UNIVERSITEIT VAN PRETORIA
UNIVERSITY OF PRETORIA
YUNIBESITHI YA PRETORIA

Department of Mechanical and Aeronautical Engineering

In-belt vibration monitoring of conveyor idler bearings by using wavelet package decomposition and artificial intelligence

By: W.A. Roos

Supervisor: Prof. P.S. Heyns

Abstract

Conveyor systems make use of idlers that support the belt and its payload as it is circulated. These idlers have bearings to ensure lower friction between the idlers and the belt. These bearings do become contaminated with dust and dirt and bearings tend to fail or even seize, adding unwanted strain and stress on the belt. These idlers are monitored and replaced when needed to minimize the damage to the belt.

There are several methods used to monitor the condition of the idlers. Thermal cameras are used to identify failing bearings that tend to run hotter than healthy bearings. Acoustic equipment exist that can capture the sound produced by the idler and processes it to indicate whether an idler is still working properly or when it is failing. These methods require an operator to travel the length of the belt, monitoring the idlers along the way. Vibrations have been used, with great success, to monitor idlers. An accelerometer is attached to the structure of the conveyor and the vibration signals are processed and from this a possible failing idler can be identified, either by an operator or an automated artificial intelligence system. However, the sensor can only monitor a few idlers close by and the cost of installing accelerometers along the entire length of a conveyor does make such a system infeasible.

A method of using an accelerometer attached to the moving belt that travels over the idlers is investigated in this study. The vibration signals of the idler are captured as the accelerometer passes it and are then analyzed and used in a decision making system to identify and classify the idler bearing conditions. The accelerometer is attached at different positions across the width of the belt to investigate the possibility of only using one or two sensors to monitor all the bearings of the idlers across the width of the conveyor. Healthy bearings are tested against bearings with inner raceway, outer raceway and rolling element defects. Contaminated bearings are tested as well. Wavelet package decomposition is used to extract the bearing features and presents it to the intelligent decision making system. Neural networks and support vector machines are used with great success to identify and classify faulty bearings. The support vector machine monitoring system has a 100% accuracy in identifying and classifying faulty bearings, regardless of the sensor position and even when a localized payload is added. The system could not only identify a faulty bearing, but also classify the fault with 100% accuracy. These accuracies were obtained in a controlled experimental environment with a simplified test setup.

The self-developed data acquisitioning system costs as much as one meter of steel reinforced rubber belt. There are some improvements needed before it could be implemented into a working conveyor, adding to the cost. A working in-belt idler monitoring system is not only plausible, but will be affordable as well.

Acknowledgements

Glory to God for all the opportunities and perseverance to complete my studies and this investigation to the best of my abilities.

A very special word of thanks to:

- My parents, Johan and Lizette Roos, for a lifetime of lessons learnt and all the countless opportunities, for all the help and assistance, for the insight, guidance and motivation.
- My mentor, Prof. Stephan Heyns, for his support, suggestions and insight and all the opportunities that he and C-AIM, The Centre for Asset Integrity Management, have given me.
- Through the Eskom Power Plant Engineering (EPPEI) programme, Dr. Mark Newby for discussing early Eskom work done in this field and their support in the test bench construction.
- Fenner Conveyor Belting, and in particular Alida van Blerk and Jose Luiz, for their assistance and the tour of their production and test facilities. Also a great thanks to their generous donation of the conveyor belt used on the test bench and the splicing thereof.
- Mr. George Breitenbach at The Sasol Laboratory for Structural Mechanics, for his assistance and insight.
- The machinists in the University of Pretoria's heavy machinery laboratory, especially Peet Kruger, Edwin Mohale and Spencer Miles Leith, for their assistance in the production of the test bench.
- The University of Pretoria, in particular my lecturers of the Department of Mechanical and Aeronautical Engineering, for my education and the opportunities they have given me.
- Chin-Chung Chan and Chih-Jen Lin, for their support vector machine library, LIBSVM, that is used with great success in this investigation.

Table of Contents

Document structure

- Chapter 1 deals with a literature study done on the workings of conveyors and what failures do occur, with the focus being on idler failure. The various methods that are currently used to monitor idler conditions are discussed as well as the feasibility of a vibration-based condition monitoring system.
- Chapter 2 contains a small scale proof-of-concept test that discusses the transmissibility of vibration through rubber conveyor belting. The conveyor test bench and the data acquisitioning system is described. The data pre-processing that is done on the vibration signals and the two artificial intelligence systems that are used to classify the idler bearing faults are also contained in Chapter 2.
- Chapter 3 presents and discusses the vibration signals of the various idler bearing faults at different measurement locations. The artificial intelligence classification results are also presented and discussed.
- The conclusions are discussed in Chapter 4.
- Proposed future work and recommendations can be found in Chapter 5.
- Appendix A contains more detail about the self-developed data acquisitioning equipment. This includes a component breakdown.

Chapter 1 - Literature study

1.1. Introduction

Conveyor belts are used in many industries; from the food industry to the mining and power generation industry. These conveyors consist of many sub-systems and these systems, like any mechanical system, are prone to failure. The failure of these systems can cause the conveyor to be stopped and repaired and during this downtime, production is lost.

One of the most expensive parts of a conveyor is the belt. The cost of the belt is approximately a third of the total installation cost. Belts tend to be damaged when the supporting idlers seize or have difficulty rotating. The seized idlers put extra strain and stresses on the belt and driving unit. Belts wear as they are dragged over a stationary idler and belts have been torn and in some cases ripped in two where the two ends of the rip have to be fixed together to form a continuous loop again. Repairing a damaged belt can be very costly.

The bearings of idlers do become contaminated with dust and dirt and this leads to bearing failures occurring and can result in the idler seizing. Some conveyors can be several kilometers in length and there may be thousands of bearings along the length of the conveyor. Any one of these idlers' bearings can start to fail and if it is not identified in time, can damage the belt to an extent where portions of the belt have to be removed and replaced.

A method for early bearing failure detection will allow the faulty bearings to be detected before the idlers seize and start to damage the belt. An automated idler monitoring system is desired to monitor the conditions of all the idler's bearings and notify an operator when a faulty bearing is detected. This system needs to be financially feasible but accurate enough to be trusted to identify any faulty bearings.

Conveyors play an important role in the operation of the mining and power generation industry. Conveyors are used to continuously feed the power generation plants with the needed quantities of coal over long distances. Conveyors can deliver their payloads continuously and the volumes can be regulated to fit the need of the process it is feeding. Conveyors play a very important role in the smooth operation of all applicable industries and the continuous monitoring of these conveyors ensure that they stay operational and working optimally.

The conditions that conveyors operate in can be very dirty and hazardous to humans if exposed to for prolonged time. In plants where conveyors are used there can be very high levels of noise and particle inhalation is also a real threat. An automated monitoring system will reduce the time an inspector has to be exposed to these conditions considerably.

1.2. Brief history of conveyor belts

With the industrialization in England in the second half of the 18th century, the conveyor belt was introduced in many industries like bakeries and abattoirs. The introduction of these conveyor belts led to a method of transporting the different products in a shorter period and at a reduced cost (Habasit, 2011). Apparently, the first steam powered conveyor belt was set into operation in 1804 to produce biscuits for the ships of the British Navy (Habasit, 2011).

The use of conveyor belts quickly spread to other industries to improve on the production efficiency. Thomas Robins developed a conveyor system in 1892 that was used to transport coal, ore and other materials (Habasit, 2011).

Richard Sutcliffe, a British mining engineer, designed a conveyor belt for underground mining, a world first that revolutionized the mining industry in 1905 (Habasit, 2011). Figure 1.1 shows one of the first conveyor belts used to transport material for the mining industry.

Figure 1.1: One of the first conveyor belts used in the mining industry (Habasit, 2011)

The conveyor belt also played an important role in the famous car manufacturer Henry Ford's assembly lines. His assembly line was the first to incorporate a conveyor belt for the purpose of car manufacturing (Habasit, 2011).

In 1957, a patent was filed for the so called "Turnover Conveyor Belt System" by B.F. Goodrich. A half-twist in the belt extended its lifetime significantly as it allowed the belt to wear on both sides and not just the one side like today's conveyor belts (Habasit, 2011). Figure 1.2 shows an extract of a patent, similar to that of B.F. Goodrich, where the half-twist can be seen. Figure 1.3 shows the Turnover Conveyor Belt System in operation.

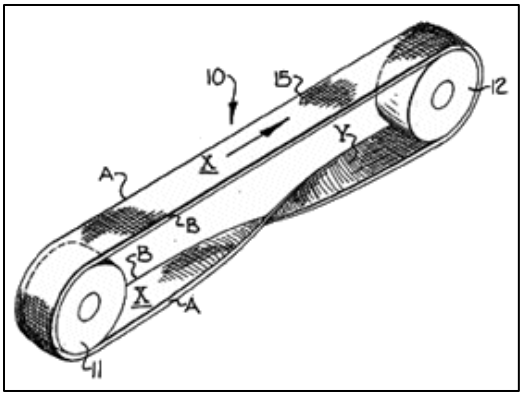

Figure 1.2: Turnover Conveyor Belt System by B.F. Goodrich (Kapp & Lehman, 1976)

Figure 1.3: Implemented Turnover Conveyor Belt (Darling, n.d.)

By twisting the belt half a turn on the bottom section of the conveyor allows the belt to wear on all of its exposed surfaces and not only on the one side like conveyor belts we know today. Although, at the time, the Turnover Conveyor Belt System was more durable than the other untwisted belts, modern day belts are more durable because they can be constructed from different layers consisting of different materials and this lead to the twist in the belt to be phased out (Darling, n.d.).

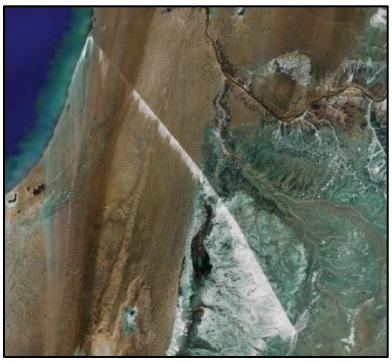

Figure 1.4: Aerial photo of world's longest conveyor belt in Western Sahara (Conveyor Belt Guide, 2005)

The longest conveyor system in use today is in the Western Sahara. The combination of conveyors has a total length of just over 100 km and has been in use for over 30 years (Habasit, 2011), (Conveyor Belt Guide, 2005). Figure 1.4 shows an aerial photo of the conveyor belts in the Western Sahara. The conveyor belts are used to transport phosphate from the mines to the coast and as some of the phosphate is blown from the belts, it leaves a distinct white line of the conveyor in the aerial photo. Belts used for the outdoor transportation of bulk materials like stone, coal and ore are made from rugged rubber and is reinforced with steel cord (Habasit, 2011).

1.3. Working principle of a conveyor

A conveyor, whether it is used in the food industry or the mining industry, has a few basic, but crucial components. A conveyor is comprised of a drive or head pulley, a tail pulley, a continuous belt, supporting idlers, a tensioning and alignment device and a driving unit that is usually geared down for improved torque to transport great amounts of payload.

1.3.1. Drive unit

The heart of the conveyor is the drive unit. The sizing of the drive unit depends on the amount of payload that needs to be transported, how fast it needs to be delivered as well the length of the belt that needs to be circulated. Some power units can be as small as a 24 V DC motor like the drive unit in an iDrive compact conveyor from Dorner (Automation Supplies Ltd, n.d.) as seen in Figure 1.5. Other drive units like those found in the mining industry can range from 45 to 3000 kW with some of the drive units rated at a maximum torque of 600 kNm (David Brown, n.d.). A large drive unit like this is shown in Figure 1.6. As seen in the figure, the yellow enclosure protects the gearbox, the flywheel and braking system. The size of the drive unit depends on the requirements of the transportation of the payload. Some conveyors make use of direct drive where the motor is connected directly to the head pulley but it is not widely used yet (Siemens, 2013).

Figure 1.5: Small drive unit of an iDrive conveyor (Automation Supplies Ltd, n.d.)

Figure 1.6: CX Conveyor Drive unit installed on site (David Brown, n.d.)

1.3.2. Head or drive pulley

The head pulley, or also known as the drive pulley, is a big drum around which the belt of the conveyor is wrapped around. The head pulley, with the assistance of the drive unit, provides the driving force that circulates the belt. The payload on the belt, and the weight of the belt itself, induces a large amount of tension on the head and tail pulley. The head and tail pulley is designed to withstand these large forces and the drum, shaft and bearings can become massive. Figure 1.7 shows a very large pulley used in a copper project in Peru where a designed tension of 1,422 kN needed to be withstood (RAS, n.d.).

Figure 1.7: Large drive pulley
(RAS, n.d.)

Another main reason for the large diameter is to accommodate the bending of the belt around the pulley. If the diameter is too small, the belt will be strained and the lifetime of the belt can be decreased or the splice (connection between the two ends of the belt to create a continuous belt) can be damaged and may lead to catastrophic failure (CKIT, n.d.).

1.3.3. Belt

The belt is the component of the conveyor system that comes into contact with the payload and carries it. There are a number of different belts available to choose from. Some belts are made from rubber with reinforcements imbedded and some belts are made completely from solid woven PVC. The type of reinforcements usually found in rubber belts differ from steel cords (metal) to Kevlar (material) (Du Pont, 2013) and can be imbedded longitudinally and/or transversely (Dunlop Conveyor Belting, n.d.).

Some belts are produced with different layers to increase the strength. The inclusion of steel cord is not uncommon when the belt's strength needs to be increased (Dunlop Conveyor Belting, n.d.). As seen in Figure 1.8, different size steel cords can be used depending on the strength needed. Some belts may only have steel cord along the longitudinal direction of the belt, but other manufacturers may also add transverse strengthening as seen in Figure 1.9.

Figure 1.8: Different steel cord and belt size
(Shandong Rubber Six Xiang Te Conveyor Belt Co., Ltd., 2015)

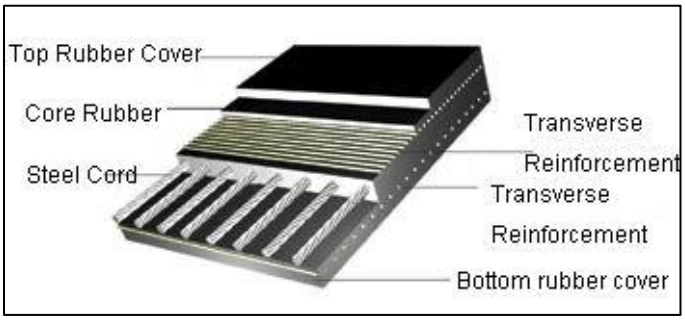

Figure 1.9: Different orientations of steel cord in a belt
(ESTAR, 2014)

Belts can be as short as a few meters or as long as 35 km – the longest single conveyor belt in the world (Conveyor Belt Guide, 2005). Some belts have flexible rubber sidewalls that can help keep the payload on the belt as it is transported as seen in Figure 1.10. A more commonly used method is to use additional idlers to form the flat belt into a trough shape as seen in Figure 1.11. This is done to help keep the payload on the belt and not spill over the edges

Figure 1.10: Conveyor belt with rubber sidewalls (C.C.Components Pty. Ltd., n.d.)

Figure 1.11: Trough created with idlers (Conveytech, 2013)

Some conveyors create a pipe or tube with the flat conveyor belt by gradually rolling the belt into a tube with the idlers as seen in Figure 1.12. The payload is not spilt nearly as much or blown by the wind as it is protected against the elements (Lakshmi Macfab, 2015).

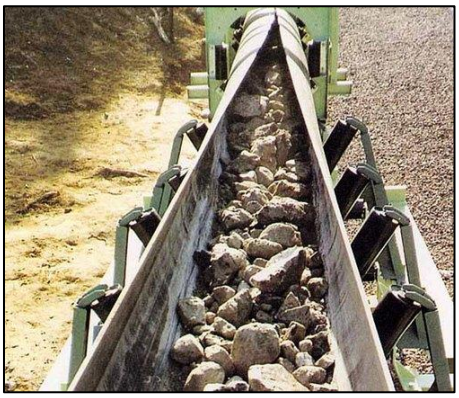

Figure 1.12: Belt formed into tube with idlers (Lakshmi Macfab, 2015)

1.3.4. Support idlers

Support idlers are small cylinders that run on bearings. They are used to support the conveyor belt as it transports the payload from one end to the other. Older idlers were made from steel cylinders with steel end-caps welded or pressed onto the top and bottom of the cylinder (Kinder, 2015). There is a bearing in each end-cap and a shaft through the bearings to support the idler. Some of the more modern idlers are made from plastic, nylon, polymer or other high density plastic parts. This is done as the parts can be moulded in one piece, keeping the

manufacturing cost down as well as the overall weight of the idler (Kinder, 2015). Some idlers are hybrids where the cylinder is still made from steel or even aluminium but with high density plastic end-caps.

Seals are used to protect the bearings from the environment, keeping dust and mud away from the bearings to increase the usable life. Bearings contaminated with dust or mud tend to seize or fail catastrophically (Kinder, 2015). The seizure or failure of a bearing can cause an entire idler to seize and then it will start to scrape or rub against the belt, causing unnecessary friction on the belt. This excess friction places additional strain on the power unit and the belt may also rip, tear or catch fire under these excessive friction forces, leading to the standstill of the conveyor.

1.3.5. Tail pulley

The tail pulley is very similar to the head or drive pulley but there is normally no driving unit coupled to the tail pulley – it is a free running pulley. In some cases the tail pulley may have a drive unit coupled to it and in effect it becomes a drive pulley that works with the primary drive pulley to circulate the belt.

The size of the tail pulley is governed, similar to the size of the drive pulley, by the bending of the belt and the load on the pulley. Some belts need a larger diameter pulley to wrap around to accommodate the bending of the strengthening structure within (CKIT, n.d.).

1.3.6. Tensioning devices

The total load on the belt is almost never constant. In the mining industry, the rate at which the payload is deposited onto the conveyor always fluctuates a bit (CKIT, n.d.). The purpose of the tensioning or take-up devices in the conveyor system are to maintain tension in the belt. The tension in the belt should be applied gradually and equally over the width of the belt to ensure the belt is not stressed excessively. When the load on the belt varies, the tensioning device should respond to keep the belt from sagging or being stretched too much (CKIT, n.d.).

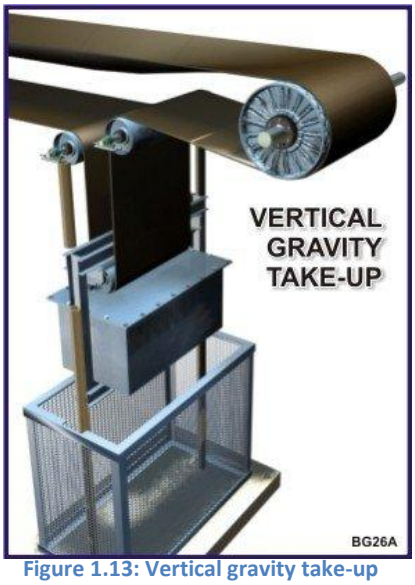

Figure 1.13: Vertical gravity take-up system (CKIT, n.d.)

An example of a tensioning device is where gravity is used to pull on a take-up pulley. This pulley can hang underneath the conveyor as seen in Figure 1.13. Weights attached to the take-up pulley with the belt wrapped around it provide the tension. The weight in the take-up system is calculated to provide the best tension regulation needed for the system.

1.4. Failures in a conveyor

Like every mechanical system, something is bound to wear and fail at some stage during the operation of the conveyor. There are plenty of individual components that make up a conveyor system and each one of them can fail or lead to subsystems failing. The conveyor can still operate and deliver the payload even when certain components fail - like the idlers. If these components are not fixed they can lead to the failure of subsystems or other components that are critical to the operation of the conveyor - like the belt.

The bearings in the drive unit, head and tail pulleys are subjected to enormous stresses. The bearings can fail and lead to catastrophic failure of the conveyor. There have been reports that the bearings became so hot that the grease inside caught fire (Owen, n.d.). The gears inside the drive unit are also under large cyclic loads. Various condition monitoring methods have been implemented on these critical components for preventative maintenance against catastrophic failure.

The belt of the conveyor system is an expensive component. For a nylon or polyester embedded belt, the cost of the belt is about one third the installation cost of the entire system and can be even more expensive if the belt is reinforced with steel cord (Owen, n.d.). Preventing damage to the belt is a good way of keeping the maintenance cost down. The belt can be damaged in a few ways. Large rocks on the belt or material build-up on the idlers can stress the belt to an extent that the strengthening structure, or carcass, of the belt gets weakened (Kinder, 2013). These weaknesses in the belt can lead to a tear in the belt or the complete severing of the belt. This will mean that the conveyor has to come to a standstill to repair or rejoin the belt. Figure 1.14 shows material build-up on an idler and how it stretches the belt, weakening and sometimes even tearing it.

Figure 1.14: Material build-up and visible belt damage (Kinder, 2013)

There are hundreds if not thousands of idlers along the length of conveyors. These idlers support the belt as the payload travels from one end to the other. The most belt failures are due to the failure of the idlers (Kinder, 2013). The free rotations of the idlers are compromised as the bearings wear and in some cases the entire idler seizes as the idler's bearings fail catastrophically. Friction between the idler and the belt increases when the bearings start to fail and the idlers do not rotate as freely. The friction between the idler and the belt wears the shell of the idler as well as the surface of the belt. In some cases the idler completely seizes and the belt, with its payload, is dragged over the stationary idler. These damaged and seized idlers wear, cut and tear into the belt (Intium, 2015).

Figure 1.15 shows an idler that had seized but that had not been replaced for a while. As the belt travelled over the idler, it wore through the steel shell. Sharp edges from the worn section could potentially slice or rip the belt.

Figure 1.15: Idler seized and belt wore through the steel shell (Intium, 2015)

Although the idlers are not as complex as the drive unit, the head and tail pulley or the tensioning mechanism, they are very crucial to the smooth operation of a conveyor. There is a very large number of idlers along the length of a conveyor. For general engineering practice, the spacing, in imperial units, of the idlers based on the belt width and the payload weight can be found in Table 1.1. The table was found in an idler selection procedure from (Goodman Conveyor, n.d.). Note the table is in imperial units.

It can be seen that the maximum spacing of the weight carrying idlers are 1.67 m (5.5 ft.) and as the belt width and the payload mass increases, the idler spacing becomes smaller to about 0.61 m (2 ft.). The spacing of the return idlers are larger seeing that they do not have to support the mass of the payload, only the mass of the belt has to be supported. The spacing for the return idlers range from 3.05 m (10 ft.) to 2.44 m (8 ft.), depending on the belt width. From this, the possible number of idlers per kilometer of conveyor can be calculated.

Table 1.1: Suggested idler spacing (feet) in engineering practice (Goodman Conveyor, n.d.)

Belt width [in]	Number of troughing Idlers Weight of Material Handled, [Lbs. per Cu. Ft]						Number of return Idlers
	30	50	75	100	150	200	
14	5.5	5.0	5.0	5.0	4.5	4.5	10.0
16	5.5	5.0	5.0	5.0	4.5	4.5	10.0
18	5.5	5.0	5.0	5.0	4.5	4.5	10.0
20	5.5	5.0	5.0	5.0	4.5	4.5	10.0
24	5.0	4.5	4.5	4.0	4.0	4.0	10.0
30	5.0	4.5	4.5	4.0	4.0	4.0	10.0
36	5.0	4.5	4.0	4.0	3.5	3.5	10.0
42	4.5	4.5	4.0	3.5	3.0	3.0	10.0
48	4.5	4.0	4.0	3.5	3.0	3.0	10.0
54	4.5	4.0	3.5	3.5	3.0	3.0	10.0
60	4.0	4.0	3.5	3.0	3.0	3.0	10.0
66	4.0	4.0	3.5	3.0	3.0	3.0	10.0
72	4.0	3.5	3.5	3.0	2.5	2.5	8.0
84	3.5	3.5	3.0	2.5	2.5	2.0	8.0
96	3.5	3.5	3.0	2.5	2.0	2.0	8.0

It was found that, according to the data in the table, a minimum of 925 or a maximum of 2,049 idler-assemblies will be needed per kilometer depending on the belt width and the payload mass. In each idler assembly, there can be up to three idlers on top to form a trough and to support the payload and one or two idlers supporting the empty returning belt. If it is assumed that there are three idlers on the top of the assembly supporting the payload and one idler supporting the empty returning belt, it equates to four idlers per assembly, or eight bearings. That means that there can be 7,400 to 16,392 bearings per kilometer. Some conveyors in the mining and power generation industry can be a few kilometers in length. That is a very large number of bearings to inspect and monitor for possible failures and any one of these bearings can fail and can potentially lead to damage of the belt.

There are a number of condition monitoring systems implemented on sub-systems like the drive unit, head and tail pulley and even the belt surface and internal structure that do not need constant human involvement or assistance. These systems are automated and notify an operator when a fault is identified. As with the other sub-systems in the conveyor, a system is needed to monitor all the bearings in the idlers and notify an operator of any possible failures that may have occurred. According to a feasibility study done at Eskom, there is a need for a system that can monitor the idlers of conveyor belts (van Tonder, 2002) but it needs to be financially feasible. The monitoring equipment has to be affordable and the remuneration of the work force needed to monitor and replace the idlers needs to be taken into account.

1.5. Current methods of monitoring the idlers on a conveyor

There are many possible points of failure as any one of the idlers can fail and cause damage to the belt. If the belt is excessively damaged or ripped, the entire system has to be stopped to fix the belt and this can cause hours of downtime. A method of identifying a damaged idler early on can be very valuable. The cost of repairing a belt is quite high in comparison to the cost of a new idler (van Tonder, 2002). If a damaged idler can be identified and replaced/repaired before it fails or before it damages the expensive belt, the cost and the hours of repairs can be reduced.

A monitoring system that can be used to monitor the conditions of all the idlers along the length of the conveyor can be very beneficial to a plant. If the conditions of all the idlers are known, the plant can prepare for the time, the type and number of repairs that has to be done in order to keep the conveyor working optimally (van Tonder, 2002). If it is known which idlers need to be repaired or replaced, the needed parts can be ordered and all of them can be repaired or replaced in a single planned outage when the dependency on a working conveyor is not as high.

There are several existing methods of identifying faulty idlers and the different types of failures that do occur. A number of investigations have been done on different ways to monitor the condition of idlers.

1.5.1. Visual inspection

The simplest form of condition monitoring is usually done by walking the length of the conveyor and looking and listening for indications of failures.

Faulty idlers can be spotted by visual inspection but sometimes failing idlers can be missed. Visual inspection cannot accurately determine the degree of failure or the urgency of an idler that needs to be replaced (van Tonder, 2002). A seized idler is easy to spot but by the time an idler has seized, the belt has already been dragged over it for a while. Some idler supporting structures are bolted to the conveyor structure and these bolts can come loose. If these bolts do come loose, the idler supporting structure can move and become misaligned. Attention to this is also needed when inspecting the conveyor. Material build-up can also be easily identified and removed.

While some failed idlers can be identified with visual inspection, not all the faults or potential failures can be identified. Some conveyors are very long, several kilometers, and it can be a tedious job to inspect the entire length of the conveyor by human visual or acoustic inspection. Some failure characteristics are better/easier to identify by specialized equipment to aid the inspectors.

1.5.2. Thermal cameras

Thermal cameras offer a great way of identifying faulty idlers. Bearings that are starting to fail will normally run slightly hotter than the other bearings. These temperature differences can easily be seen on a thermal image like that of Figure 1.16 and Figure 1.17 and the faulty idler can be identified and repaired. Thermal cameras make for a quick inspection (Maras, 2013).

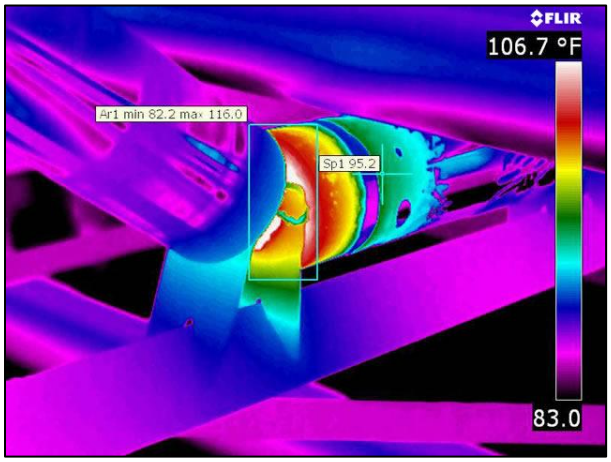

Figure 1.16: Thermal image of a hot idler bearing (FLIR, 2015)

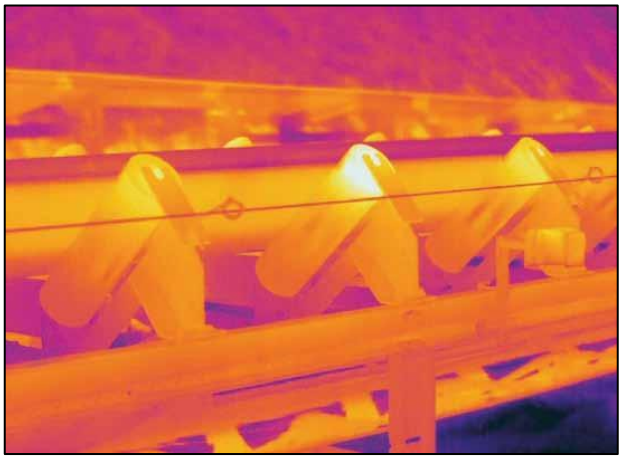

Figure 1.17: Clear thermal indication of a faulty idler (Maras, 2013)

Most thermal cameras have interchangeable lenses (FLIR, 2015). A wide angle lens can be fitted to a thermal camera and a large portion of the conveyor can be inspected with ease. The wide angle (90°) lens can also be used when there is not a lot of space and the camera has to be close to the idlers. A telephoto (7°) lens can be used to capture the heat signatures of idlers that are far away and difficult to access (FLUKE, 2015). Figure 1.18 shows an overlay of a thermal photo and a normal colour photo of an idler that is difficult to reach.

Figure 1.18: Thermal image overlay of elevated conveyor (FLUKE, 2015)

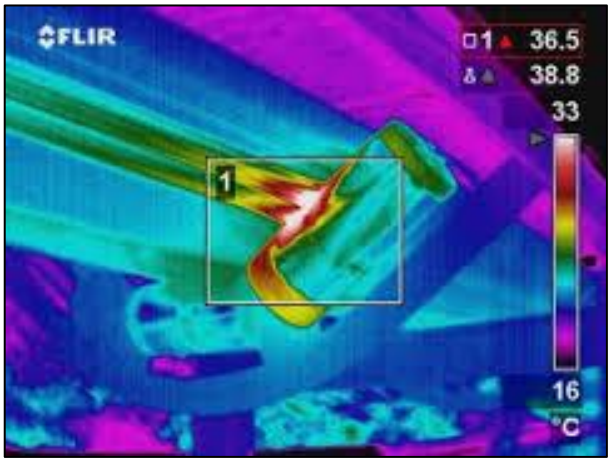

Figure 1.19: Heat streaks on belt due to uneven loading (Nuatitech, 2015)

The thermal cameras are not only used to identify faulty idlers, but can also be used to identify uneven belt loading. When the belt is not laden evenly, the pressures on the belt as it travels over the idlers are not uniform. This uneven pressure creates heat streaks on the belt and this can be captured by the thermal cameras (Nuatitech, 2015). Figure 1.19 shows such heat streaks due to uneven loading. A camera operator still needs to travel the length of the belt to capture the heat signatures of all the idlers. This can also take some time to complete.

1.5.3. Acoustic sensing equipment

To help the inspector to identify possible faults or failures, acoustic equipment are used to identify audible and inaudible noise. Specialized acoustic equipment like SKF's idler sound monitor kit, depicted in Figure 1.20, can be used to identify small deviations in bearing vibrations and serve as a fault identifier (SKF, n.d.).

The SKF monitor works with headphones and can be operated with one hand, making it safer for the inspector. The SKF monitor can identify a faulty idler bearing from 3 m away and even when the inspector walks at a pace of 2 km/h (SKF, n.d.).

Figure 1.21 shows the SFK monitor while a bearing is spun close to the microphone. The bearing vibration signal is displayed on the monitor itself. The monitor can then process the signal and indicate the level of noise as seen in Figure 1.20. The green light indicates low vibration energy and indicates that the bearing is still functioning properly. A red light indicates a failing bearing.

Figure 1.20: SFK idler sound monitor kit (SKF, n.d.)

Figure 1.21: SKF monitor displays noise signal of a bearing (Edilson S Ribeiro, 2012)

1.5.4. Vibration

The vibrations of mechanical equipment can reveal the condition it is in and vibration analysis is a commonly used tool in fault diagnosis (Li, et al., 2013). The vibration signal of equipment that theoretically has no faults, is referred to as a good or healthy signal. The monitoring of the equipment's vibration and comparison to the healthy signal can be a good indication of the equipment's health. The key of vibration analysis is extracting the fault features (Li, et al., 2013). Deviations from the healthy signal is also a good indication of faults occurring as the vibration of equipment will change when faults occur (Li, et al., 2013).

Vibrations have been used to monitor the conditions of conveyor idlers before with success. By looking at the vibration signal of the idlers, the state of the idler can be monitored. By knowing the state of the idlers, potential problematic idlers can be identified and decisions can be made on whether to replace or just repair these idlers and when to do so. The on-line or real time capabilities of such a monitoring system allow potential faulty idlers to be identified and to notify an operator before failure occurs.

An investigation was done on the vibrations of conveyor idlers by the School of Mechanical and Electrical Engineering of the China University of Mining and Technology. (Li, et al., 2013). This investigation looked at the vibrations of the idlers and identifying which of the idlers close by is failing. The vibrations were captured by accelerometers placed on the supporting structure of the conveyor as seen in Figure 1.22. Seeing that some conveyors can be very long, and having an accelerometer at every idler can become costly, a single accelerometer was used to monitor three idlers – the idler at the accelerometer and the two neighbouring idlers. Figure 1.23 shows the three idlers that were monitored in the investigation. The accelerometer seen in Figure 1.22 is placed at the idler marked "Idler 2". The accelerometer was then used to monitor the neighbouring idlers as well - "Idler 1" and "Idler 3".

Figure 1.22: Accelerometer attached to the conveyor's supporting structure
(Li, et al., 2013)

Figure 1.23: Three idlers being monitored by a single accelerometer
(Li, et al., 2013)

An artificial intelligence system was then used to analyze the vibration signal of the accelerometer and inform an operator of any failing or faulty idlers. This method of monitoring the idlers can be very accurate seeing that the intelligent system is trained with the type of idlers and bearings used in that specific plant.

Figure 1.24 shows the classification of faults on a mechanical fault simulator. The simulator was used to illustrate the feasibility of using wavelet package decomposition and artificial intelligence to classify mechanical faults (Li, et al., 2013). An output of 1 was given for a normal, healthy state. Depending on a gear defect in the mechanical fault simulator, either a 2, 3 or 4 were given as output. Figure 1.24 shows the classification of the gear faults. The red data set represents the classification of the faults with a neural network and the blue data set the classification by a support vector machine. It can be seen that the support vector machine classifies the faults more specifically - the output is one of four values, where the neural network classifies the faults with a little less certainty. It has been found that the support vector machine is the more accurate classifier (Li, et al., 2013) and was then used for faulty idler identification and classification.

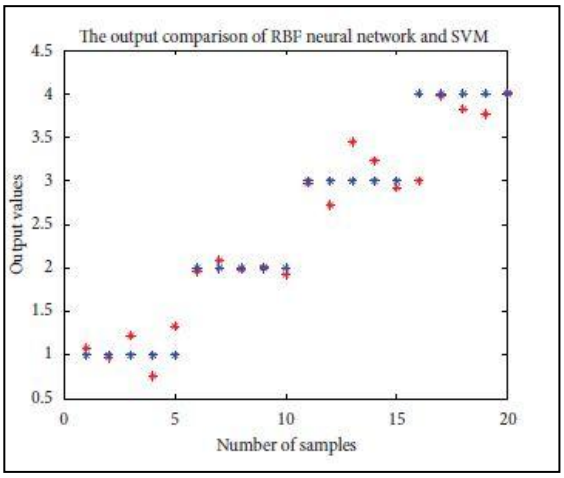

Figure 1.24: Neural network (Red), Support vector machine (Blue) classification of gear faults (Li, et al., 2013)

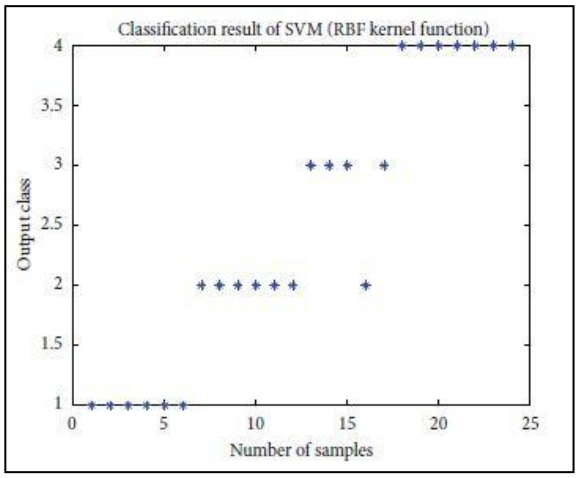

Figure 1.25: Support vector machine classification of idler faults (Li, et al., 2013)

A support vector machine, that made use of a radial base function (RBF), was used to identify the faulty idlers and the classifications can be seen in Figure 1.25. The investigators found that their support vector machine was 91.67% accurate (22 of 24 datasets) in classifying the idler conditions, whether it was where no idlers were faulty or where either one of the idlers were faulty. Only 2 out of 24 samples were not classified correctly. The investigation group then used the support vector machine to create an online monitoring system that could inform an operator of a faulty idler within a fraction of a second (Li, et al., 2013).

From this successful idler monitoring technique, it can be seen that vibration based monitoring can be very accurate and successful to identify faulty idlers of conveyors. The use of wavelet package decomposition, for signal pre-processing, and neural networks and support vector machines, as classifiers, were very effective in monitoring conveyor idlers (Li, et al., 2013).

The accelerometer was only used to monitor three idlers. An accelerometer is not sensitive enough to pick up the change in vibrations of the idlers that are far from the measuring point (Li, et al., 2013). Although this is a very accurate and nearly autonomous monitoring method, there is a downside. The number of accelerometers needed to monitor an entire conveyor will be too much and the cost of such a system will be too expensive to justify (Li, et al., 2013). Even if an operator uses a single accelerometer and moves from one idler to the next, it will still take as much time to set up as it would to use a thermal camera or an acoustic monitoring system.

The research being done in this report intends to address the possibility of using a conventional vibration based condition monitoring approach on idler bearings, because of the excessive number of bearings that would be required to do so. The feasibility of placing an accelerometer and all the data acquisitioning equipment on the moving conveyor belt, and having the sensor monitor the vibrations of each idler it passes, will be investigated.

In essence the methods used in the investigation done by the School of Mechanical and Electrical Engineering of the China University of Mining and Technology (Li, et al., 2013) will be used, albeit now with the data acquisitioning done on the moving belt and not on the stationary supporting structure. This choice is based on the results obtained by pre-processing the signals with wavelet package decomposition and classifying the faulty idlers with intelligent systems.

The idea of placing the data acquisitioning equipment on the conveyor belt comes from a patent (Freeman, 2010) that was originally filed in 2008 in the United States of America by Vincent Neil Freeman. This patent describes a possible solution where the sensors are installed or imbedded into the belt rather than on the supporting structure. Figure 1.26 shows an extract of the patent.

As the belt moves over all the idlers (parts 108a to 108h), all the vibration signals are captured by the sensors (included in parts 110, 112 and 114). Rather than having a vast number of accelerometers or having someone walk the length of the belt with measuring equipment, the belt will transport the measuring equipment (parts 110, 112 and 114) along the conveyor. A smaller number of sensors are needed to monitor the entire conveyor.

Although the proposed system uses only a few accelerometers, some other hardware is now required for the system to function. The signals need to be captured and stored on the belt until it can be transmitted to a computer. A source of power is also needed for the entire duration of the monitoring process.

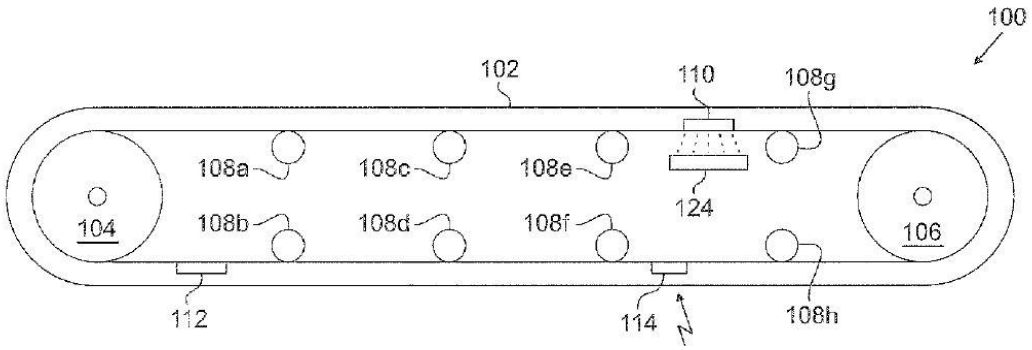

Figure 1.26: Side-view of conveyor with embedded sensors (Freeman, 2010)

1.6. Feasibility of vibration-based condition monitoring on conveyor idlers

In 2002, Eskom did a feasibility study of an in-belt on-line idler monitoring system to see whether there is a demand for such a system to replace their current methods of idler condition monitoring – visual inspection aided with thermal cameras and temperature sensors (van Tonder, 2002). Questionnaires were sent to all the Eskom power stations to gather information on what their opinion was on the matter, the frequency of idler failures and repairs as well as the details of their plant's belts.

It was found that there is a need for an on-line idler monitoring system seeing that the current methods that were used were quite expensive, but the labour needed for the inspections even more so (van Tonder, 2002). The two main factors that contribute to the need for an on-line monitoring system are the long lengths of conveyors that are very laborious to inspect manually and the critical areas such as inclines and transfer chutes that has to be monitored closely (van Tonder, 2002). It is essential to have a system that can accurately monitor idlers seeing that visual inspection sometimes misses failing idlers and visual inspection cannot determine the degree of failure or the urgency of an idler that needs to be replaced (van Tonder, 2002).

The feasibility of an in-belt on-line idler monitor, as described by the questionnaires, depends on cost of the monitoring system embedded within the conveyor belt in relation to the cost of the belt that is being monitored. The cost of not implementing a monitoring system with all the repair, maintenance and inspection costs has to be weighed against the cost of implementing and maintaining the monitoring system (van Tonder, 2002). Data was gathered from the questionnaires in terms of the number of idlers that had been replaced, whether they have failed or were failing, the cost of idlers, the cost of lengths of belts used, the cost of splicing a belt, the cost of labour to inspect the belt and even the cost of load loss or plant shut down. An

estimated cost of an in-belt on-line monitoring system and the maintenance of the system was determined, and it was found that the monitoring system would cost less than the visual inspection methods used at the time, but not by a significant margin. The total estimated cost of an in-belt monitoring system was about 90% of the current inspection methods (van Tonder, 2002). The cost of the monitoring equipment has decreased over the years but another feasibility study has to be done to find accurate values.

A focus group meeting was held in 2002 where the implementation of an in-belt on-line idler monitoring system was discussed. It was mentioned that the technology that was intended for the monitoring system was too expensive. It was recommended that the market should be scanned for newer, cost effective technology that would be more financially viable (van Tonder, 2002) seeing that the sensory equipment used in the estimation contributed to about 73.5% of the total solution. It was also mentioned that the preferred methods of determining an idler failure was through noise or heat monitoring.

Visual inspection of conveyor idlers can become dangerous if the necessary precautions are not taken. In coal fired power stations, like those of Eskom in South Africa, there are large amounts of coal dust, noise, coal spillage and moving conveyor equipment. There are risks of coal dust particle inhalation, slippage on coal spillage and even being caught between moving components (Mjelo, 2013). Specified personal protective equipment (PPE) has to be worn when inspections are done and guidelines have been provided for the correct and safe inspection of idlers (Mjelo, 2013). Time to visually inspect an entire conveyor belt, even with additional equipment like thermal cameras, will take significantly longer than when the idlers are monitored with an in-belt on-line monitoring system.

A preliminary test will be done first to investigate the feasibility of measuring vibrations through the rubber conveyor belt. A data acquisitioning system prototype was developed for measuring vibrations on the conveyor belt and can sample at about 1 kHz. The final self developed data acquisitioning system is discussed later in Chapter 2.3 and Appendix A. The type of idlers and the running conditions of the system that will be used in the final tests were not known at this stage as a feasibility test is done first, thus the fundamental bearing fault frequencies were not known but was expected to be below the 1 kHz that the data acquisitioning system will be able to sample at. To investigate the transmissibility through the belt for the entire frequency range that the system will be able to sample, 0 Hz to 1 kHz was chosen as the frequency range of the feasibility test.

The feasibility and accuracy of a low-cost in-belt idler bearing vibration monitoring system should be investigated.

Chapter 2 - The development of an in-belt idler monitoring system and test bench

2.1. Small scale test - Vibration transmissibility through conveyor belt

Figure 2.1 shows a frequency plot of the vibrations found in a bearing as it fails. The first signs of bearing failure can be detected in the ultrasonic frequency range above 20 kHz (Graney & Starry, 2012). Stage two is where the natural frequencies of the structure are excited (Graney & Starry, 2012). Stage three are the frequencies associated with the bearing components like the race pass frequencies and the roller element frequencies also known as the bearing fault frequencies (Graney & Starry, 2012). Stage 4 is where the harmonics of the bearing fault frequencies appear.

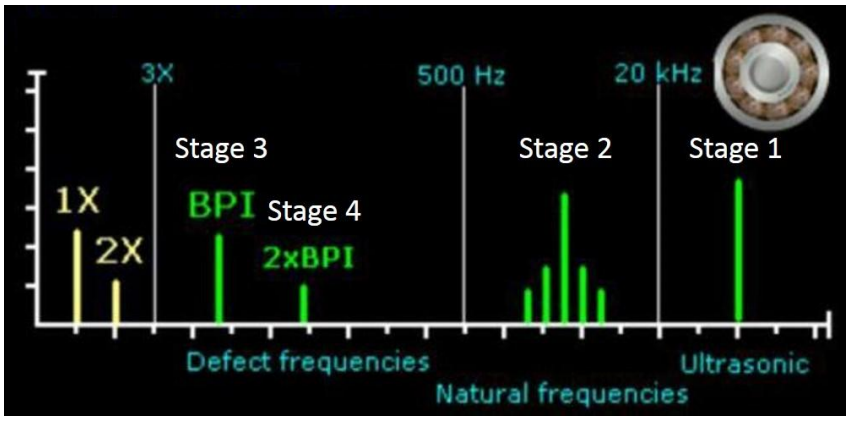

Figure 2.1: Vibration stages of failing bearings

For very early fault detection one can focus on the first stage of bearing failure. Monitoring the ultrasonic vibrations will give a very early insight to a bearing's health. These frequencies are very high and the sensors and data acquisitioning equipment that can measure at these high frequencies are more expensive. More readily available equipment can be used to measure at the lower frequencies and monitor the bearing fault or defect frequencies. This will be more financially viable but will only indicate later stage failure. Faulty idlers will be replaced when it is in the later stages of failure as it makes no sense to replace a bearing when there is still significant life left. It would be beneficial to be able to identify a faulty bearing when it is in the initial stages of failure, but identifying the bearing in the third stage of failure should give the operators enough time to evaluate the severity of the failing bearing.

There are a few concerns when measuring the vibrations of the idler bearings by placing an accelerometer on or in the belt. The biggest concern is the potentially low transmissibility of the vibrations from the bearings, through the idler body and the rubber belt to the sensor.

To better understand the risks involved due to this effect, a simple experiment was conducted before commencing with the study. This was done to investigate if it is possible to measure the vibrations through the rubber belt at various distances from the source.

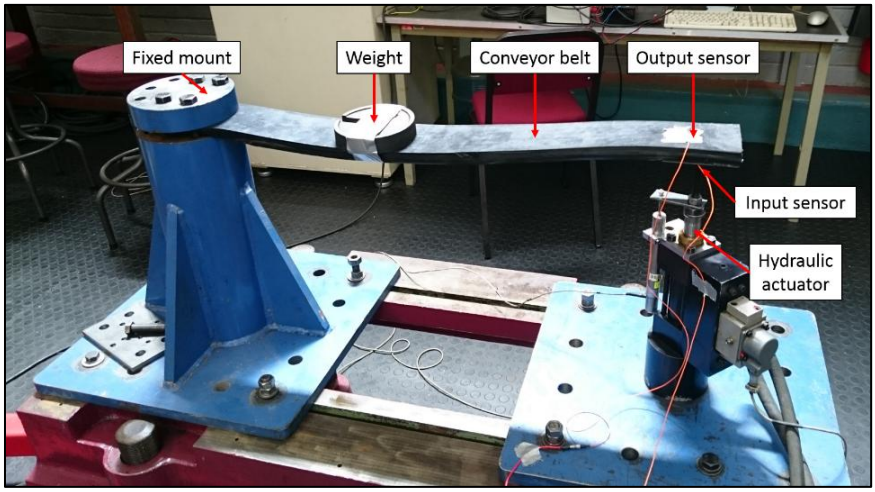

Figure 2.2: Transmissibility test bench

Figure 2.2 shows the small scale experiment that was used to investigate the transmissibility. The major components are labelled on the figure:

- A hydraulic actuator was used as the source of the vibration. A frequency sweep was done from 0Hz to 1000Hz. This range was chosen because low range frequencies, rather than high or ultrasonic frequencies, are more important to characterize properly seeing that later stage failure occurs at these frequencies.
- An accelerometer was used to measure the vibration signal generated from the hydraulic actuator. The input sensor was fixed to the underside of the belt on its centreline where the hydraulic actuator connected to the belt. This represented the source of the vibrations that is induced by the idler.
- The output sensor was used to measure vibrations on the centreline on top of the belt. This is where the sensor of the real-world application ought to be installed. The sensor was first placed over the source (as seen in Figure 2.2) and was then moved in 50mm increments away from the source. This was done up to a distance of 400mm away from the source. 800mm is the average distance between two idlers as seen in Figure 2.2. At a distance halfway between idlers, the sensors will start to associate the measured signal with the next idler. For this reason, tests were only done up to 400mm.

- A weight was used to crudely simulate the effects of a payload on the belt. The weight was concentrated and does not represent the uniform loads found in the real-world accurately. The weight was placed just to the left of the furthest point of measurement. The other end of the belt was fixed to a rigid post. The total distance of the belt that was free to move was 800mm in length.
- The conveyor belt used is a sample that was cut from a steel cord reinforced rubber belt. This belt is produced by Fenner for the materials handling industry. It is this industry that this monitoring method is aimed at, and this type of belt will be used in the tests for this reason.

The transmissibilities at a certain distance from the source were calculated by comparing the input or source vibration to the measured output vibration. The time signals of both accelerometers were analyzed in the frequency domain. A simple fast Fourier transform (FFT) was done on the measured signals. The two sensors were both connected to the same data logger so that both signals had the same sampling frequency. In the frequency domain, each value of the two signals that corresponded to the same frequency were used to determine the transmissibility. From eq. 2.1, the transmissibility T for a given frequency f is given by the ratio between the signal magnitudes, in the frequency domain, of the output M^o and the input M^i.

$$T_n = \frac{|M^o{}_f|}{|M^i{}_f|} \qquad \text{(eq. 2.1)}$$

The transmissibilities for the entire frequency range and for all nine measured distances were calculated. Figure 2.3 shows the gradient filled contour plot of the transmissibility of vibrations through the belt.

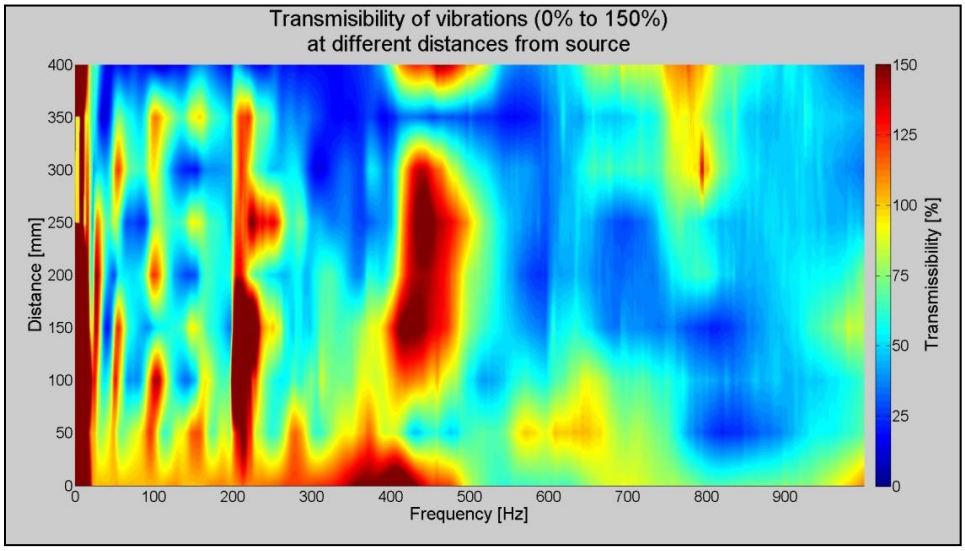

Figure 2.3: Transmissibility of vibrations through the belt

As seen in Figure 2.3, the transmissibilities of the vibrations are very good close to the source for a wide range of frequencies. In the region on the belt from 0mm to 50mm and at a frequency of 0 Hz to 500 Hz there is a yellow-orange and red region, this corresponds to 100% transmissibility and higher. The sensor is still close enough to the source that the dynamics of the belt does not influence the transmissibility too much. At higher frequencies the transmissibility reduces quite dramatically. It is also seen that at some positions on the belt, transmissibility is larger than 100% - red regions. This can be due to the belt resonating at its natural frequencies. The resonating belt can help amplify the underlying bearing frequencies if the bearing frequencies correspond with the belt's natural frequencies and these induced vibrations are large enough to excite the belt. There are however sections of the belt that attenuate the source vibrations - blue and green sections. If a sensor is measuring in these regions at those frequencies, the bearing vibrations may be difficult to capture.

Referring to Figure 2.4 that only shows the regions that have a transmissibility of 75% and higher, it can be seen that up to 50mm away from the source, the transmissibility of vibrations up to 400Hz is well above 75%. This region, indicated with the bounding box, has a transmissibility of 100% and higher and it is comforting to know that sensor readings in this region will not be attenuated close to the source when tests will be done on the moving conveyor.

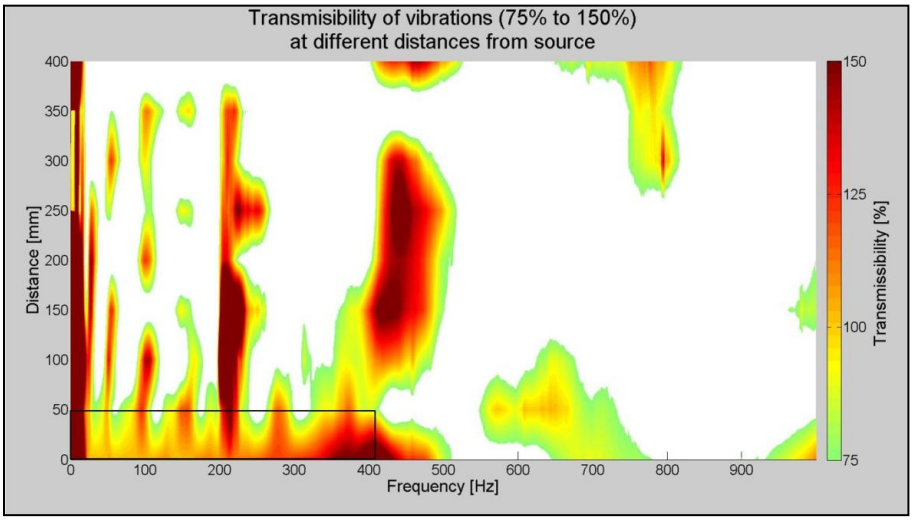

Figure 2.4: 75% Transmissibility and higher

Figure 2.5 show the regions that has a transmissibility of 50% and higher. It is shown that at a distance of 100mm the transmissibility is higher than 50% for vibrations up to about 760Hz. The transmissibility is also well above 50% for frequencies up to 280Hz for distances up to 300mm away from the source, but there are sections within this range where the transmissibility is

below 50% - shown as the white voids in the contour plot. This is due to the mode shapes of the belt at different frequencies that have an attenuating effect on the transmissibility.

The belt has mode shapes at some frequencies where troughs and peaks in the wave magnitude can be seen in the abovementioned figures. These mode shapes change as the frequencies do and explain why, at some frequencies, the transmissibility can be very high at some point on the belt, and be very low just a short distance away. Take 150Hz in Figure 2.3 as an example, at 50mm, 150mm, 250mm and 350mm the transmissibility is just below 100% (yellow-orange region) but in between can be as low as 25% or even lower (dark blue).

From the contour plots it can be seen that the vibrations are, as expected, attenuated more at high frequencies far from the source.

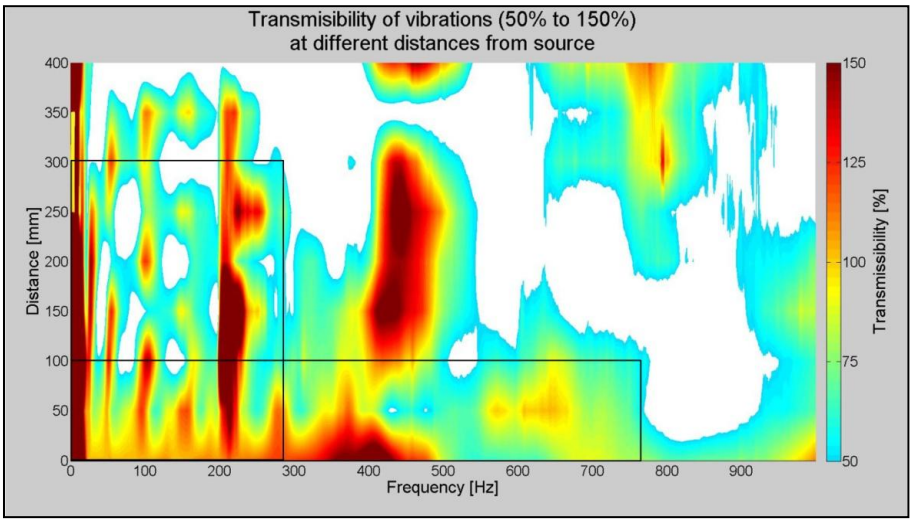

Figure 2.5: 50% Transmissibility and higher

This experiment was done to investigate the magnitude of the attenuation effect of the steel reinforced rubber belt on a vibration signal, possibly from an idler bearing, and what influence it would have on the capabilities of measuring said signal.

From the experiment it can be expected that the vibration signals from an idler bearing can be measured with little loss to the signal strength, close to the source over a wide range of frequencies, and still clearly at low frequencies far from the source. The measuring equipment should be able to measure bearing vibrations as it approaches the idler and even as it passes and moves away. The next concern is measuring the bearing vibrations as the sensor moves towards and away from the idler. A conveyor test bench was built to investigate this.

2.2. Conveyor test bench

A test bench was needed to recreate a more realistic signal that would represent the vibrations associated by the bearings in an idler and the different faults found in such a bearing. At first, an actuator was considered to shake a piece of belt with an input signal that corresponded with theoretical fundamental bearing frequencies, thereafter adding bearing fault frequencies to the signal. There are numerous real-world influences that would have an effect on the vibration signal that would not be simulated by this method. A better representation of the real-world conditions was needed.

A short conveyor was designed and built. Figure 2.6 shows the test bench that was used to acquire vibration signals of different idler bearing faults. The test bench has a head pulley, drive motor, tail pulley and an idler. The 1.5 kW motor has a belt reduction to aid with the acceleration of the inertias. The motor was powered by a variable speed drive which gave great control over the start-up and operational speeds. The rotational speed for all the tests were kept constant with the variable speed drive with as little variations as possible (<5%) and confirmed with a handheld tachometer. Both the head and tail pulley has tensioners and alignment mechanisms. These mechanisms were used to tension and align the drive belt and the conveyor belt alternatively and can be seen in Figure 2.7 and Figure 2.8. The idler is easily removed by releasing the tail pulley tension – allowing the conveyor belt to be lifted. This allows the removal of the idler without having to release tension of the drive belt and having to re-align it every time a new idler condition has to be tested. The idler was positioned a bit higher than it would normally be found on a conveyor. This was done to easily apply a downwards force on the idler, simulating the effect of a payload on the conveyor. Figure 2.9 shows the idler and the belt wrap.

Figure 2.6: Test bench representation of a conveyor

The conveyor belt used on the test bench is only 200mm wide. This decision was made to keep the cost and weight of the test bench low. The test bench was designed so that the data acquisitioning equipment could be installed on top of the belt - no supporting idler underneath the conveyor. It was decided to attach the equipment on top of the belt rather than in the belt at this stage because the sensor position relative to the faulty bearing will be varied to investigate the influence of the sensor placement on the system's accuracy. Only one idler is being used to simplify the test bench and the data processing.

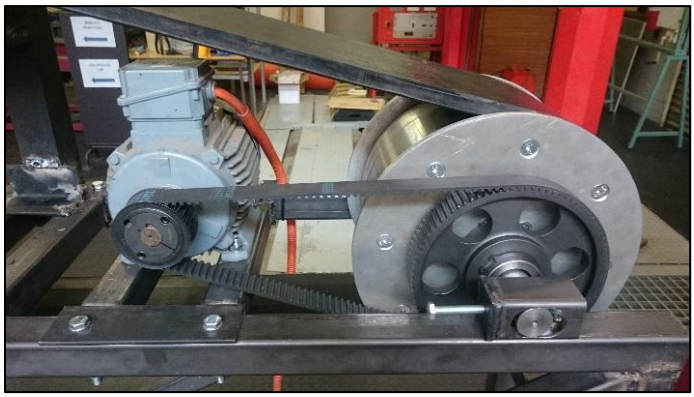

Figure 2.7: Drive pulley and motor

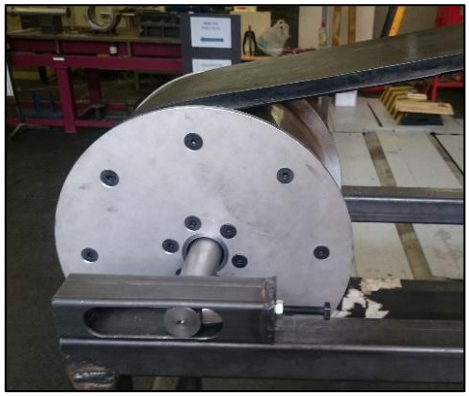

Figure 2.8: Tail pulley and tension/alignment mechanism

Figure 2.9: Idler and wrapped conveyor belt

2.3. Data acquisitioning equipment

The data acquisitioning equipment used in the earlier transmissibility tests are too large and heavy to be attached to the moving belt. The mass and size of the data logger will influence the vibration signals and the motion of the belt while the conveyor is operational. A smaller, compact data logger is needed but small, compact commercial data acquisitioning equipment are quite expensive. A DTS Slice Micro is a data logger that is very compact and has great sampling specifications that allow them to be used in applications like car crash test dummies. The downside is that the DTS Slice Micro is very expensive. The hardware is in excess of R90 000 as quoted by ESTEQ on 19 November 2015. The software is an additional cost. Using a DTS Slice Micro will not be financially feasible.

A data logger was self-developed for the purpose of measuring the vibrations of conveyor idlers. A prototype was built with a 16 MHz Arduino Micro and the sampling rates were as high as 600 Hz with 12 bit resolution up to a ± 16g range. To improve on the specifications, a new data logger was built with a Teensy 3.2 micro controller. This data logger can be seen in Figure 2.10. The Teensy 3.2 has a clock speed of 96 MHz – a big improvement on the Arduino. The data logger reached sampling frequencies of up to 1 kHz with 16 bit resolution up to a range of ±16g. The logger has a built-in anti-aliasing filter.

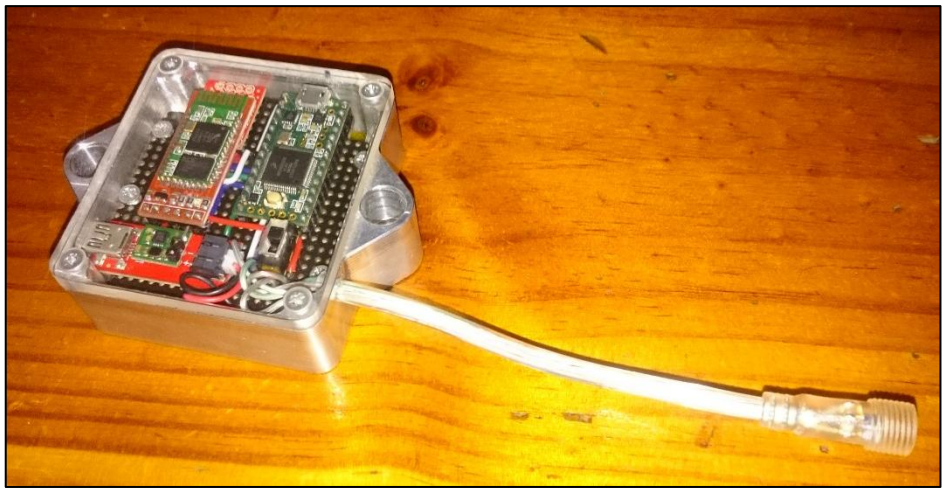

Figure 2.10: Self-developed data logger

The micro-controller is used to acquire the acceleration data from an accelerometer and to store it on an SD card and/or broadcast it over Bluetooth. The logger has an SD card module that allows the accelerometer data and timestamp to be stored on an SD micro card of up to 64 Gb. The Bluetooth capabilities allow the data to be streamed live over 10m away. The Bluetooth also allows for settings to be changed without having to connect a laptop to the logger. The filename and the acceleration range can be set and the live stream capabilities can be toggled on or off with a cell phone and a serial communication application. A sampling frequency of 1 kHz is achieved if the live stream is switched off. The settings are text based and can be changed easily with any Bluetooth enabled device. The data logger has a 2000 mAh Lithium-polymer battery built in. This enables the continuous data logging for over 50 hours. The battery can be charged with a cell phone charger. A protective aluminium case was machined to protect all the components within and a Perspex cover allows the status indication lights to still be visible. The overall cost of this data logger is under R2000. This is considerably less than the cost of a DTS Slice Micro and should be more financially feasible.

The accelerometer used is an LSM6DS33 system-package. It is a 3 degree of freedom accelerometer and a 3 degree of freedom gyroscope on a single microchip no larger than 23mm x 14mm x 2.5mm and costs less than R300. The data logger can communicate with the

accelerometer over an Inter-Integrated Circuit protocol (also called I^2C). The sensor has 16 bit resolution and can measure up to a range of ±16g at a maximum frequency of 6.6 kHz. The microcontroller and the combination of all the components and features restrict the sampling frequency to about 1 kHz. The sensor is built into a protective casing and can be seen in Figure 2.11. The data logger and the sensor connects through a 4-wire screw connector that ensures good connection but allows the two to be separated if one needs to be removed as seen in Figure 2.12

Figure 2.11: LSM6DS33 sensor encased

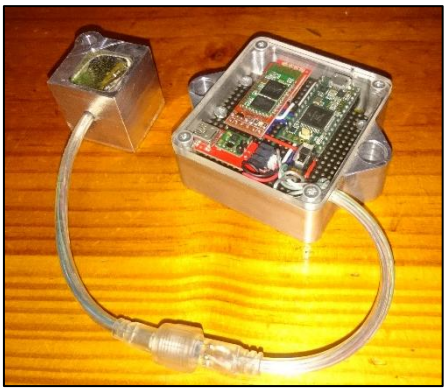

Figure 2.12: Logger and sensor connected

Figure 2.13 shows the data logger and the sensor fixed to the belt. The data logger is fixed with springs between the bolt head and the casing to accommodate the wrapping over the pulleys and idler. The sensor is bolted to the belt to ensure good connection between the sensor and the belt. The nuts have been sunk into the underside belt to ensure there are no protruding parts underneath the belt.

Figure 2.13: Data logger and sensor fixed to the belt

The current developed data logger is too large to encase in the belt and has to be fixed on top of the belt. For the test bench it is sufficient because there are no support idlers on the bottom return side. The circuit board of the data logger is on top of the battery. In the future, the data logger can be reduced in height by placing the battery next to the circuit board. This will increase the footprint, but the data logger can be encased in the belt in separate portions to accommodate for belt flex so that the circuit does not break or snap. This will enable the entire data acquisitioning system to be embedded in the belt – increasing the protection from the idlers and the payload. The data can be extracted from the SD card over Bluetooth to any device.

The self-developed data logger and sensor can be used as an alternative to expensive data acquisitioning equipment to monitor the vibrations of conveyor idlers. With some work it can be developed into an embeddable monitoring system. More detail regarding the data acquisitioning equipment can be found in Appendix A - Data acquisitioning details.

2.4. Pre-processing of sampled data

Different faults in bearings show in a frequency analysis at different frequencies. There are a few elements in an idler bearing that can fail. The inner and outer ring, or raceway, of the bearing can crack or pit and this can lead to the failure of the bearing. The rolling element, whether it's a ball or roller bearing, can pit and can cause damage to the inner and outer raceways, also leading to the failure of the bearing.

The different bearing elements, and the type of failures associated with them, correspond to different frequencies. As a fault progresses, the magnitude of the associated frequency is expected to increase. It is very difficult to identify any obvious changes or differences in the signals. Intelligent systems (or artificial intelligence as it is also known) are widely used to recognize a change in these features that might indicate a faulty idler or any other potential faults within the bearing. These intelligent systems are used seeing that, when they are trained correctly, they can be very accurate and consistent in identifying and classifying features like those associated with faulty bearings. The accelerometer data is first pre-processed to extract the bearing features to be used in the identification and classification of the bearing condition.

2.4.1. Extracting each idler's signal

The accelerometer is continuously measuring vibrations as it travels over the idler and around the pulleys. When the sensor is in the vicinity of the idler, it captures the vibrations of the bearings in the idler better than when it is at a distance from the idler. Extracting the section of the signal when the sensor is close to the idler and examining it should produce better and clearer results as discovered in the transmissibility tests of Chapter 2.1.

Figure 2.14 shows the vibration signal measured for multiple sensor passes over the idler. The sensor measures gravitational acceleration of the Earth as well and that is why the signal has a +1g offset when the sensor is on the top part of the conveyor and a -1g offset when the sensor is upside down when it is on the bottom of the conveyor. This swing between the returning and the forward passes is used as a trigger because that is when the sensor moves to the top of the conveyor and is in the proximity of the idler. A moving average is applied to the signal and a trigger value on the rising and falling edge is used to extract the portion of the signal close to the idler.

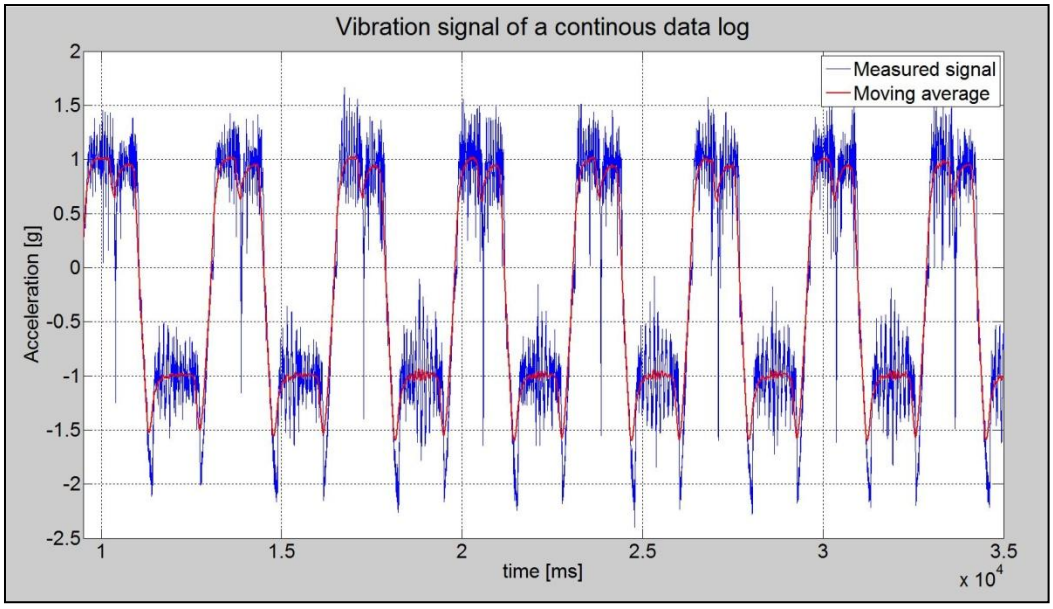

Figure 2.14: Vibration signal of multiple idler passes

Figure 2.15 shows an extracted signal of a single idler pass. With the triggers, the section of the vibration signal is extracted when the sensor is on top of the belt and close to the bearing. The signal that is used to identify the underlying bearing frequencies is extracted from halfway between the tail pulley and the idler to halfway between the idler and the driven pulley. This is done so that the bearing signal extraction is done after the dynamics between the belt and pulley have had enough time to die out and before the approaching pulley affects the signal. The extracted signal should contain the bearing vibrations with minimal inclusions of the other components in the system. This section of the vibration signal that contains the bearing signal will be used, after some pre-processing, by the artificial intelligence to identify and classify the bearing condition. Each pass of the idler will be used as a separate dataset. The large spike in the middle of the signal is caused by the sudden change in vertical direction of the sensor as it passes the idler - negative vertical acceleration.

There is a noticeable belt hop that is present between the pulleys and the idler and can be seen as the higher amplitude waves in the signal. The belt hop is included in the raw bearing signal but it is at a much higher frequency than the fundamental bearing fault frequencies (will be discussed in Chapter 3) and should not have an influence on the frequencies that is of importance for identifying the bearing conditions.

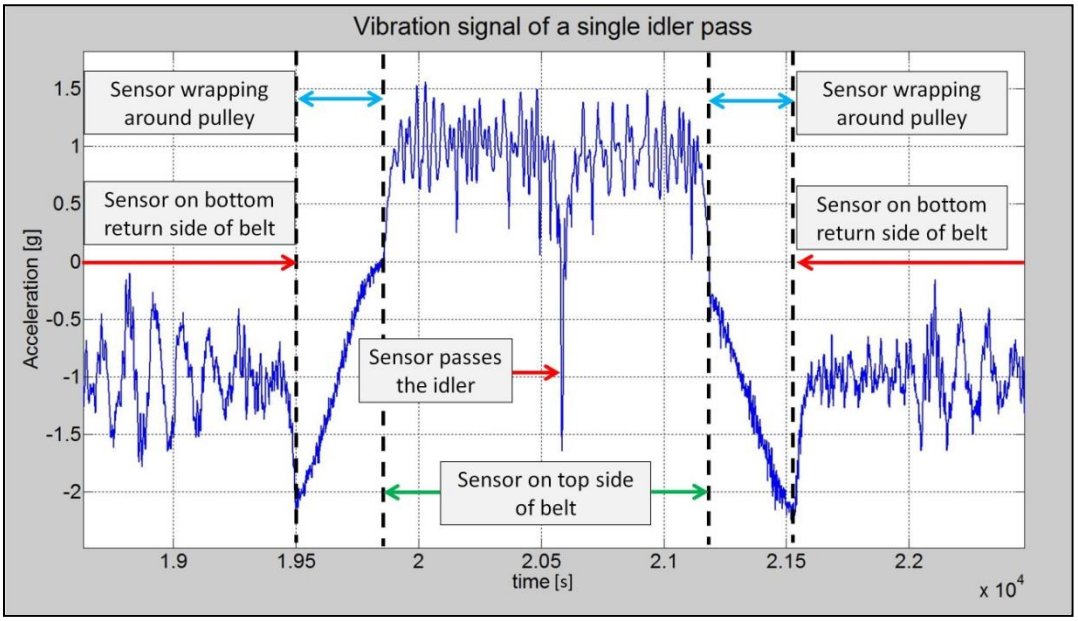

Figure 2.15: Single idler pass extract

Together with the acceleration, the timestamp of each data point is also logged. The time between each data point is not exactly the same but may differ by a few microseconds. This is caused by the microcontroller sending a request to the sensor for its acceleration data and having to wait for a response with the value. This happens hundreds of times a second and small time differences do occur. All the data sets have been sampled under, but close to, 1000 Hz. All the data sets have been resampled with software to 1024 Hz to keep it constant over the entire data range. Because all the data samples are resampled to the same frequency, they can be analyzed in the frequency domain with the same sampling frequency throughout.

2.4.2. Wavelet package decomposition and energy distributions

It is easier to identify the underlying frequencies of a time signal by using a Fourier transform (FT). With a Fourier transform of the time signal, the underlying frequencies can be identified and used to analyze the different bearing elements' health. As each idler is monitored on its own, each idler's signal needs to be analyzed on its own. A time domain localization can be used to focus on each idler individually. A short-time Fourier transform (STFT) can be used seeing that a small window of the signal is analyzed at a time with a Fourier transform. This has

a limited frequency resolution as a fixed window size is used (Ocak, et al., 2007). The window size can be changed but it is fixed for the entire signal.

A method where variable sized windows are used is called a wavelet transform (WT) and has been used, as discussed previously in Chapter 1.5.4, with success to process bearing frequencies for fault identification and classifying. This is a more flexible method for representing a signal in the time-frequency domain. Long time windows are used to get a finer low-frequency resolution and a short time window is used to get high-frequency information (Ocak, et al., 2007). Precise frequency information at both low- and high-frequencies can be obtained by using wavelet transforms, making it ideal for the analysis of irregular data patterns.

A wavelet package decomposition is performed on all the bearing time domain data sets by making use of quadrature mirror filters as low- and high-pass filters seeing that these filters have been used before with success to process bearing frequencies for fault identification and classifying (Ocak, et al., 2007). Figure 2.16 shows the high-pass and the low-pass quadrature mirror filters that are used to decompose the bearing signals into wavelets.

By applying a level 1 wavelet decomposition on the signal, two decompositions of the signal are obtained. These two decomposed signals are in the time domain, but one contains the low- and the other the high-frequency components of the signal. The low frequency component of the signal is known as the approximation (A) and the high frequency component is known as the detail (D). Figure 2.17 shows the level 1 wavelet decomposition that is done on a bearing signal.

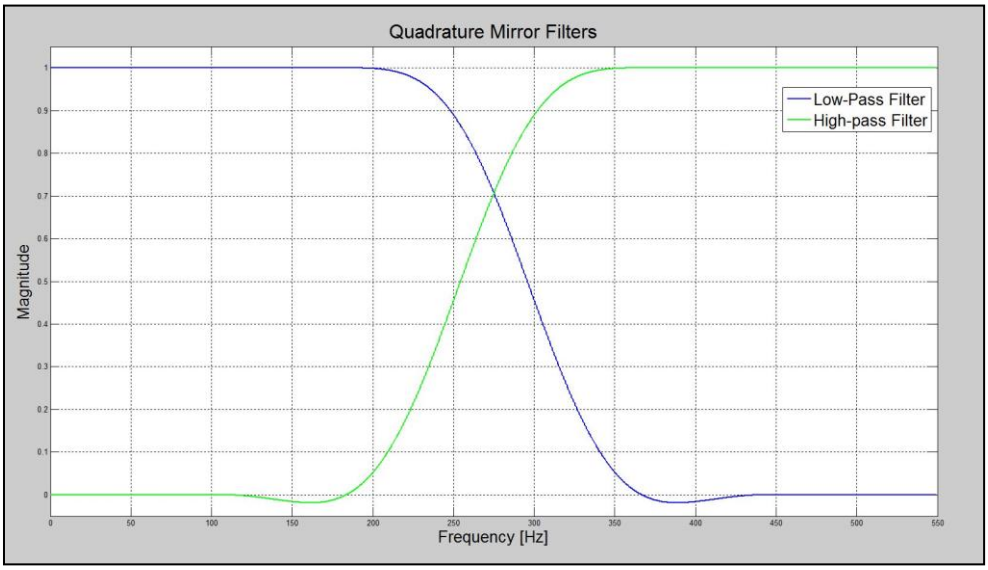

Figure 2.16: Quadrature mirror filters - First level Wavelet package decomposition

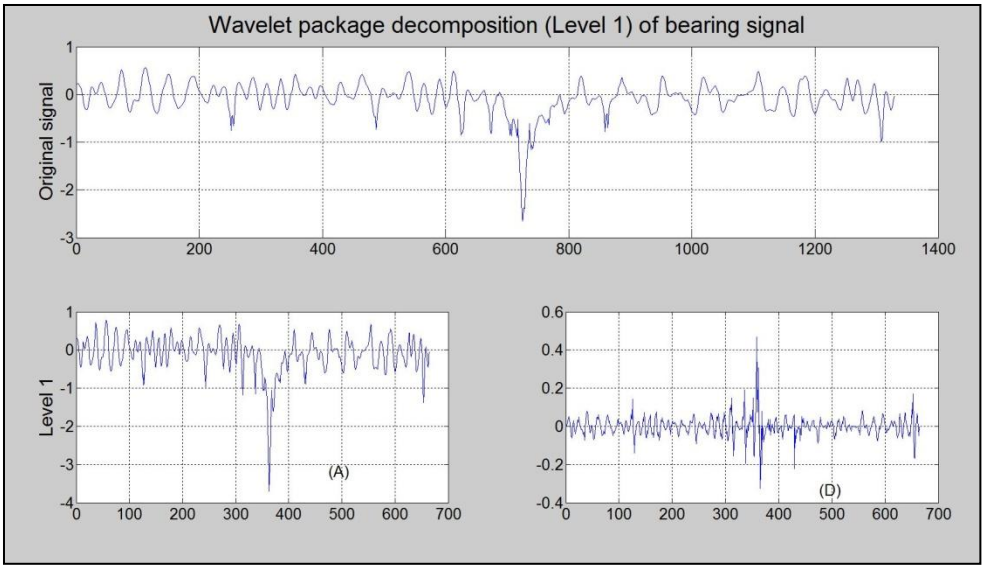

Figure 2.17: Level 1 wavelet package decomposition

A level 2 wavelet package decomposition is where the approximation (low-frequencies) and the detail (high-frequencies) signals of the first level of the decomposition is decomposed again. Now the original signal can be decomposed into four signals; approximation of the approximation (AA), detail of the approximation (DA), approximation of the detail (AD) and the detail of the detail (DD). Figure 2.18 shows the level 2 wavelet decomposition that is done on a bearing signal.

Higher level wavelet package decompositions can be done on the original signal. Figure 2.19 shows a level 3 wavelet package decomposition that is done on a bearing signal. The higher level decompositions divide the original signal into more signals that distinguish the base signal and the underlying vibration signals even better from one another.

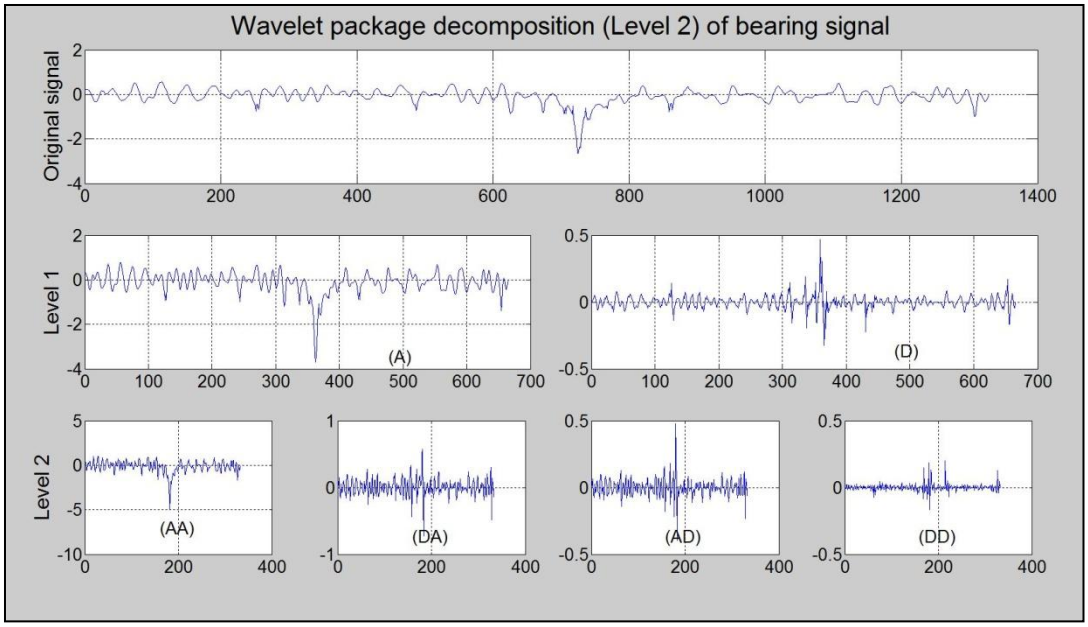

Figure 2.18: Level 2 wavelet package decomposition

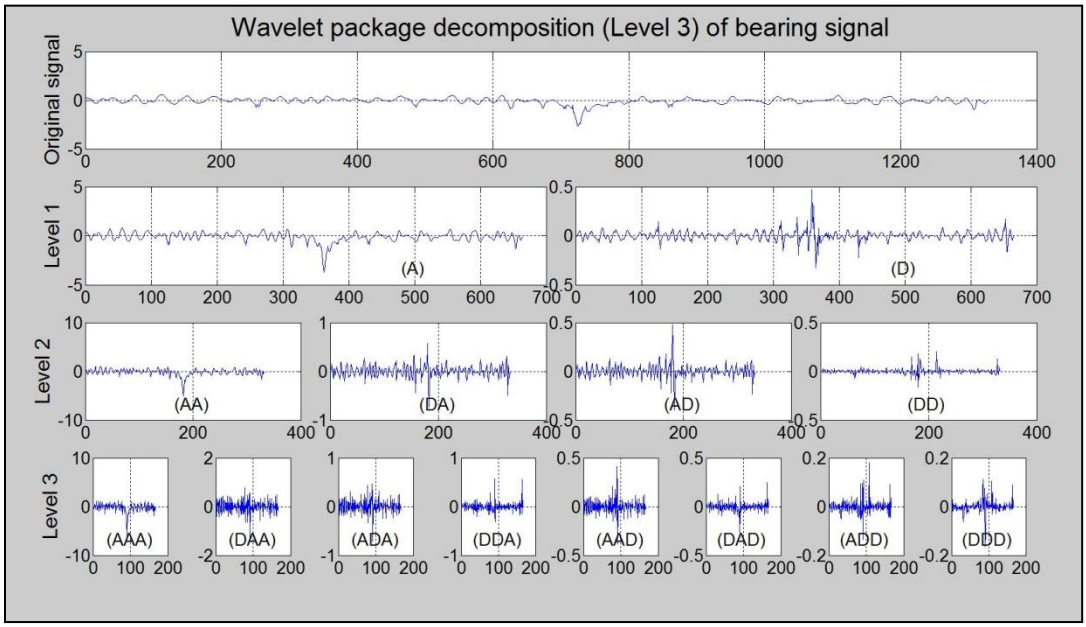

Figure 2.19: Level 3 wavelet package decomposition

If the different fundamental bearing frequencies can be captured in their own frequency bands, it should ease the process of identifying and classifying the bearing faults. For this reason, it was decided to apply a level 7 wavelet package decomposition as it should capture small signal wavelets, small enough to capture each fundamental fault frequency in its own wavelet.

A frequency analysis is done on each of the wavelets to determine the underlying frequency data. It will be difficult to use all the data points of the entire frequency spectrum of the all the wavelet packages as inputs for the intelligent system as there will simply be too much. To reduce the number of inputs to the intelligent system, an energy value representing each of the wavelets' frequency spectrums is calculated. By using the energy values of the wavelets, the number of inputs for the intelligent systems are reduced, but the energy values are still good representations of the frequency spectrum that, in essence, build up the original signal.

The energy value of a wavelet is calculated by summing the squares of the frequency magnitudes of the entire frequency spectrum. For the energy values to be better used in the intelligent system, they are non-dimensionalized by calculating each wavelet's percentage contribution to the total energy of all the wavelets. This method reduces the number of inputs needed for the intelligent system and will reduce the solving, training and testing time.

2.5. Intelligent systems used for fault identification and classification

There are many different intelligent systems to choose from, each having its own advantages and disadvantages over the other. The two main systems used in the identification and classification of errors, as in cases like the fault identification and classification in idler bearings, are neural networks (NN) or support vector machines (SVM) (Li, et al., 2013). These two classification methods are very accurate if trained well. The two systems will be compared to one another to identify the more accurate and reliable system.

2.5.1. Neural networks

Neural networks mimic the way the human brain works. Figure 2.20 show a schematic of a neural network. As seen in Figure 2.20, there are inputs to the neural network (denoted by x), and each input is connected to neurons (denoted by z), and these neurons may be connected to other neurons and eventually some neurons are connected to outputs (denoted by y). The connections are illustrated with the solid lines. In Figure 2.20, there is only one hidden level - one level of neurons between the inputs and outputs. Depending on the complexity of the neural network that one wants to use, the number of hidden levels can be increased as well as the number of neurons in each hidden level. Not all hidden levels have to have the same number of neurons (Bishop, 2006). The tendency is that each input is connected to each of the neurons in the neighbouring hidden level, and then each of those connected to each neuron in the next hidden level as seen in Figure 2.20 (Bishop, 2006). Eq. 2.2 shows how the input of each neuron in the first level, ${Z^{(1)}}_N$, is connected to each of the neural network inputs, x_i, and weighted with the first level weights ${\omega^{(1)}}_{Ni}$. The same methodology is applied in the levels that follow. Cases do exist where an input might not be connected to every neuron in the neighbouring hidden level or may even connect to a neuron in a hidden level one over. It is the weights between the inputs, neurons and outputs that are adjusted when the neural network is

trained to best predict the outputs depending on the inputs. The inputs and neurons denoted by x_o and z_o are usually constants called biases and are normally set to 1 as the weighting on each connection will adjust the magnitude of the bias (Bishop, 2006).

$$Z^{(1)}{}_{N,\ N=1\ to\ M} = \sum_{i=0}^{D} x_i \times \omega^{(1)}{}_{Ni} \qquad \text{(eq. 2.2)}$$

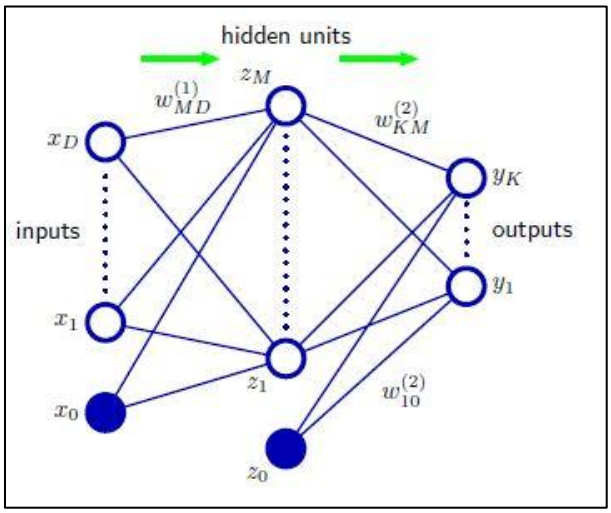

Figure 2.20: Schematic of a Neural network (Bishop, 2006)

At the neurons themselves, there is an activation function that takes the sum of the neuron's inputs and returns an output. The sum of the inputs at the neuron produces a single output through the activation function. There are several different functions that can be used as the activation function (Bishop, 2006). The form of the activation function depends on how the output of the neuron should behave depending on the value of the input.

A number of data sets are used to train and test the neural network. The data sets are divided into training sets and testing sets. The ratio is not fixed but should be chosen so that the neural network is not under or over trained. If the neural network is under trained, it might not have been exposed to all the different possible input and output combinations (insensitive) and if it is over trained, it might be too focused on one type of output that all the other possible outputs are seen as one class (over sensitive) (Bishop, 2006).

There are several ways of training a neural network. The activation function is usually kept constant throughout and that only leaves the weights of each connection that can be changed. Some neurons might be more influential on the outputs than others and their weights will be adjusted accordingly. The one way of adjusting the weights is to manually alter the weights and

analyzing the outputs and adjusting some more as needed until the success of the neural network is satisfactory. Another way is to randomize the weights and adjusting the range of the randomization algorithm until the output is satisfactory. These methods can take quite some time to find the ideal combination of weights that will take inputs and accurately estimate the outputs.

Another way of finding the weights is by a method called gradient based back propagation. Gradient based back propagation is a method where the weights are calculated automatically. Initial weights are chosen at random and the inputs are used to produce outputs based on these initial weights. The calculated outputs of the neural network are then compared to the target outputs needed for the set of inputs. The derivative of the activation function is used to calculate the outputs' dependency on the different neurons connected to it - the method is thus called gradient based. The differences between the calculated and the target outputs are then taken and the local gradient is calculated. The weights of the connections feeding into the output are then adjusted by the local gradient. The weights between hidden levels are adjusted in the same way. The more a connection's weight contributes to the error, the more it is adjusted to minimize the error of the neural network. These adjustments can be done for a set number of iterations or until a small enough error is made. It has been found that back propagation gives the greatest accuracy and numerical efficiency (Bishop, 2006). It is for this reason that a gradient based back propagation neural network will be used to identify and classify the bearing faults in the idler. Each of the non-dimensionalized energy values of the decomposed wavelets will be used as an input to the neural network and the signal will be classified based on the underlying bearing fault.

2.5.2. Support vector machines

Support vector machines are popular for solving problems in classification, regression and novelty detection (Bishop, 2006). A Support vector machine is a classifier where data sets are separated into classes. The basic support vector machine is the two-class classification problem using linear model in a 2D feature space (Bishop, 2006). The objective of a support vector machine is to classify data to certain areas. Assuming that the support vector machine is working in a 2D feature space with a linearly separable data set, the support vector machine will separate the classes of the data set with a linear line and will also maximize the distance between the line and the closest data points of either class as a constrained optimization problem (Bishop, 2006).

Figure 2.21 illustrates a data set in 2D feature space that can be separated linearly. The red line is separating the two classes and is also called the decision boundary. The margin is defined as the perpendicular distance between the decision boundary and the closest data points of both

classes. The margin is represented as the space between the blue lines in Figure 2.21. The purple circles are the data points of both classes that are closest to the decision boundary and lie on the margin. These data points are called the support vectors seeing that vectors perpendicular to the decision boundary can be drawn to each of these data points and all the vectors have the same maximum magnitude. It is these vectors that are maximized by solving the optimization problem. The rest of the data points of each class are found on either side of the margin.

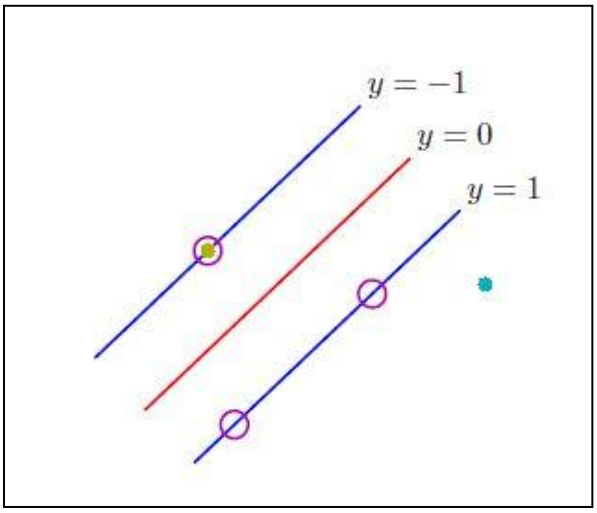

Figure 2.21: Linear separable data points in feature space
(Bishop, 2006)

It might happen that for a 2D data space, the data set cannot be separated linearly. To be able to classify these data sets, the support vector machine makes use of a non-linear kernel function that enables the data sets to be linearly separable in a non-linear feature space (Bishop, 2006). Figure 2.22 shows a data set in a 2D feature space (x-y plane) that has been classified by a non-linear kernel function. The contour lines represent values of the same height (z-direction). A kernel function has been applied to the x-y coordinates of the data set and a z-value (height) obtained for each data point. The data points can now be represented in 3D space and can be separated by a linear plane. It can be seen in Figure 2.22 that the data set is separated into two classes by a non-linear contour line. The data points marked with green circles are the support vectors.

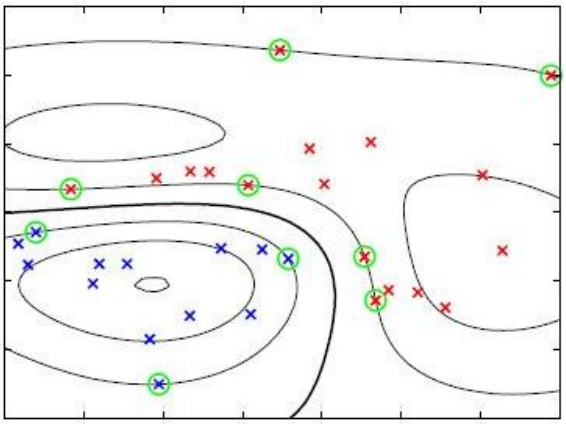

Figure 2.22: Non-linear classification of data by using a non-linear kernel function
(Bishop, 2006)

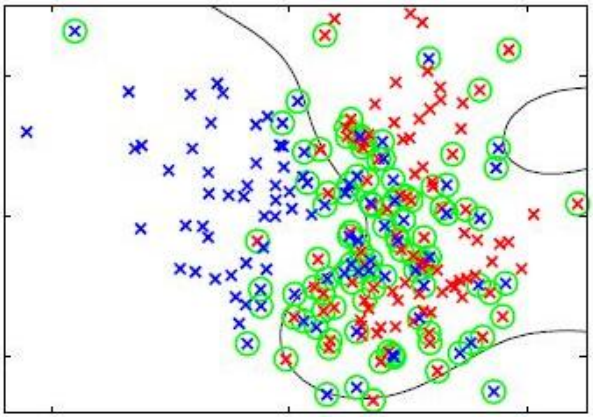

Figure 2.23: Overlapping classification to ease the optimization problem
(Bishop, 2006)

A kernel function can be of almost any form. The most common kernel functions that are used are linear, polynomial and radial based functions (Bishop, 2006). Some data sets are more accurately classified with a certain kernel function. By investigating the accuracy of the support vector machine with the different kernel functions, the more accurate kernel function for the certain case can be found. By solving the optimization problem, the different parameters of the kernel function are determined to produce the optimal function to classify the data set.

For some cases, it may be very difficult to classify a data set in 2D or even 3D. Attempts can be made to classify the data set by making use of a higher dimension kernel function but computational power needed to solve the optimization problem becomes quite high (Bishop, 2006). Rather than trying to solve a complex problem, some data points are allowed to be misclassified. A certain number of data points are allowed to be on the wrong side of the decision boundary. The optimization problem is altered to allow for data points to be on the wrong side of the decision margin and a penalty is assigned to the wrongfully classified data points depending on how far they are from the decision boundary. The optimization problem tries to solve the problem as before, but also tries to minimize the penalties by trying to fit the decision boundary as close to the wrongfully classified data points (Bishop, 2006). Figure 2.23 shows a data set in 2D feature space that has been classified but has allowed some data points to be misclassified in order to simplify the optimization problem. The data points marked with a green circle are the support vector. There are a few data points that are on the wrong side of the decision boundary.

As seen in Figure 2.23, it might be very difficult for a human being to allocate a certain data point to a specific class. The support vector machine is a great tool for accurately classifying data into classes that would otherwise be very difficult.

A data set does not have to consist of an x- and y-coordinate as depicted in Figure 2.21 to Figure 2.23. There are no limits to the dimensions that a data set can be. The higher the dimension, the more computational power may however be needed to solve the optimization problem. Each of the non-dimensionalized energy values of the decomposed wavelets will be used as an input to the support vector machine and the signal will be classified based on the underlying bearing fault.

2.6. Conclusion of small-scale test and data pre-processing

It has been found that vibrations can be accurately measured through the conveyor belt up to a certain distance from the source. The transmissibility of the vibrations is very good for a fair distance from the idler over a fairly wide frequency range - up to 400 Hz. The use of wavelet package decomposition, for data pre-processing, will extract the features of the underlying bearing fault of the idler and ease the process of classification when used in an intelligent system. The use of wavelet package decomposition and assigning energy values to each wavelet has been successful in previous investigations of faulty idlers. The same method of data pre-processing, feature extraction and intelligent systems should, if trained well, help in idler bearing fault identification and classification even if the sensor is mounted on top of the belt and moving over the idler. Gradient based back propagation neural networks and different support vector machines will be used to identify and classify faulty idler bearings seeing that these intelligent systems have been used before with great success in similar investigations. Each of the non-dimensionalized energy values of the decomposed wavelets will be used as an input to the intelligent system and the bearing signal will be classified based on the underlying bearing fault.

Chapter 3 - Conveyor belt tests and results

A bearing has three main fundamental frequencies: the inner-, outer- and rolling element fundamental frequency. There are numerous ways in which a bearing can fail and these different faults can present themselves at the fundamental frequencies within the bearing. These changes in the frequency spectrum are widely used to identify faults in bearings and other mechanical equipment. There are a number of components in a bearing that can fail, each having a different outcome on the frequency spectrum, and for this reason, different bearing fault cases will be tested on the conveyor test bench. There will be five bearing conditions tested:

- Healthy bearing. Seeing that there are idlers that have no bearing faults, it is also important to include this as one of the bearing conditions. This also serves as a baseline to compare the faulty bearing signals to. Knowing what the baseline is can help to identify the deviations of faulty bearings and these deviations can be used to better identify and classify faults.
- Outer raceway. Pits forming in the surfaces of bearing raceways are very common bearing faults that occur and can lead to bearing failure. Seeing that pitting is a very common bearing fault, a pit is formed in the outer raceway of the bearing with a Dremmel and the pit can be seen in Figure 3.1.
- Inner raceway. A similar pit is formed in the inner raceway with a Dremmel for the same reason as the outer raceway and the pit can be seen in Figure 3.2.
- Rolling element. A small pit is created on the surface of the rolling element. These pits, although small, also impact the raceways and can lead to similar failure. Figure 3.3 shows a small pit created on the rolling element.
- Contamination: Bearings do become contaminated with dust and dirt and this contamination can lead to the acceleration of bearing failure. When failing bearings are replaced, it will be beneficial to know which bearings, although not damaged yet, are contaminated. Contaminated bearings may not show significant signs of failure, but one may want to replace them as a preventative measure. For this reason, bearings are contaminated with fine sand as well and are tested in the hope that they may also be identified and classified.

The geometry of a bearing has an influence on the frequency at which the rolling elements passes certain points on the inner and outer raceways. The bearings used in the idlers are NIS 6205 deep groove ball bearings. The various geometry properties of the bearing that are needed to calculate the fundamental fault frequencies are listed in Table 3.1. The idler's rotational speed is kept constant throughout the tests with as little variations as possible with a tachometer at 311 RPM. This relates to a rotational frequency of 5.183 Hz and is also tabulated.

Figure 3.1: Outer raceway defect

Figure 3.2: Inner raceway defect

Figure 3.3: Rolling element defect

Table 3.1: NIS6205 deep groove bearing properties

Pitch diameter	D	38.5 mm
Rolling element diameter	d	7.94 mm
Contact angle	θ	20°
Number of rolling elements	Z	9
Idler rotational speed		311 RPM
Idler rotational frequency	f_s	5.183 Hz

With the idler shaft being stationary, the bearings inner raceway will also be stationary and suitable equations are needed to calculate the different fundamental fault frequencies. Assuming no slip between the rolling element and the raceways, the rolling element contact on a rotating outer raceway frequency, f_{outer} for short, at which a defect on the outer raceway is passed by a rolling element is calculated by equation 3.1 (Norton & Karczub, 2003). The rolling element pass on a fixed inner raceway frequency, f_{inner} for short, at which a defect on the inner raceway is passed by a rolling element is calculated by equation 3.2 (Norton & Karczub, 2003). The rolling element spin frequency, or f_{roll} for short, is the frequency at which a defect on the rolling element passes the inner and outer raceways and is calculated by equation 3.3 (Norton & Karczub, 2003).

$$f_{outer} = Zf_s\left[1 - 0.5\left(1 + \frac{d}{D}\cos(\theta)\right)\right] \quad \text{(eq. 3.1)}$$

$$f_{inner} = \frac{Zf_s}{2}\left[1 + \frac{d}{D}\cos(\theta)\right] \quad \text{(eq. 3.2)}$$

$$f_{roll} = f_s\left(\frac{D}{d}\right)\left[1 - \left(\frac{d}{D}\cos(\theta)\right)^2\right] \quad \text{(eq. 3.3)}$$

The fundamental fault frequencies are calculated and tabulated in Table 3.2. These frequencies are the rates at which a reference point, or defect, on different bearing elements are in contact with one another. These frequencies are expected to appear in a frequency analysis of the bearing signals when investigating different bearing conditions with different induced bearing faults. These frequencies have no relation to the resonant frequencies of the different bearing components.

Table 3.2: Bearing fundamental fault frequencies

f_{outer}	18.97 Hz
f_{inner}	27.68 Hz
f_{roll}	48.51 Hz

The transmissibility of vibrations through the conveyor belt was tested in Chapter 2.1 for a frequency range of 0 to 1000 Hz. This was done to investigate a large spectrum of frequencies as the fundamental bearing frequencies were not known yet. Now that the fundamental bearing frequencies are known, it can be seen that the frequency range is substantially smaller than the range tested in the transmissibility investigation. From the transmissibility tests it can be seen that the bearing frequencies should be transmitted clear enough to capture and represent the actual underlying frequencies accurately when test on the conveyor belt is done.

As discussed in Chapter 2.3, the sampling frequency of the data logger is in the region of 1 kHz. This sampling frequency is higher than needed for capturing the fundamental bearing frequencies but it can still capture high frequency noise and harmonics if they should appear. The sampling frequency of this self developed data acquisitioning system is in the region of 1 kHz but will capture the fundamental fault frequencies that should be lower than 50 Hz.

The failure mechanism that is of interest is physical defects on the inner and outer raceway as well as the rolling element and the geometry and operational speed have an influence on the fundamental bearing fault frequencies. These frequencies are very low and would be captured clearly with a sampling frequency of 100 Hz.

The experiment (Li, et al., 2013) conducted by the School of Mechanical and Electrical Engineering of the China University of Mining and Technology as mentioned in Chapter 1.4.4. was first replicated to some extent. The idler vibrations were measured on the stationary shaft of the idler and the data acquisitioning equipment was also stationary while the conveyor test bench was in operation. This was done to compare the measured data of the bearing vibrations to the calculated fundamental frequencies to ensure that the data acquisitioning equipment captured the bearing vibrations and did it accurately.

3.1. Vibrations measured on the stationary supporting structure

As discussed in Section 1.5.4. vibrations have been used with success to identify bearing faults in conveyor idlers and monitor them. Before the accelerometer was fixed to the moving belt, the same investigation was done to ensure the equipment, pre-processing and intelligent systems worked and was as accurate as the current monitoring done on the supporting structure. This was also done to validate if the measured frequencies corresponded to the calculated fundamental frequencies. The accelerometer was fixed to the shaft of the idler with a bolt and some wax in between to help with vibration transmission. Figure 3.4 shows the accelerometer bolted to the shaft of the idler. The sensor was attached near the faulty bearing and measured the vibrations in the vertical direction.

Figure 3.4: Accelerometer attached to idler shaft

The bearing in the idler nearest to the accelerometer was interchanged with different bearings, each with an artificially induced fault. The healthy bearing was compared to a bearing with an inner raceway defect, an outer raceway defect, a rolling element defect and a bearing that was contaminated with sand and dirt. A number of datasets were measured of the healthy bearing installed in the idler and then the bearing was removed and replaced by one of the faulty idlers and more measurements were done until a large number of datasets were obtained for each of the different bearing conditions.

3.1.1. Signal analysis

The inner raceway was fixed, and a belt speed of 1 m/s was maintained with as little variations as possible throughout the test with the use of a variable speed drive. The idler speed was monitored as well with a hand-held tachometer. Figure 3.5 shows the fast Fourier transform, or FFT, of a vibration signal measured with the accelerometer when both bearings in the idler were healthy. The three fundamental frequencies are also indicated on the figure. The fundamental frequency produced by the outer raceway was calculated to be 18.97 Hz and was measured on the FFT to be 18.63 Hz, a 1.8% difference. The fundamental frequency that corresponded to the inner raceway was calculated as 27.68 Hz and was measured at 26.79 Hz, a 3.2% difference. The fundamental frequency of the rolling element was calculated as 48.51 Hz and was measured at 47.63 Hz, a 1.8% difference. From this, it can be seen that the accelerometer measured vibration signals produced by the bearing that corresponded to the calculated fundamental frequencies. A total of 16 vibration signals were measured of a healthy bearing in the idler.

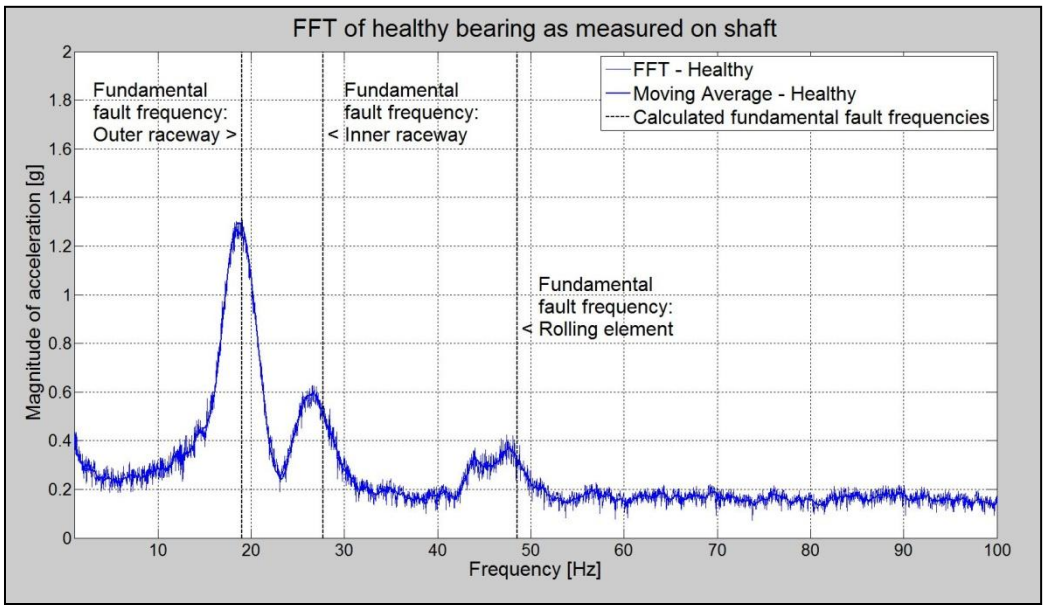

Figure 3.5: FFT of healthy bearing measured on the shaft

A bearing with an inner raceway defect was installed into the idler and the accelerometer fixed to the shaft closest to the faulty bearing. Figure 3.6 shows the FFT comparison of the healthy bearing and the bearing with an inner raceway fault. The moving average of the FFT is also used and is also shown. Only five data points before and five data points after were used in the calculation of the moving average as it still kept the general shape of the frequency spectrum.

As the rolling element impacted the inner race fault, it increased the magnitude of the inner raceway fundamental frequency in the frequency spectrum - it impacted the fault at that specific frequency. A total of 12 datasets were measured on the shaft of the idler when a bearing with an inner raceway defect was installed.

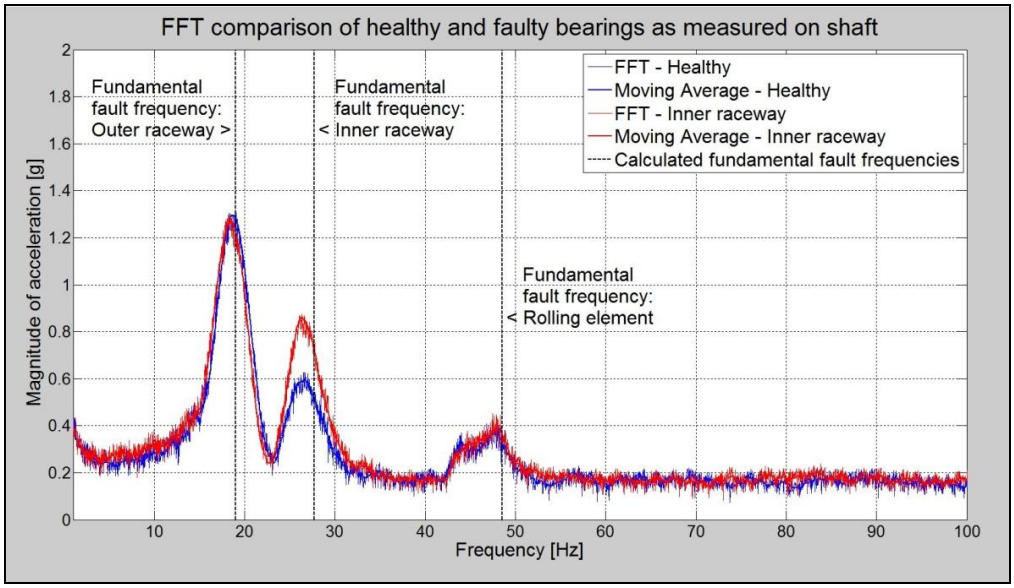

Figure 3.6: FFT of an inner raceway fault as measured on the shaft

A bearing with an outer raceway defect was installed into the idler where the previous faulty bearing was. The accelerometer was fixed to the shaft closest to the faulty bearing. Figure 3.7 shows the FFT comparison of the healthy bearing and the bearing with an outer raceway fault. The moving averages of the FFTs are also used and are also shown. The same moving average was used throughout all the tests; only five data points before and five data points after were used in the calculation of the moving average.

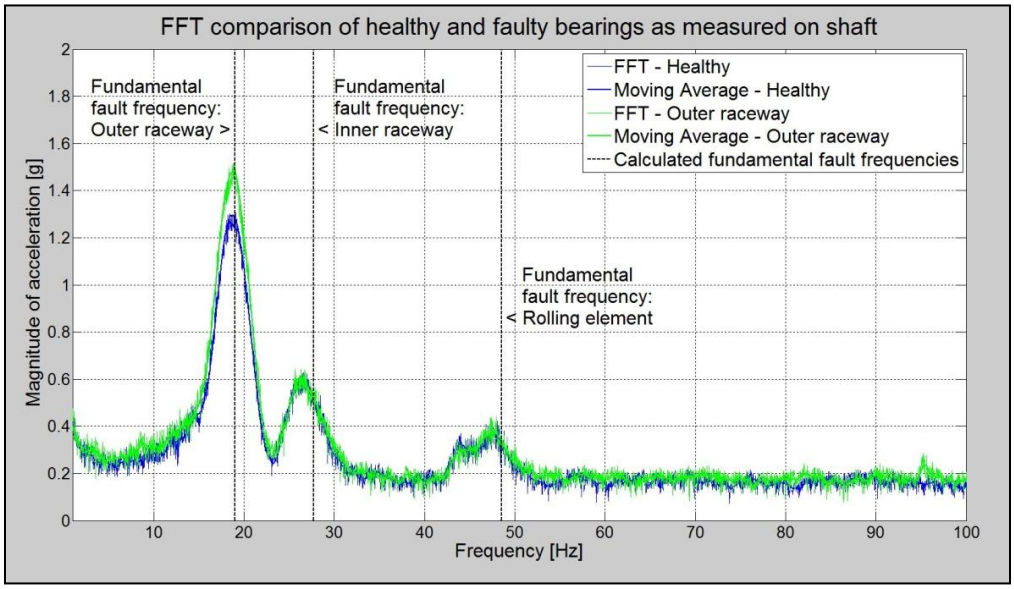

Figure 3.7: FFT of an outer raceway fault as measured on the shaft

As expected from the analysis of the inner raceway fault, there was an increase in the magnitude of the outer raceway fundamental frequency in the frequency spectrum. Just as with the case where the inner raceway defect was introduced, only the magnitude of the frequency corresponding to the fault in the bearing increased significantly. This increase can be coupled to the impact of the rolling elements on the bearing fault at the corresponding rate. The measured fundamental frequencies of the signals still corresponded to the calculated fault frequencies with very little error. A total of 14 datasets were measured on the shaft of the idler when a bearing with an outer raceway defect was installed.

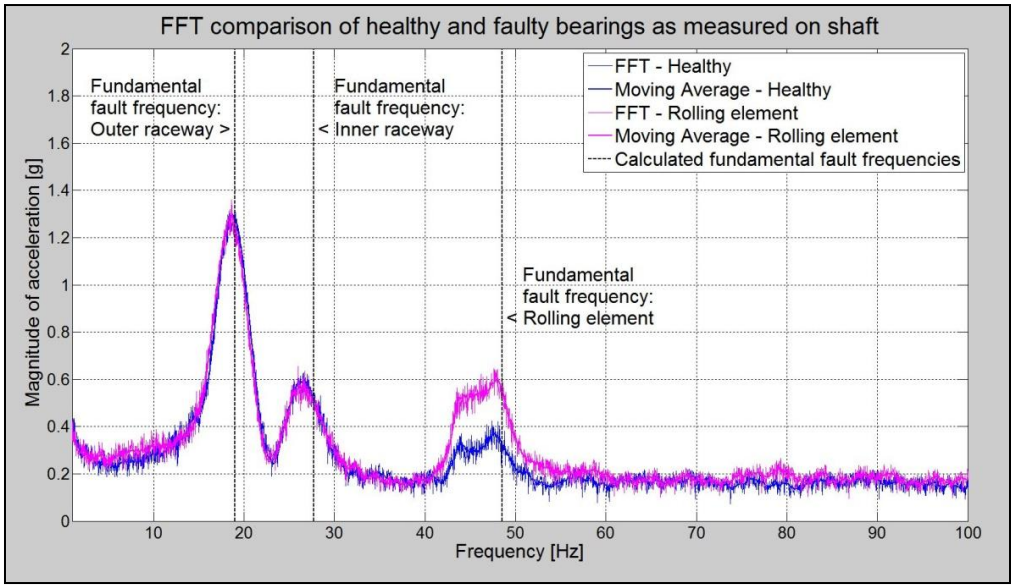

Figure 3.8: FFT of a rolling element fault as measured on the shaft

A bearing with a rolling element defect was installed into the idler where the previous bearing with the outer raceway fault was installed. The accelerometer was fixed to the shaft closest to the faulty bearing. Figure 3.8 shows the FFT comparison of the healthy bearing and the bearing with a rolling element fault. The moving averages of the FFTs are also used and are also shown.

A substantial increase in the magnitude of the rolling element fundamental frequency could be seen. The region where the rolling element's fundamental frequency was calculated to be, had a wider range of frequencies present compared to the inner and outer raceway fundamental frequencies, which had prominent peaks. The peak with the highest magnitude in the region near the calculated rolling element fundamental frequency, had a frequency that corresponded to that of the calculated fundamental frequency. The other frequencies present in this region had a lower frequency than that of the rolling element fundamental frequency, indicating that there might have been a small amount slippage between the rolling element and the raceways - slightly slower rotational speed of the rolling element.

The impact of the defect on the rolling element with the inner and outer raceway increased the magnitude of the rolling element fundamental frequency. These cyclic impacts between the rolling element and the two raceways increased the magnitude of the rolling element fundamental frequency and this can clearly be seen in Figure 3.8. A total of 16 datasets were measured on the shaft of the idler when a bearing with a rolling element defect was installed.

A contaminated bearing was installed into the idler where the previous bearing with the rolling element fault was installed. The accelerometer was fixed to the shaft closest to the faulty bearing. Figure 3.9 shows the FFT comparison of the healthy bearing and the contaminated bearing. The moving averages of the FFTs are also used and are also shown.

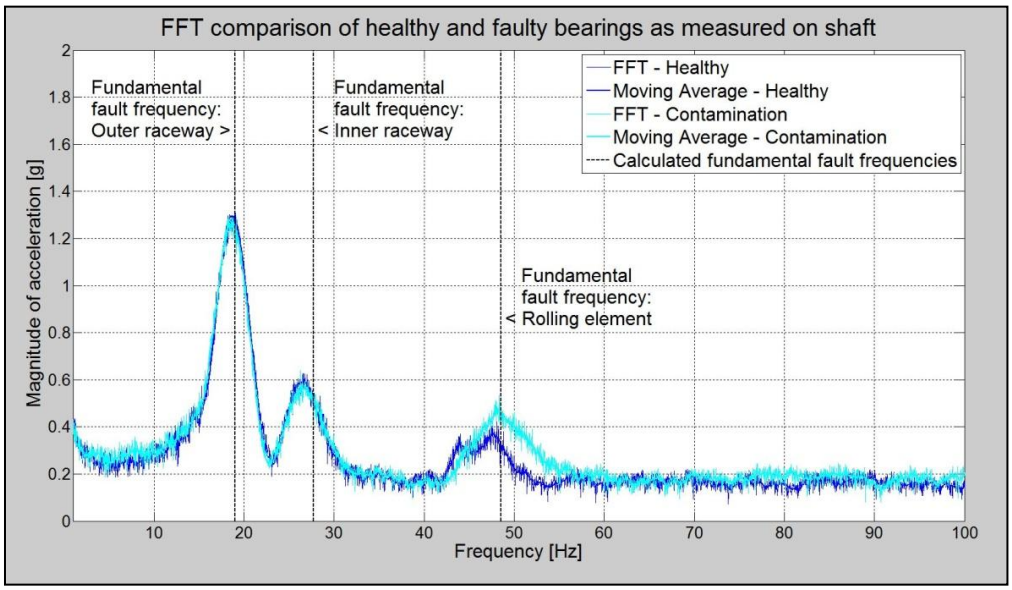

Figure 3.9: FFT of a contaminated bearing as measured on the shaft

The FFT of the contaminated bearing shows a prominent peak at the calculated rolling element fundamental frequency. Some of the contaminating particles in the bearing were caught between the rolling element and the raceways, causing small impacts as the rolling element passed over them and could be heard as the test bench was operational. There may have been more than one particle rolled over in a single rotation of the rolling element, increasing the rate at which these impacts occurred. This was observed as if there were more than one defect on the rolling element. The frequency range in which these impacts occurred was larger than that of the bearing with only one rolling element fault. The amplitude of the rolling element fundamental frequency in the presence of contaminants was not as high as when an actual defect was present on the rolling element. The defect was larger than the contaminants' size. A total of 14 datasets were measured on the shaft of the idler when a contaminated bearing was installed.

The signals shown in this section were of single datasets used to illustrate the differences between the signals of different bearing conditions. A total of 72 different bearing fault signals were measured and captured on the shaft. Of the 72 signals captured, 36 were used to train the intelligent systems and 36 were used to test their accuracy. Figure 3.10 shows a typical moving average of each of the five different bearing conditions to illustrate all the differences between the different signals. Each bearing condition has a unique frequency spectrum and it is these differences that were used to distinguish the one condition from the other. Although only one signal is shown per bearing fault, 72 data sets were obtained for this case of which half (36) were used for training and the other half were used to test the identification and classification process. The number of test sets are tabulated in each case's results table.

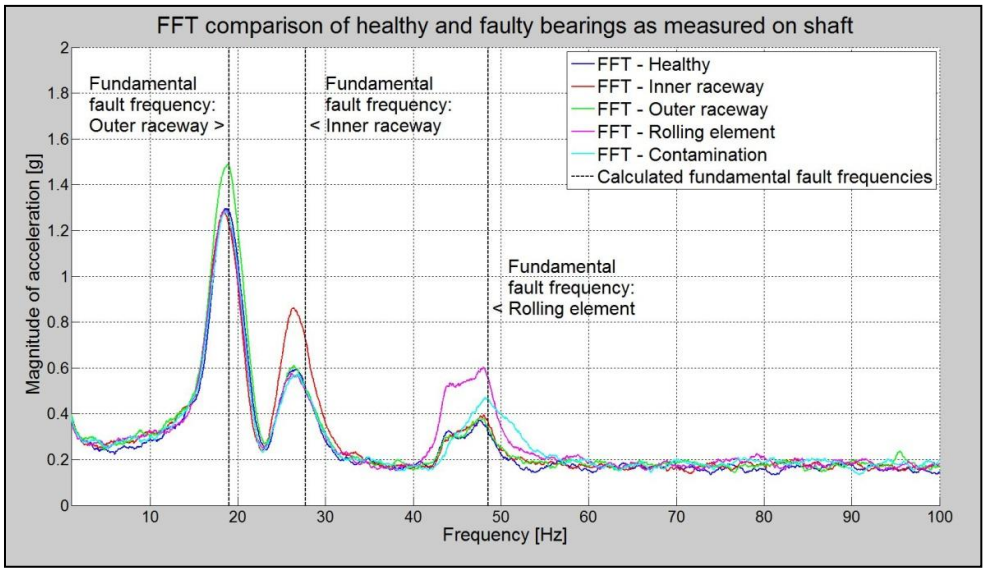

Figure 3.10: Moving averages of the different bearing conditions as measured on the shaft

A level seven WPD was applied to each signal of all the different bearing condition. A level seven WPD was chosen because it had very good resolution - divided the signals into small enough sections so that each defect could be placed in its own pair of wavelets but still resembled the original signal. The level 7 WPD, in essence, divided the frequency spectrum into 2^7 frequency bands and an energy value for each band was then calculated as discussed in Chapter 2.4.2.

To normalize the energy levels of the wavelets, the percentage contribution of each wavelet of the signal was used and is shown in Figure 3.11. The different energy distributions were used to identify and classify the bearing faults with an intelligent system. Only the first 13 levels are shown seeing that the remaining energy bands are very small in comparison to the low-frequency bands. It can be seen that some frequency bands are dominated by the fundamental frequency that is present within that frequency range.

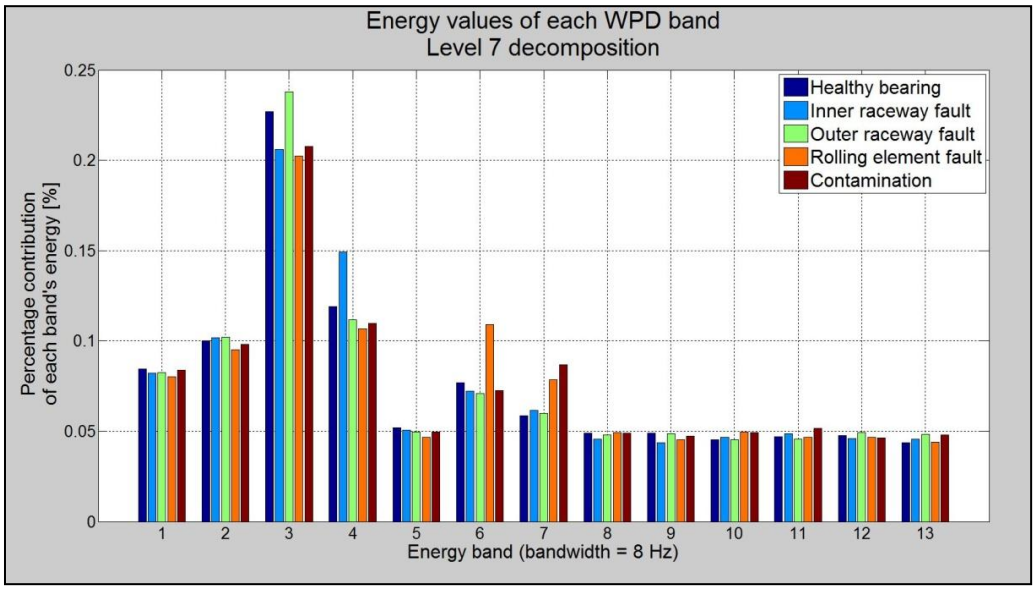

Figure 3.11: WPD of the different bearing defects as measured on the shaft

3.1.2. Identification and classification of the bearing faults

Neural networks and support vector machines are very popular intelligent systems used to classify datasets, even those of different bearing faults. Both of these systems were used to identify and classify the different bearing faults measured on the shaft.

Vibration measurements were taken of the five bearing conditions. All these measurements were pre-processed as discussed in Chapter 2.4.2. Each bearing condition's datasets were divided into two equal parts, one for training and the other for testing the intelligent system.

The gradient based back propagation neural network was trained and tested as discussed in Chapter 2.5.1. The 36 training datasets were first used to train the neural network to distinguish a healthy bearing from a faulty one, regardless of the fault. It was found that the neural network had a 100% accuracy (36 of 36 testing datasets) when it had to distinguish a healthy bearing from a faulty bearing. The neural network was then retrained to not only distinguish a healthy bearing from a faulty bearing, but also classify the type of fault when a faulty bearing was detected as either an inner raceway, outer raceway or a rolling element fault or a contaminated bearing. The retrained neural network had a 100% accuracy (36 of 36 datasets) when it had to identify a faulty bearing and had to classify the fault if one was found.

Figure 3.12 shows the five different classes and the classified datasets. The green markers indicate the datasets that were classified correctly. Note that the output of a neural network isn't a definite value that corresponds to a class value, but rather a value that, when within a range from a specified class value, can be associated with that class. Table 3.3 shows the statistics of the neural network classification.

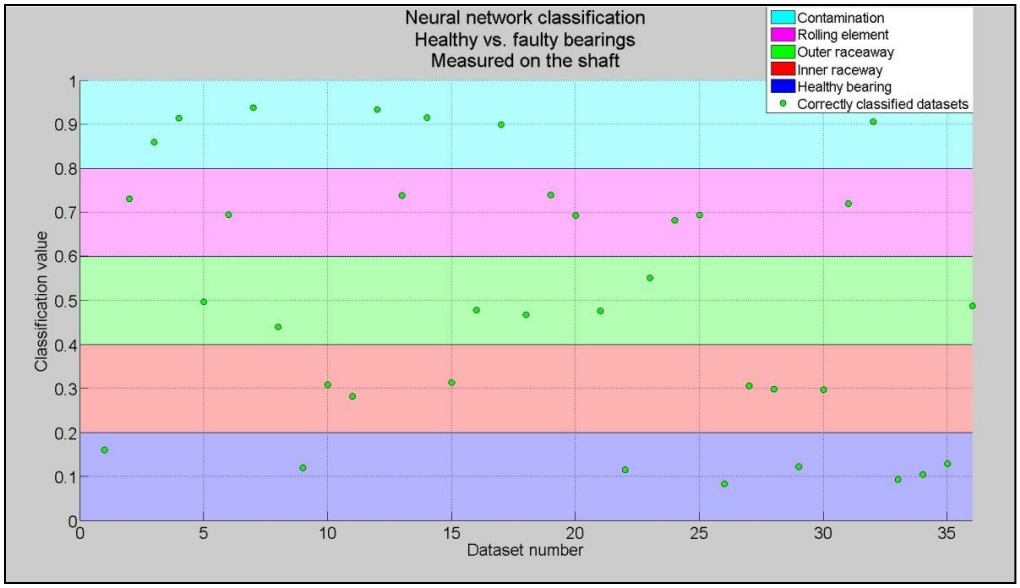

Figure 3.12: Five-class Neural network classification measured on the shaft

Table 3.3: Neural network accuracy when measured on the shaft

Neural network classification of faulty bearings as measured on the shaft			
Bearing condition	Number of datasets	Correctly classified	Accuracy
Healthy bearing	8	8	100.00%
Inner raceway	6	6	100.00%
Outer raceway	7	7	100.00%
Rolling element	8	8	100.00%
Contaminated bearing	7	7	100.00%
Total	36	36	100.00%

The same datasets were used to train and test the support vector machine as discussed in Chapter 2.5.2. A radial base function was used and with a grid search, a cost value of 3.4953×10^{2} and a gamma value of 7.4623×10^{-7} produced the highest accuracy. The support vector machine did not only classify the datasets into the two classes of healthy and faulty, but classified all the different faults with 100% accuracy (36 of 36 test datasets). A single support vector machine classified a dataset into any of the five bearing conditions; healthy bearing, inner raceway defect, outer raceway defect, rolling element defect or contaminated bearing. Figure 3.13 shows the five different classes and the classified datasets. Table 3.4 shows the statistics of the support vector machine classification. The output of the support vector machine is distinct class values.

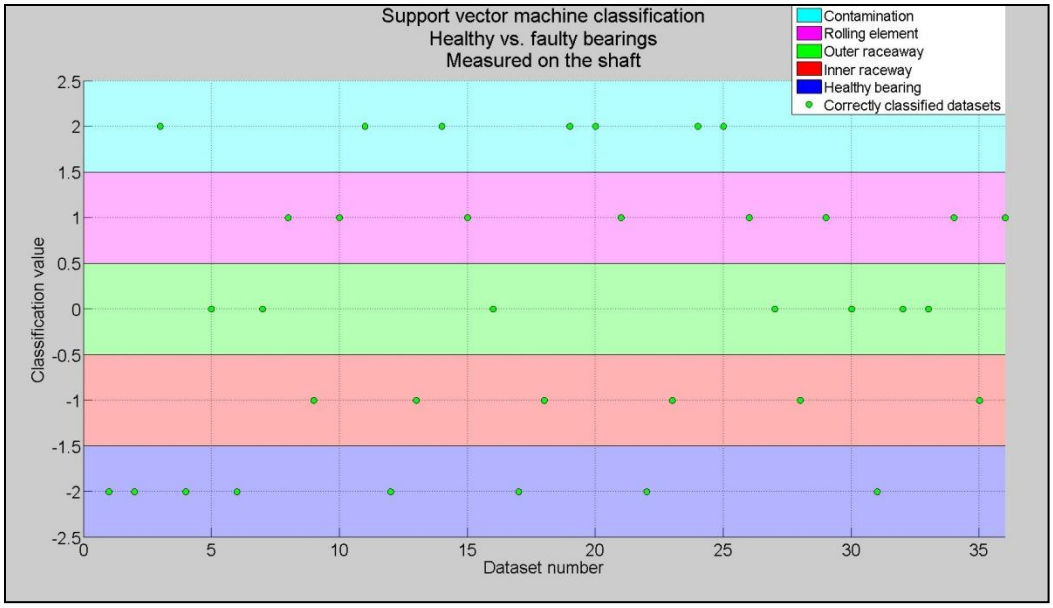

Figure 3.13: Five-class Support vector machine classification as measured at the shaft

Table 3.4: Support vector machine accuracy when measured on the shaft

SVM classification of faulty bearings as measured on the shaft			
Bearing condition	Number of datasets	Correctly classified	Accuracy
Healthy bearing	8	8	100.00%
Inner raceway	6	6	100.00%
Outer raceway	7	7	100.00%
Rolling element	8	8	100.00%
Contaminated bearing	7	7	100.00%
Total	36	36	100.00%

3.1.3. Conclusion

The geometry and physical properties of the bearing, together with the operating speeds and conditions, has an influence on the different fundamental frequencies of the bearing. Different component faults in a bearing effects the different fundamental frequency corresponding to the specific bearing fault. An increase in the magnitude of the frequency in the frequency spectrum was noted. It was these noticeable changes to the different fundamental frequencies that enabled an intelligent system to identify a faulty bearing and distinguish one bearing fault from the other.

The investigation conducted by the School of Mechanical and Electrical Engineering of the China University of Mining and Technology was successfully recreated on the conveyor test bench. The test bench was smaller than the conveyor used in their investigation, and this might have contributed to the high intelligent system accuracies obtained, but it was confirmed that idler bearing faults can be identified and classified with success. The identification and classification was successfully done by implementing wavelet package decomposition on the vibration signals. The energy contributions of each wavelet were used to train and test a neural network and a support vector machine with great success. Both the gradient based back propagation neural network and the support vector machine, that used a radial base function, were able to identify and classify a bearing fault with 100% accuracy when the vibrations were measured on the stationary shaft of the idler.

The fundamental frequencies of the signals, as measured on the shaft of the idler, corresponded to the calculated fundamental bearing frequencies with minimal errors. From these tests it could be seen that the self developed data acquisitioning equipment captured the fundamental frequencies of the bearing accurately and that the sampling frequency was sufficient to capture the needed detail of the signals. The equipment can now be used with confidence on the conveyor belt to measure the vibrations of the idler bearings.

The measuring of the bearing vibrations of the different bearing conditions also provided insight into what changes to the fundamental frequencies are to be expected depending on the bearing faults present. The knowledge of the fundamental frequencies, and how they respond to different faults, will help in the understanding, interpretation and comparison of the frequency responses obtained from measuring idler vibrations on the moving conveyor belt.

3.2. Measuring vibrations on the moving belt

Measuring the idler vibration on the supporting structure confirmed the range where the calculated fundamental frequencies were expected to be measured.

In practice, there might be more than one idler on the same supporting structure. Troughs are widely used to keep the payload on or in the centre of the belt to reduce spillage as discussed in Chapter 1.3.3. These troughs are usually made by placing three idlers side by side as seen in Figure 3.14.

Figure 3.14: Trough made with idlers

On the top side of the conveyor, there are a total of three idlers per supporting structure, thus six bearings in total. Rather than placing a sensor at each bearing, one or two sensors would be ideal to keep costs down. On the conveyor test bench, the sensor was placed on three different positions to investigate the number of sensors that might be needed to monitor a conveyor in full.

The sensor was placed on three different positions across the width of the belt. The first position was almost directly above the faulty bearing. If the faulty bearing could only be identified and classified at this position, and not at the others, a sensor would be needed for every bearing across the width of the belt. This position can be seen in Figure 3.15 as the "Near position".

The second position was in the middle of the belt. If the faulty bearing could be identified and classified from this position, it was assumed that only one sensor per idler was needed across the width of the belt. This position can be seen in Figure 3.15 as the "Middle position".

The third position was almost directly above the healthy bearing. This was the furthest the sensor could be placed from the faulty bearing on the belt of the test bench. If the faulty bearing could be identified and classified at this position, the number of sensors needed could be reduced to having a common sensor between two idlers.

As with the case of having three idlers creating a trough, there could be a possibility of only having two sensors across the width of the belt. This position can be seen in Figure 3.15 as the "Far position".

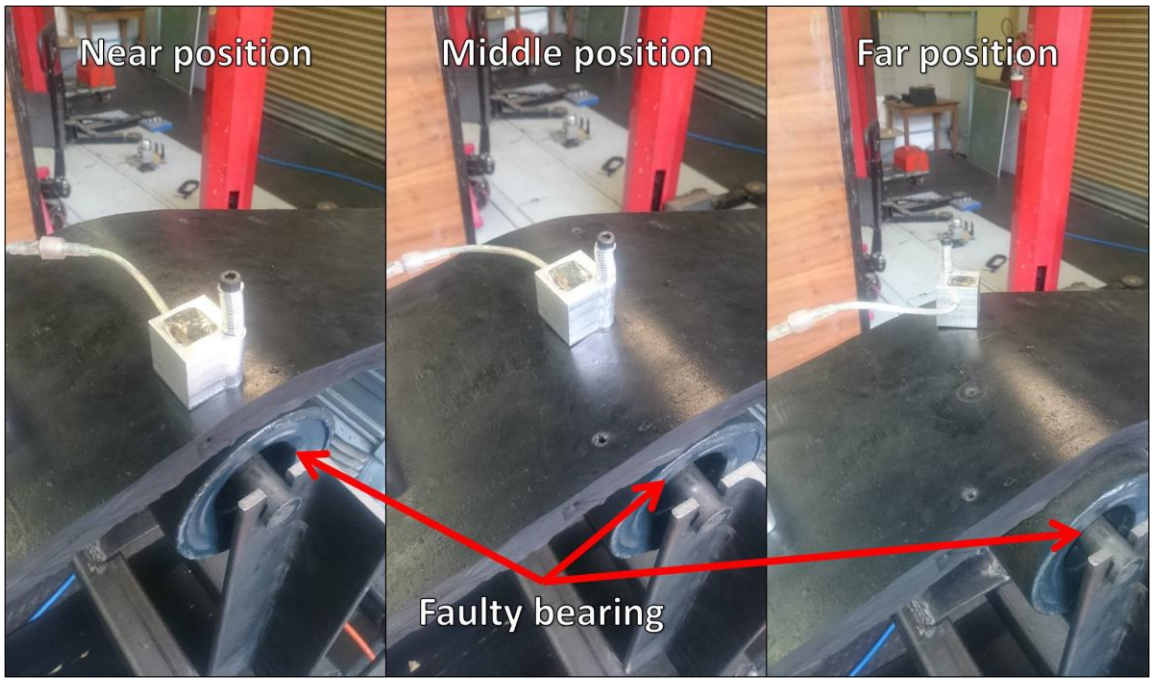

Figure 3.15: Different sensor positions on the belt

3.2.1. Measuring near the faulty bearing

3.2.1.1. The different bearing conditions and faults

The different bearing faults were investigated first by attaching the sensor to the belt close to the faulty bearing. The vibrations of the healthy bearing were measured first. Figure 3.16 shows the FFT of the healthy bearing signal. The moving average of the FFT is also used and is also shown. A simple moving average was used throughout the tests. Only five points before and five points after were used to eliminate most of the noise but still kept the general shape of the frequency spectrum.

As discussed in Chapter 3.1, there were three distinct frequency regions seen on the frequency spectrum. The first, and lowest frequency that was observed corresponded to the outer raceway fundamental frequency. The second frequency was that of the inner raceway fundamental frequency. These two fundamental frequencies were easily observed on the FFT and the moving average. The rolling element's fundamental frequency could be seen in the FFT but was not as prominent as the other two fundamental frequencies. The deviations in the faulty bearings' fundamental frequencies, from that of the healthy bearing, would be used to identify and classify the bearing faults.

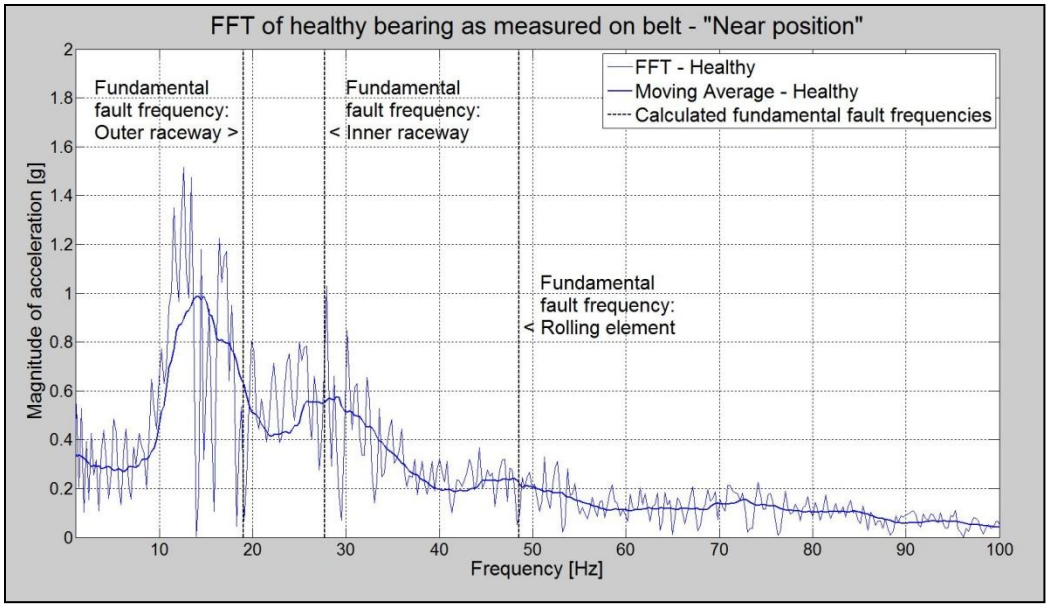

Figure 3.16: FFT of a healthy bearing as measured near the bearing

Each dataset that was captured was of a single pass over the idler as discussed in Section 2.4.1. A total of 616 datasets were recorded of the healthy bearing in the idler when the sensor was fixed in the near position on the belt. After the healthy bearing was tested, it was removed and replaced with a bearing with an artificially induced inner raceway fault.

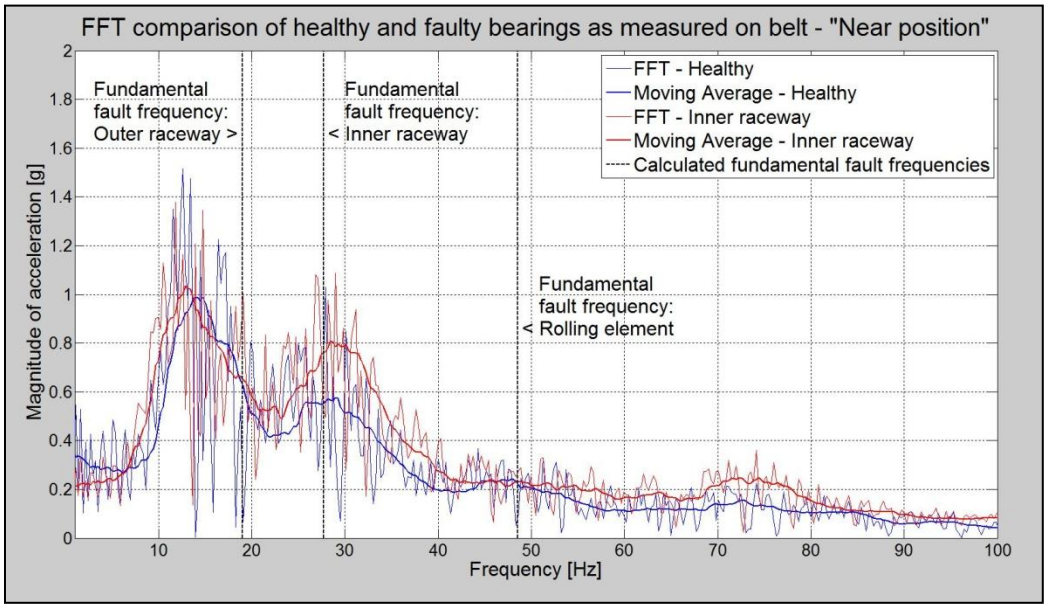

Figure 3.17: FFT of an inner raceway fault as measured near the faulty bearing

Figure 3.17 shows the FFT of a bearing with an inner raceway fault that was measured at the near position. The FFT of a healthy bearing is also included to compare. The moving averages of the FFTs are also shown. From Figure 3.17, it can be seen that the magnitude of the frequency corresponding to that of the inner raceway fundamental frequency was larger in the faulty bearing than in the healthy bearing, as expected from the previous tests. There was very little change in the outer race frequency as well as in the rolling element fundamental frequency. A total of 394 datasets were recorded of the bearing with an inner raceway fault. The faulty bearing was removed and replaced with a bearing with an artificially induced outer raceway fault.

Figure 3.18 shows the FFT of a bearing with an outer raceway fault that was measured at the near position. The FFT of a healthy bearing is also included to compare. The moving averages of the FFTs are also shown. A clear increase in the magnitude of the outer raceway fundamental frequency was visible. Not only the magnitude of the outer raceway fundamental frequency, but the magnitude of the inner raceway fundamental frequency had increased. The magnitude increase of the outer raceway fundamental frequency could be clearly seen. A total of 276 datasets were recorded of the bearing with an outer raceway fault. The faulty bearing was removed and replaced with a bearing with an artificially induced rolling element fault.

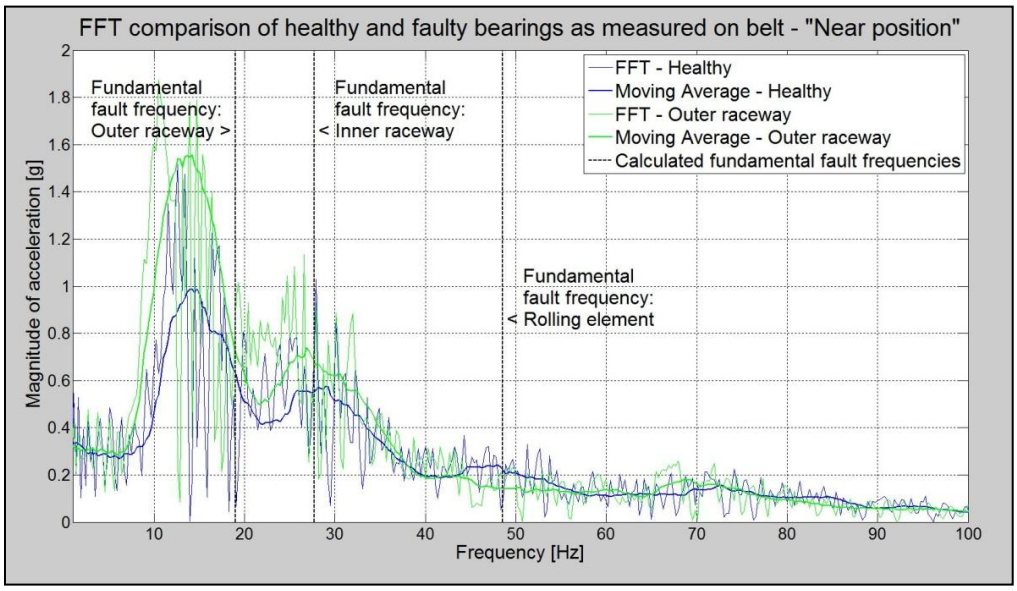

Figure 3.18: FFT of an outer raceway fault as measured near the faulty bearing

Figure 3.19 shows the FFT of a bearing with a rolling element fault that was measured at the near position. The FFT of a healthy bearing is also included to compare. The moving averages of the FFTs are also shown. There was a distinct increase in the rolling element fundamental frequency as expected.

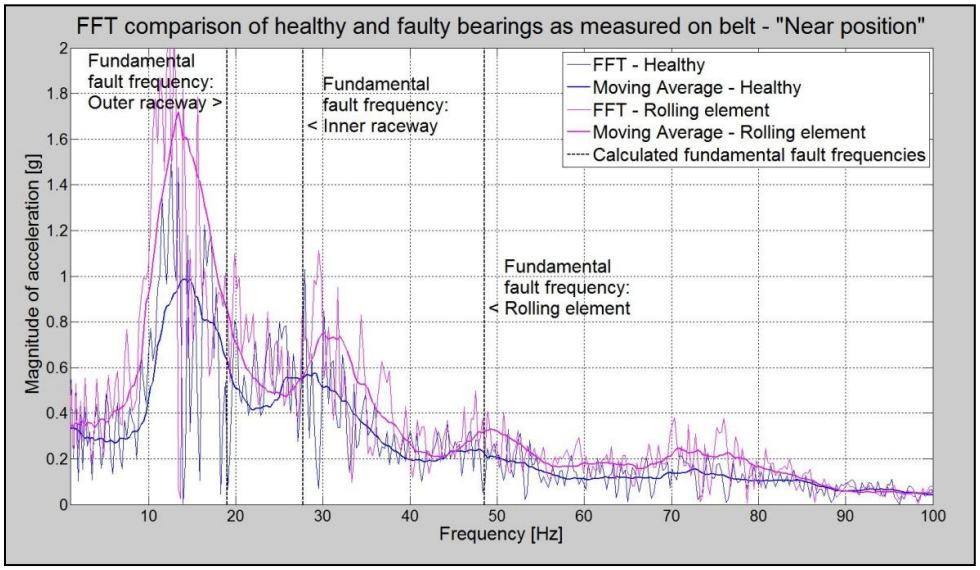

Figure 3.19: FFT of a rolling element fault as measured near the faulty bearing

The impact of the defect on the rolling element with the inner and outer raceway increased the magnitude of the frequency of the rolling element, but also that of the inner and outer raceway. Both the inner and outer raceways were impacted by the rolling element as the fault passed the raceways' surfaces. These cyclic impacts on all three components increased the magnitude of the three fundamental frequencies of the bearing. This could be seen in Figure 3.19 as all three fundamental frequencies have increased in magnitude. A total of 428 datasets were recorded of the bearing with an artificially induced rolling element fault. The faulty bearing was removed and replaced with a bearing that was contaminated with fine sand and dust.

Figure 3.20 shows the FFT of a contaminated bearing. The FFT of a healthy bearing is also included to compare. The moving averages of the FFTs are also shown. As with the rolling element defect, there was a distinct increase in the magnitudes of all three fundamental frequencies of the bearing. Some of the contaminating particles in the bearing were caught between the rolling element and the raceways. When the rolling element moved over a particle, small impacts occurred between the rolling element and the raceways. These impacts increased the magnitude of the fundamental frequencies of both the raceways as well as that of the rolling element. The FFT of the contaminated bearing shows a deviation in the rolling element's fundamental frequency from that of what was expected. .

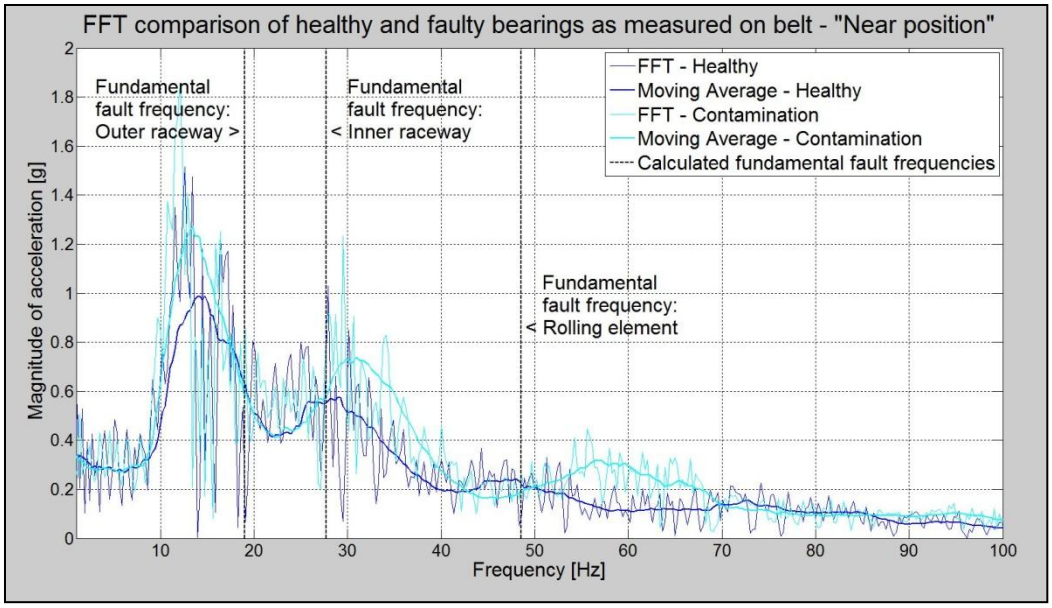

Figure 3.20: FFT of a contaminated bearing as measured near the bearing

As seen in Figure 3.20, the measured frequency corresponding to the rolling element is noticeably higher than the calculated frequency and the frequency observed in the healthy bearing. This could be due to the contamination particles. As the rolling element rolled over the surfaces of the raceways, particles would get trapped and caused the impacts. The slight increase in the frequency magnitude associated with the rolling element suggest that there may have been more than one particle rolled over in a single rotation of the rolling element, increasing the rate at which impacts occurred between the rolling element and the raceways. The frequency range in which these impacts occurred was slightly wider and at slightly higher frequencies than that of the bearing with only a rolling element fault, seeing that there was a wide range of different impact rates in the contaminated bearing. A total of 432 datasets were recorded of the contaminated bearing.

It was noticed that when the accelerometer was attached to the shaft of the idler, the measured fundamental frequencies corresponded to the calculated values with very little deviation, as seen in Figure 3.5 to Figure 3.9. Deviations as little as 3.2% were found between the calculated and measured fundamental frequencies. When the accelerometer was attached to the belt, the measured bearing fundamental frequencies did not correspond to the calculated values as well as the case where it was fixed to the shaft. Larger deviations were noted as seen in Figure 3.16 to Figure 3.20. Some of the largest deviations found were in the order of 6.3 Hz from the 18.97 Hz outer raceway fundamental frequencies, a 33.2% deviation. The magnitudes of the deviations were not excessive, but still noticeable.

When the accelerometer was attached to the shaft, the system showed characteristics of a linear system where the frequencies of the measured vibrations corresponded to the frequencies of source vibration, albeit the calculated source frequencies. The stiff idler shaft transmitted the source vibration to the accelerometer with very little dampening.

When the accelerometer was attached to the belt, the system did not show these characteristics of a linear system anymore. The accelerometer was placed on top of the rubber conveyor belt that is known to have viscoelastic properties and dampening effects. While the belt was moving it had a low frequency hop. The idler has a slight eccentricity that adds additional forced vibrations to the system. A classic characteristic jump was also noted that has an influence on the natural frequency of the belt and it changes as the belt speed changes. Efforts were made to maintain the belt at a constant speed, but small variations were observed. These are all characteristics of a non-linear system as described by (Moon & Wickert, 1997) that studied natural frequencies of non-linear belt systems.

High-speed footage of the conveyor test bench was recorded and motion amplification was done on the video. From the video it can clearly be seen that the system and the belt in particular behaves in a non-linear way as described in (Zhang & Zui, 1998) and (Kim & Lee, 1999). Figure 3.21 to Figure 3.23 show screenshots taken from the footage. From the footage it can clearly be seen that there is belt hop present and this is also supported by the time-domain signals recorded on the belt as seen in Figure 2.15 where low-frequency waves are present before and after the sensor passes the idler.

The vibrations measured on the belt had frequency spectrums that looked similar to those measured on the shaft, but the measured fundamental fault frequencies did not correspond to the calculated source frequencies. The non-linear conveyor belt system showed belt hop between the pulleys and the idler and other characteristics that corresponds to the observations, analysis and modelling done of non-linear belt systems by (Zhang & Zui, 1998) and (Kim & Lee, 1999). Non-linear vibration systems have been investigated by (Narayanan & Jayaraman, 1991) and (Choi & Noah, 1988) and it has been found that non-linear systems can have subharmonic, superharmonic and chaotic responses to harmonic excitation. This shows that the fundamental fault frequencies as measured on the belt can appear at higher or lower frequencies due to the non-linearity of the on-belt monitoring system and still contain the underlying bearing fault data.

The characteristics of this non-linear system can be investigated in future to better understand and predict the frequencies of the measured vibrations when the accelerometer is placed on top of a moving conveyor belt.

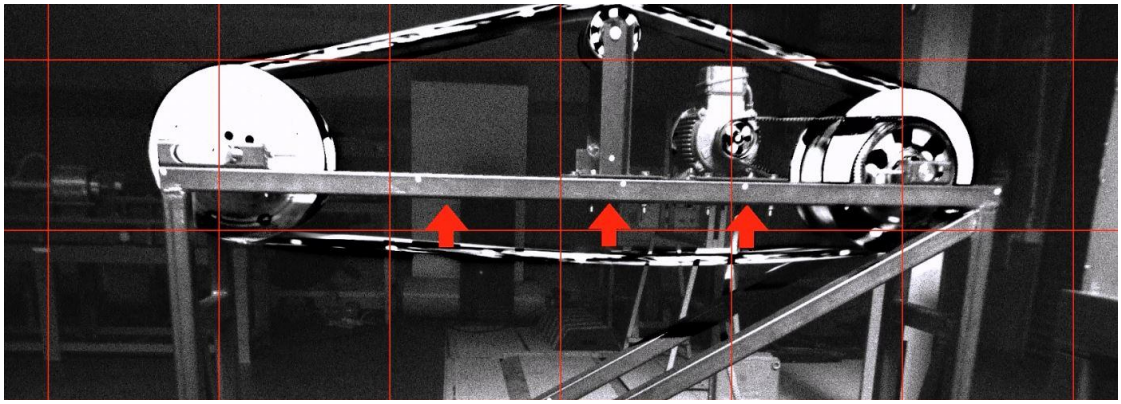

Figure 3.21: High-speed footage screenshot 1

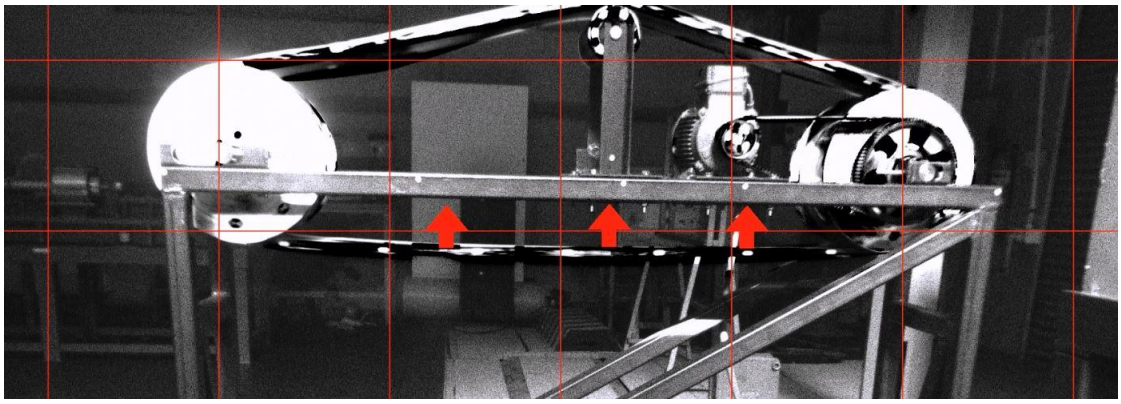

Figure 3.22: High-speed footage screenshot 2

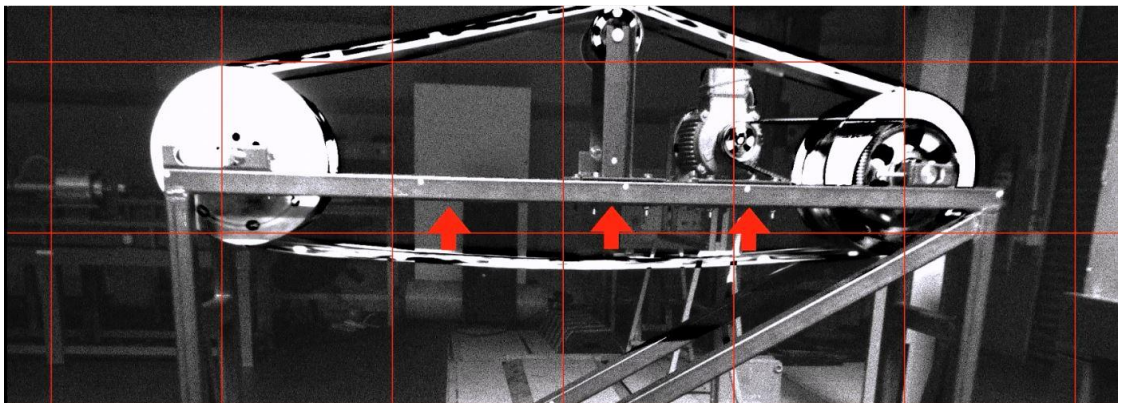

Figure 3.23: High-speed footage screenshot 3

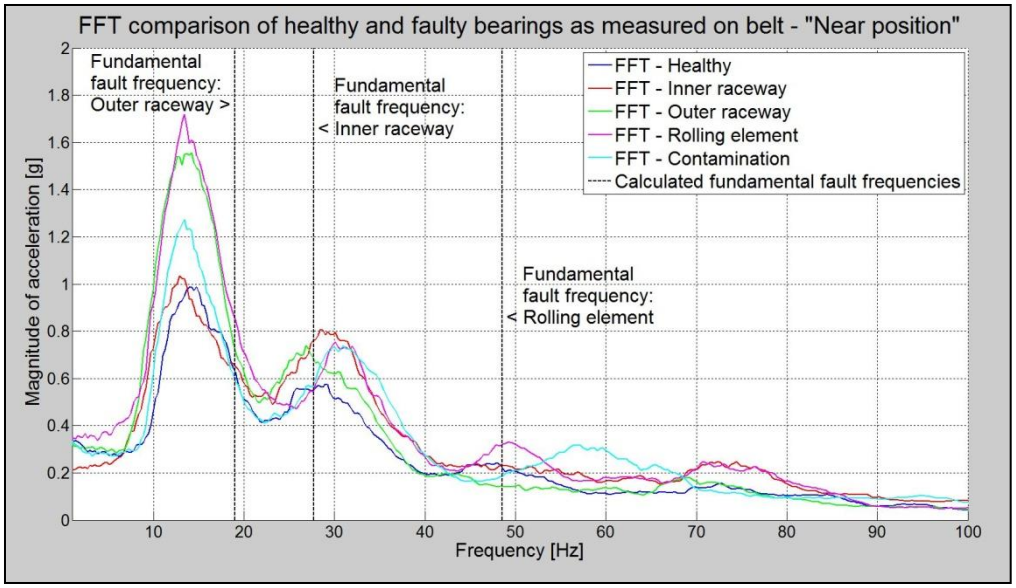

Figure 3.24: Moving averages of different bearing conditions as measured near the bearing

Figure 3.24 shows the moving averages of the five different bearing conditions. It is clear that the frequency spectrum of each bearing condition has a unique shape and it was this uniqueness that was used to distinguish the one condition from the other. Figure 3.25 shows the energy values of the different bearing conditions depicted in Figure 3.24. A level seven WPD had been applied and the energy levels were calculated.

A level seven WPD was applied to each bearing dataset. A level seven WPD was chosen because it had very good resolution - divided the signals into small enough sections so that each defect could be placed in its own pair of wavelets but still resembled the original signal. The level 7 WPD, in essence, divided the frequency spectrum into 2^7 sections and an energy value for each section was calculated as discussed in Chapter 2.4.2. It can be seen from Figure 3.25 that each bearing condition has a different energy distribution and it was these differences that were used to identify and classify the bearing faults. Only the first 13 levels are shown seeing that the remaining energy bands are very small in comparison to the low-frequency bands.

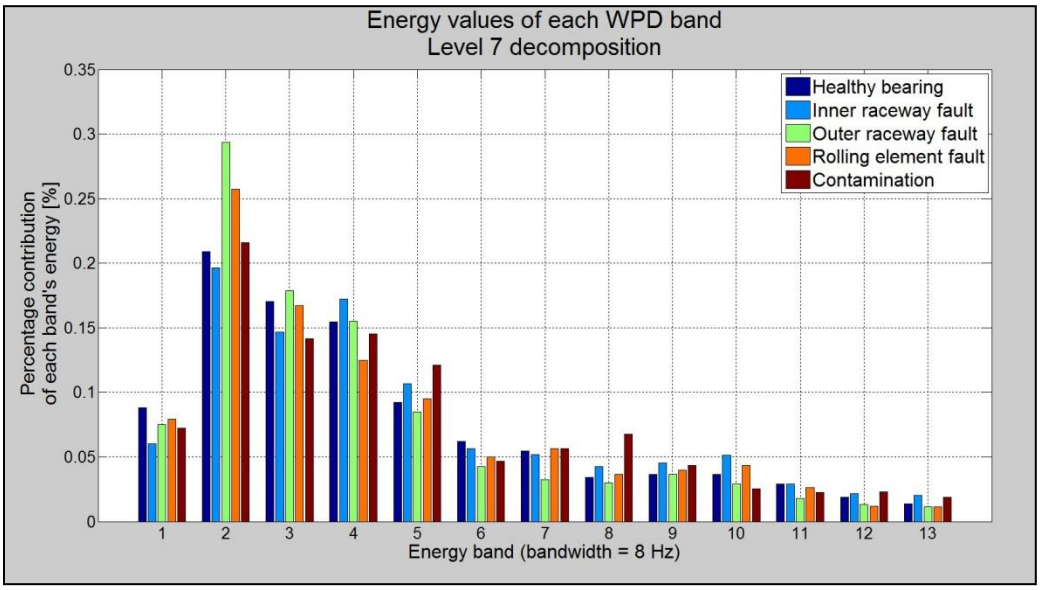

Figure 3.25: WPD of the different bearing defects as measured near the faulty bearing

3.2.1.2. Identification and classification of the bearing faults

There are two popular intelligent systems used to classify datasets. These are neural networks and support vector machines. Both of these systems were used to attempt to identify and classify the different bearing faults that were measured near the faulty bearing.

A large number of measurements were taken for each of the five bearing conditions. All these measurements were pre-processed, as discussed in Chapter 2.4.2, and the energy values of each measurement were used to train and test the intelligent systems. Each bearing condition's datasets were divided into two equal parts, one for training and the other for testing the intelligent system.

The gradient based back propagation neural network was trained and tested as discussed in Chapter 2.5.1. Firstly it was investigated to see if the neural network could distinguish a healthy bearing and a faulty bearing, regardless of the fault. It was found that the neural network had a 94.41% accuracy (1013 of 1073 datasets) when distinguishing a healthy bearing from a faulty one. It was however not as accurate in classifying the fault. The neural network only had a 58.90% accuracy (632 of 1073 datasets) when trying to classify the bearing fault.

Being able to tell if a bearing is faulty with 94.41% accuracy is quite good but the error is too large when looking at the amount of idler bearings there can be in a single conveyor. The neural network was not very accurate when classifying the type of fault. Only 58.90% (632 of 1073 datasets) were classified correctly. This may have been because the signals of the faulty bearings were too different from one fault to the other for the neural network to distinguish

them properly. But when the different bearing faults were combined as one class, the faulty bearing class, and compared to the healthy bearing class, the differences seemed to be prominent enough for the neural network to distinguish the faulty bearings from the healthy ones. This made the identification of a faulty bearing easier and more accurate but the classification of the fault could not be done. Figure 3.26 shows the two classes, healthy and faulty, and the different classifications of the datasets. The green markers indicate the datasets that are classified correctly and the red markers indicate those that are misclassified.

Note that the output of the neural network (most neural networks in general) was not a fixed output value or class value like a support vector machine would be. The output of a neural network was not a definite value that corresponded to a class value, but rather a value that, when within a range from a specified class value, could be associated with that class. Table 3.5 shows the statistics of the neural network classification. The majority of the misclassified datasets were from the healthy bearing class, roughly 13% of this class had been misclassified.

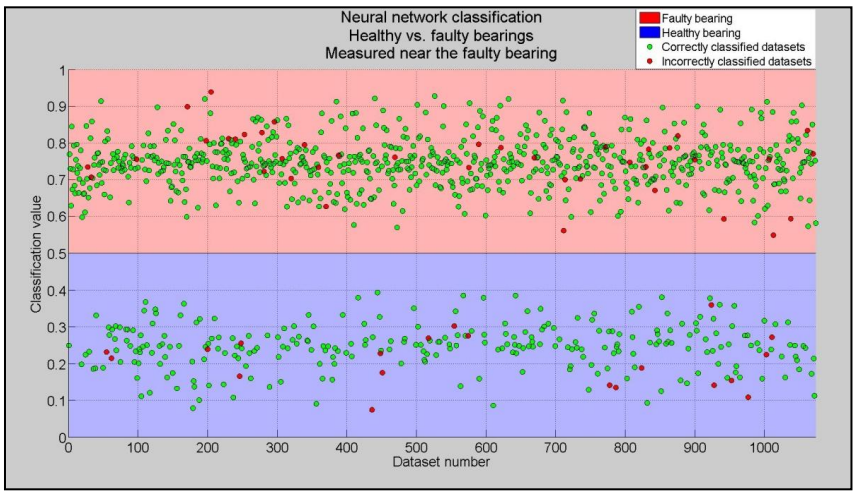

Figure 3.26: Two-class, near bearing, Neural network classification

Table 3.5: Neural network accuracy when measured near the faulty bearing

Neural network classification of faulty bearings (Measured at near position)				
Bearing condition	Number of datasets		Correctly classified	Accuracy
Healthy bearing	308	308	268	87.01%
Inner raceway	197	765	745	97.39%
Outer raceway	138			
Rolling element	214			
Contaminated bearing	216			
Total	1073		1013	94.41%

The support vector machine had a fixed value for each class's output, unlike the neural network, which made it such a popular classifier. The support vector machine was trained and tested, as discussed in Chapter 2.5.2, with the same datasets as with the neural network. A radial base function was used and with a grid search, a cost value of $1.3347 \times 10^{7}$and a gamma value of 1.5447×10^{-9} was found to produce the highest accuracy. The support vector machine did not only classify the datasets into the two classes of healthy and faulty, but classified all the different faults with 100% accuracy (1073 of 1073 test datasets). A single support vector machine could classify a dataset measured at the near position into any of the five bearing conditions; healthy bearing, inner raceway defect, outer raceway defect, rolling element defect or contaminated bearing. Figure 3.27 shows the five different classes and the classified datasets. Table 3.6 shows the statistics of the support vector machine classification.

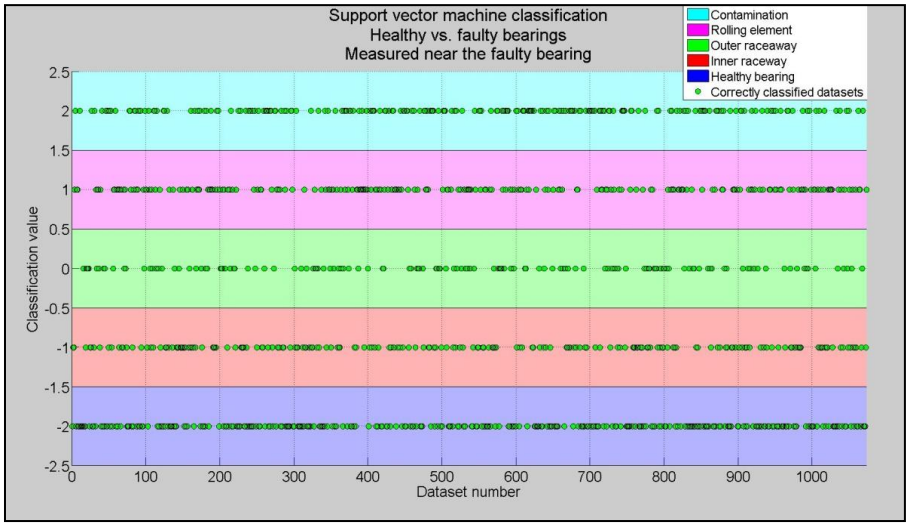

Figure 3.27: Five-class, near bearing, Support vector machine classification

Table 3.6: Support vector machine accuracy when measured near the faulty bearing

SVM classification of faulty bearings (Measured at near position)			
Bearing condition	Number of datasets	Correctly classified	Accuracy
Healthy bearing	308	308	100.00%
Inner raceway	197	197	100.00%
Outer raceway	138	138	100.00%
Rolling element	214	214	100.00%
Contaminated bearing	216	216	100.00%
Total	1073	1073	100.00%

3.2.1.3. Conclusion

The different bearing faults and conditions had more or less the same frequency spectrums but the small deviation from one another was what enabled an intelligent system to distinguish them from one another. The vibrations measured on the belt, right above the faulty bearing, were used to identify and also classify these faults with very high accuracy. A 100% accurate classification (with a SVM) of over a thousand different datasets is a very good indication that it is possible to measure and monitor idler bearing vibrations through a rubber conveyor belt as it moves at speed. This means that it is possible to make use of accelerometers, fixed to a conveyor belt, to monitor the conditions of the idler bearings. With the success of this test, it can be said with confidence, that having a sensor over each bearing across the width of the belt will enable the monitoring of all the idler bearings with high accuracy. Further investigations will be done to try and reduce the number of sensors used.

3.2.2. Measuring at other positions on the belt

3.2.2.1. Influence of sensor placement on signal clarity

When the accelerometer was placed on the belt so that it travelled directly over the faulty bearing, it was possible to identify when the bearing was faulty and even classify the different faults. It would be possible to monitor all the bearings of the idlers if a sensor was placed over each bearing position. This requires a number of sensors and can become costly. To reduce the number of sensors needed to monitor all the bearings across the width of the belt, different sensor positions will be investigated. Figure 3.28 shows how the sensor was placed in the middle of the belt and over the other, healthy, bearing as well - as far from the faulty bearing as possible on the test bench. The accelerations were measured perpendicular to the belt surface and the sensor rotation about this axis, as in the far position depicted in Figure 3.28, had no influence on the measured data.

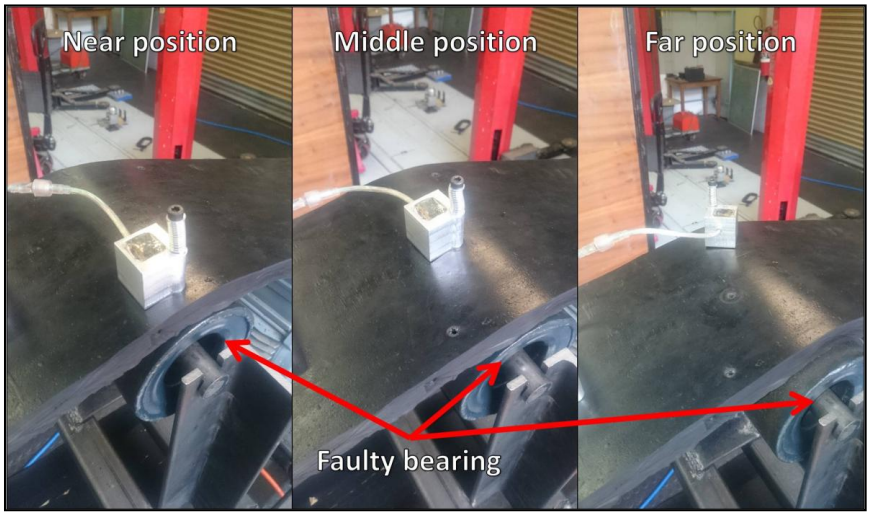

Figure 3.28: Different sensor placement on the belt

Figure 3.29 shows the moving averages of the case where both bearings in the idler were healthy. It can be seen from the FFTs of the signals that were measured directly over the bearings were very similar. The magnitudes of the different fundamental bearing frequencies were close to one another for the near and far positions. This was expected seeing that both bearings were healthy. When measured in the middle of the belt, the FFT magnitudes were lower than the other two positions, but by a small margin. This could be due to the further distance between the sensor and the source of the vibrations, reducing the transmissibility. A total of 226 datasets were recorded on the middle of the belt when both bearings were healthy and a total of 222 datasets were recorded over the healthy bearing in the far position.

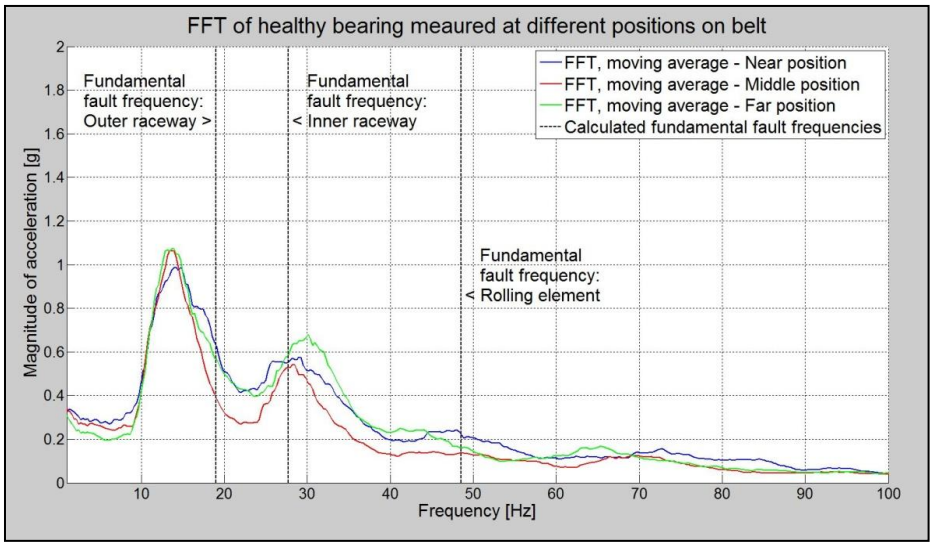

Figure 3.29: FFT of healthy bearings at different positions

Figure 3.30 shows the moving averages measured at the three positions when a bearing with an inner raceway defect was installed at the near position. It was noted the FFTs had the same shape, independent of the position where measurements were taken from. There was very little change in the magnitude of the fundamental frequency associated with an inner raceway fault, independent of the sensor position, but there was a difference between the healthy bearing and the bearing with an inner raceway defect.

As expected, there was an increase in the magnitude of the fundamental frequency corresponding to the inner raceway fault. These magnitudes were larger than expected. It was expected for the magnitudes of the middle position to be lower than the near position and the far position even lower. The hard rubber compound of the belt seemed to be a good medium for transmitting vibrations at these distances. It is comforting to see that the inner raceway fault could be seen in the FFTs for both the middle and the far sensor placements. A total of 388 datasets were recorded on the middle of the belt and a total of 206 datasets were recorded by the sensor in the far position when a bearing with an inner raceway fault was installed in the idler.

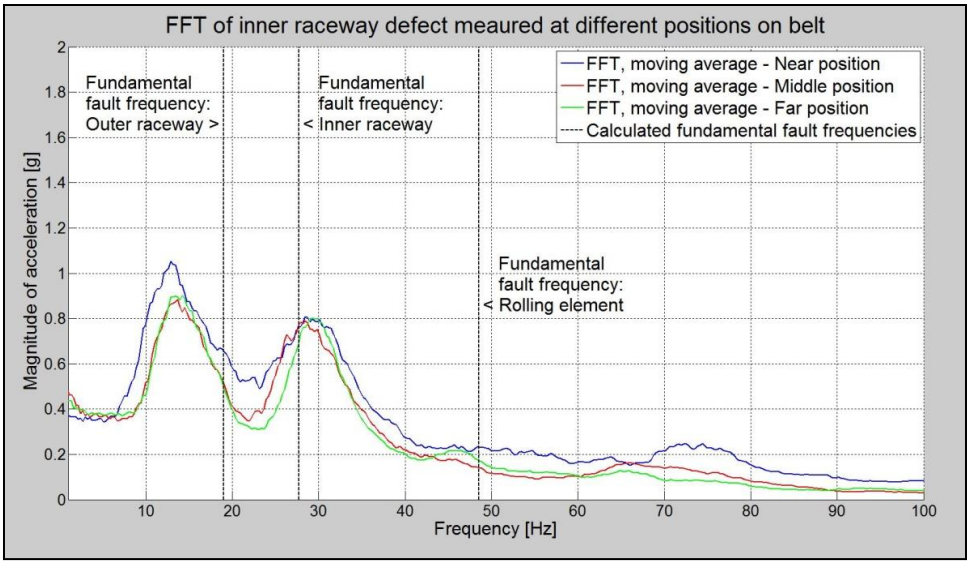

Figure 3.30: FFT of inner raceway faults at different positions

Figure 3.31 shows the moving averages of the case where a bearing with an outer raceway defect was installed at the near position. It could be seen that, just like when measured near the faulty bearing, the magnitude of the outer raceway fundamental frequency had increased when measuring at the other two positions. It was noted that the magnitudes of the frequency spectrums of the signals measured at the middle position were slightly lower than that of the near position. The magnitudes of the frequency spectrums of the signals measured at the far position were the lowest of the three sensor positions, as expected. The distance from the faulty bearing to each of the measuring positions had an influence on the transmissibility of the bearing vibrations. The further the sensor from the faulty bearing, the less of the underlying frequencies were captured by the sensor, but the losses were very small.

The sensor captured the vibration due to both bearings in the idler. Depending on where the sensor was placed, it would capture more of the one bearing than the other seeing that the transmissibility of the bearing closest to the sensor would be better. This is why, when the sensor was placed near the faulty bearing, the magnitudes of the fundamental frequencies were so much higher than the other two positions. The middle position can be seen as a midway between the two bearings, capturing both bearings' vibrations equally. It is comforting to see that the sensor captured the faulty bearing's signal when it was placed at the far position and that it could be seen from this signal that there was a fault in the bearing. A total of 284 datasets were recorded on the middle of the belt and a total of 298 datasets were recorded by the sensor in the far position when a bearing with an outer raceway fault was installed in the idler.

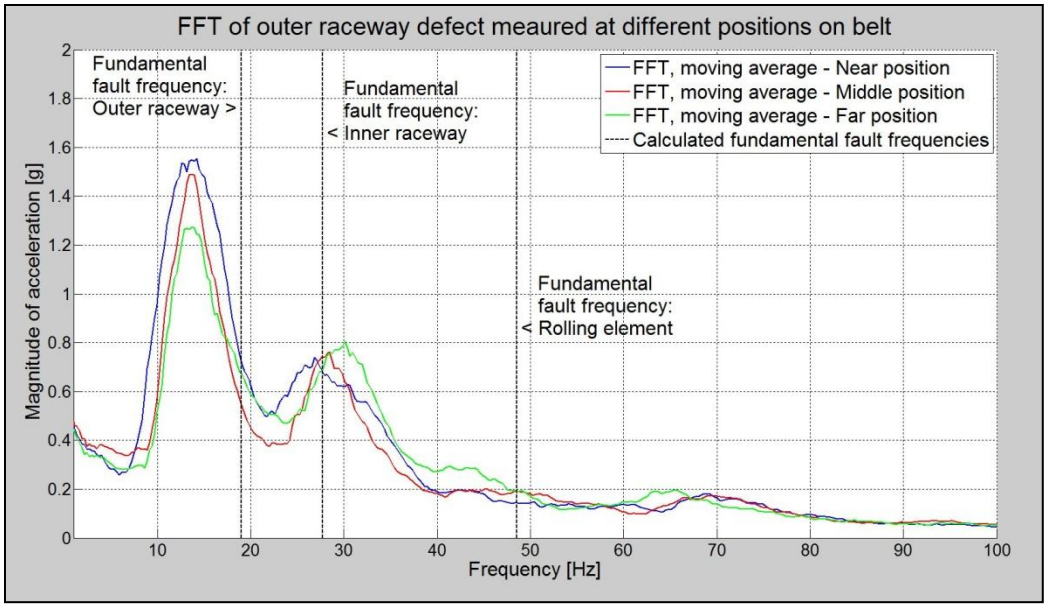

Figure 3.31: FFT of outer raceway faults at different positions

Figure 3.32 shows the moving averages of the case where a bearing with a rolling element defect was installed at the near position. The presence of a rolling element fault was clear when the frequency spectrums of the different sensor placements were inspected. The higher magnitude of the rolling element fundamental frequency was an indication that there was a rolling element fault in the bearing. As expected, the magnitude of the frequencies, as measured near the fault, was higher than that of the middle position and even higher than the far position. A total of 240 datasets were recorded on the middle of the belt and a total of 246 datasets were recorded by the sensor in the far position when a bearing with a rolling element fault was installed in the idler.

Figure 3.33 shows the moving averages of the case where a contaminated bearing was installed at the near position. It can be seen that there was a rolling element related fault in the bearing because the magnitudes of all three the bearing fundamental frequencies had increased. As with the case where the sensor was placed near the faulty bearing, there was a larger-than-normal range of frequencies present around the rolling element fundamental frequency as discussed in Chapter 3.2.1. The ranges of the rolling element frequencies of the cases where the sensor was placed at the middle and the far positions were at lower frequencies. It looks like the rubber of the belt and the idler itself had a dampening effect on the additional high frequency vibrations of the contaminants. The base fundamental frequency of the rolling element was prominent on the frequency spectrums with less high frequency data. There was however a difference between these signals and the signals of a healthy bearing. A total of 262 datasets were recorded on the middle of the belt and a total of 294 datasets were recorded by the sensor in the far position when a contaminated bearing was installed in the idler.

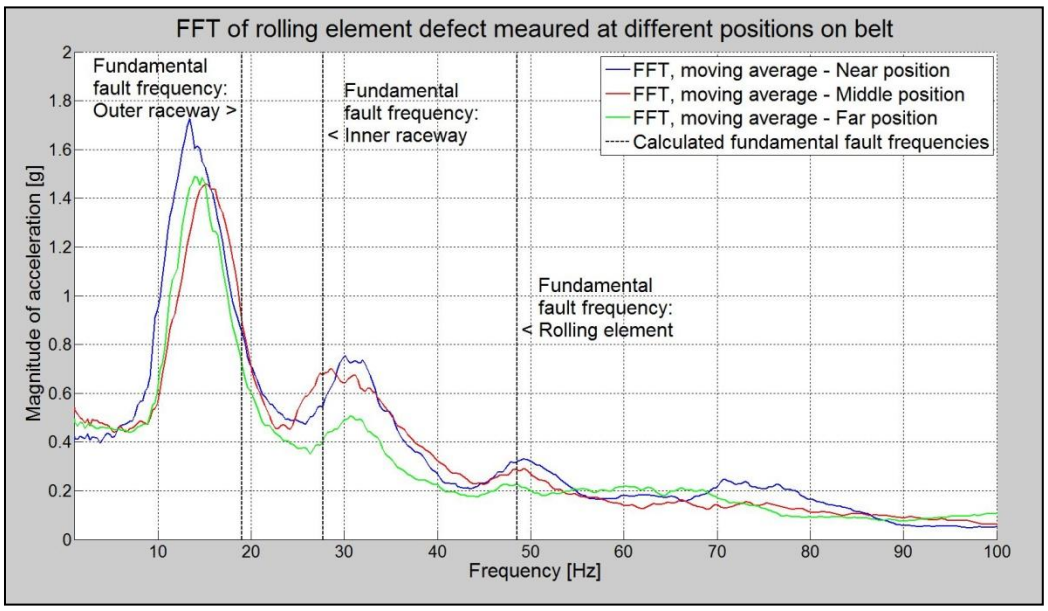

Figure 3.32: FFT of rolling element fault at different positions

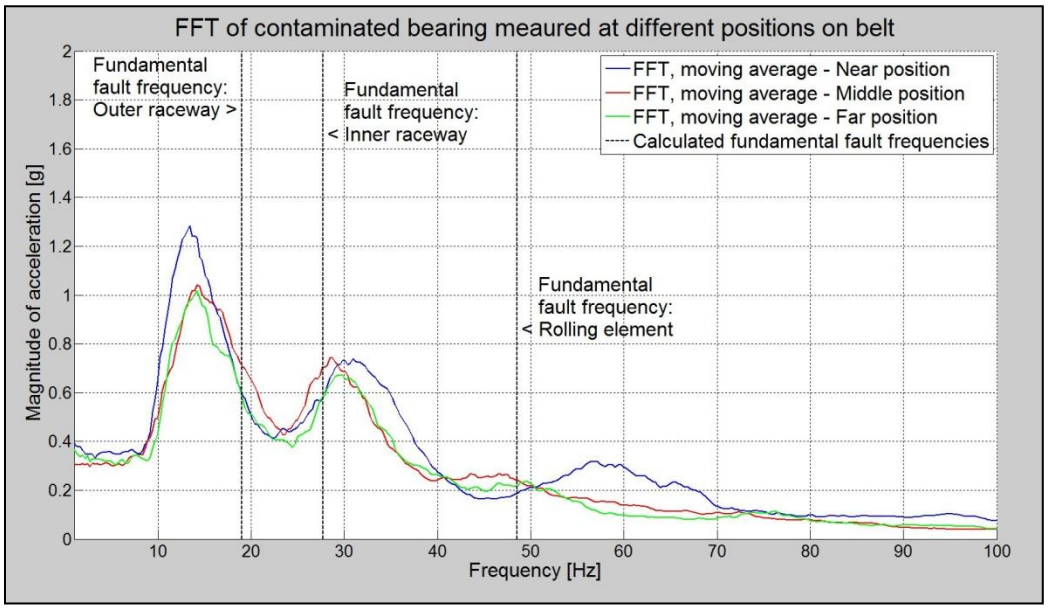

Figure 3.33: FFT of contaminated bearing at different positions

3.2.2.2. Identification and classification with sensor in the middle of the belt

Data was sampled for each of the five bearing conditions at both the middle and far positions. All these measurements were pre-processed and the energy values calculated as discussed in Chapter 2.4.2. Each bearing condition's datasets were divided into two equal parts, one for training and the other for testing the intelligent system.

The gradient based back propagation neural network was trained and tested, as discussed in Chapter 2.5.1, with data measured in the middle of the belt. Firstly it was investigated to see if the neural network could distinguish a healthy bearing and a faulty bearing, regardless of the fault. It was found that the neural network had a 96.86% accuracy (678 of 700 test datasets) when distinguishing a healthy bearing from a faulty one. It was however not as accurate in classifying the fault. The neural network only had a 75.43% accuracy in trying to classify the bearing fault.

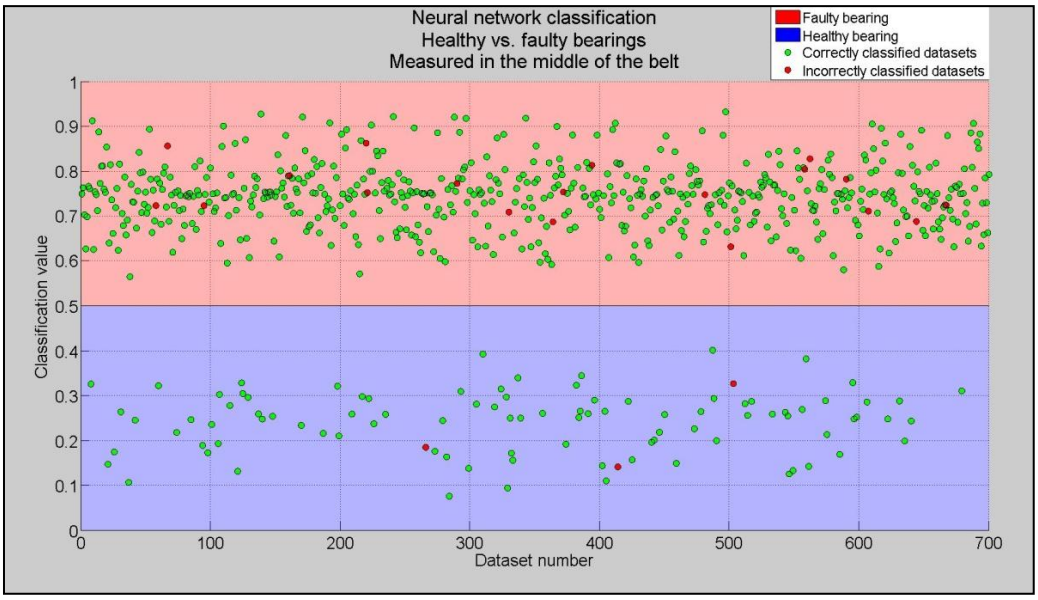

Figure 3.34: Two-class, middle of the belt, neural network classification

Figure 3.34 shows the two classes, healthy and faulty, and the different neural network classifications of the datasets as measured in the middle of the belt. The green markers indicate the datasets that were classified correctly and the red markers indicate those that were misclassified. Table 3.7 shows the statistics of the neural network classification for this sensor position. The majority of the misclassified datasets were from the healthy bearing class - almost 17% of this class had been misclassified. Although 83.19% of the healthy bearings had been correctly classified, it's not accurate enough to say with confidence whether a bearing is healthy or not when there can be thousands of bearings in the idlers of a conveyor. The large misclassification could be due to the large amount of faulty bearing datasets when they were all combined. The neural network can become oversensitive or over trained for faulty bearings.

Table 3.7: Neural network accuracy when measured in the middle of the belt

Neural network classification of faulty bearings (Measured at middle position)				
Bearing condition	Number of datasets		Correctly classified	Accuracy
Healthy bearing	113	113	94	83.19%
Inner raceway Outer raceway Rolling element Contaminated bearing	194 142 120 131	587	584	99.49%
Total	700		678	96.86%

As discussed in Chapter 2.5.2, the support vector machine was trained and tested with the same datasets as with the neural network. A radial base function was used with a grid search and a cost value of 2.3269×10^{3} and a gamma value of 9.5491×10^{-5} was found to produce the highest accuracy. The support vector machine did not only classify the datasets into the two classes of healthy and faulty, but classified all the different faults with 100% accuracy (700 of 700 test datasets). A single support vector machine classified a dataset into one of the five bearing conditions; healthy bearing, inner raceway defect, outer raceway defect, rolling element defect or contaminated bearing. Figure 3.35 shows the five different classes and the classified datasets. Table 3.8 shows the statistics of the support vector machine classification.

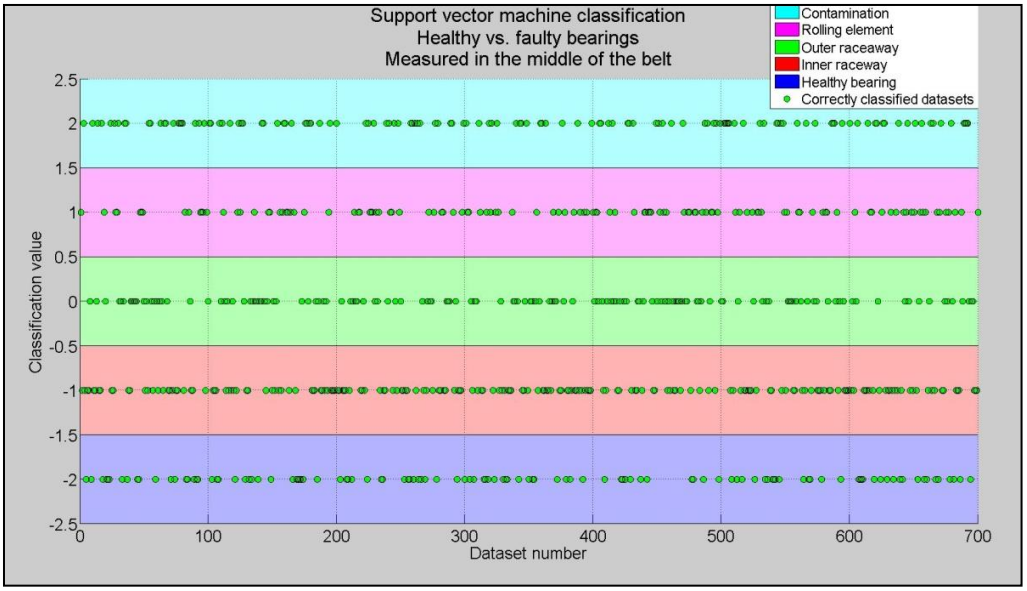

Figure 3.35: Five-class, middle of the belt, Support vector machine classification

Table 3.8: Support vector machine accuracy when measured in the middle of the belt

SVM classification of faulty bearings (Measured at middle position)			
Bearing condition	Number of datasets	Correctly classified	Accuracy
Healthy bearing	113	113	100.00%
Inner raceway	194	194	100.00%
Outer raceway	142	142	100.00%
Rolling element	120	120	100.00%
Contaminated bearing	131	131	100.00%
Total	700	700	100.00%

3.2.2.3. Identification and classification with sensor far from the faulty bearing

The gradient based back propagation neural network was trained and tested, as discussed in Chapter 2.5.1, with the data measured far from the faulty bearing. Firstly it was investigated to see if the neural network could distinguish a healthy bearing and a faulty bearing, regardless of the fault. It was found that the neural network had a 98.74% accuracy (625 of 633 test datasets) when distinguishing a healthy bearing from a faulty one. It was however not as accurate in classifying the fault. The neural network only had a 79.30% accuracy in trying to classify the bearing fault. It was noted that the accuracies had increased from the case where the sensor was placed near the faulty bearing to the case where it was placed in the middle of the belt and the highest for the case where the sensor was placed far from the faulty bearing. A summary of the accuracies can be seen in Table 3.11. As the tests progressed, the faults may have increased slightly in size, making it easier for the neural network to identify the faulty bearings.

Figure 3.36 shows the two classes, healthy and faulty, and the different neural network classifications of the datasets as measured far from the faulty bearing. The green markers indicate the datasets that were classified correctly and the red markers indicate those that were misclassified. Table 3.9 shows the statistics of the neural network classification for this sensor position.

Table 3.9: Neural network accuracy when measured far from the faulty bearing

Neural network classification of faulty bearings (Measured at far position)				
Bearing condition	Number of datasets		Correctly classified	Accuracy
Healthy bearing	111	111	103	92.79%
Inner raceway	103	522	522	100.00%
Outer raceway	149			
Rolling element	123			
Contaminated bearing	147			
Total	633		625	98.74%

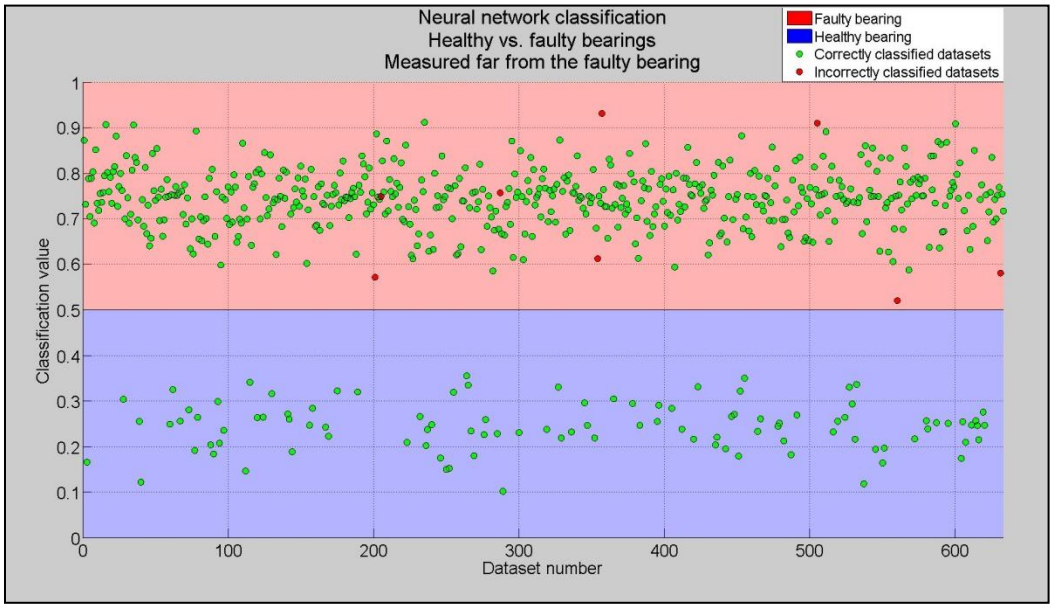

Figure 3.36: Two-class, far from the bearing, Neural network classification

The support vector machine was trained and tested, as discussed in Chapter 2.5.2, with the same datasets as with the neural network. A radial base function was used, and with a grid search, a cost value of 4.7428×10^{6} and a gamma of 7.9635×10^{-6} was found to produce the highest accuracy. The support vector machine did not only classify the datasets into the two classes of healthy and faulty, but classified all the different faults with 100% accuracy (633 of 633 test datasets). A single support vector machine could classify a dataset into any of the five bearing conditions; healthy bearing, inner raceway defect, outer raceway defect, rolling element defect or contaminated bearing. Figure 3.37 shows the five different classes and the classified datasets. Table 3.10 shows the statistics of the support vector machine classification.

Table 3.10: Support vector machine accuracy when measured far from the faulty bearing

SVM classification of faulty bearings (Measured at far position)			
Bearing condition	Number of datasets	Correctly classified	Accuracy
Healthy bearing	111	111	100.00%
Inner raceway	103	103	100.00%
Outer raceway	149	149	100.00%
Rolling element	123	123	100.00%
Contaminated bearing	147	147	100.00%
Total	633	633	100.00%

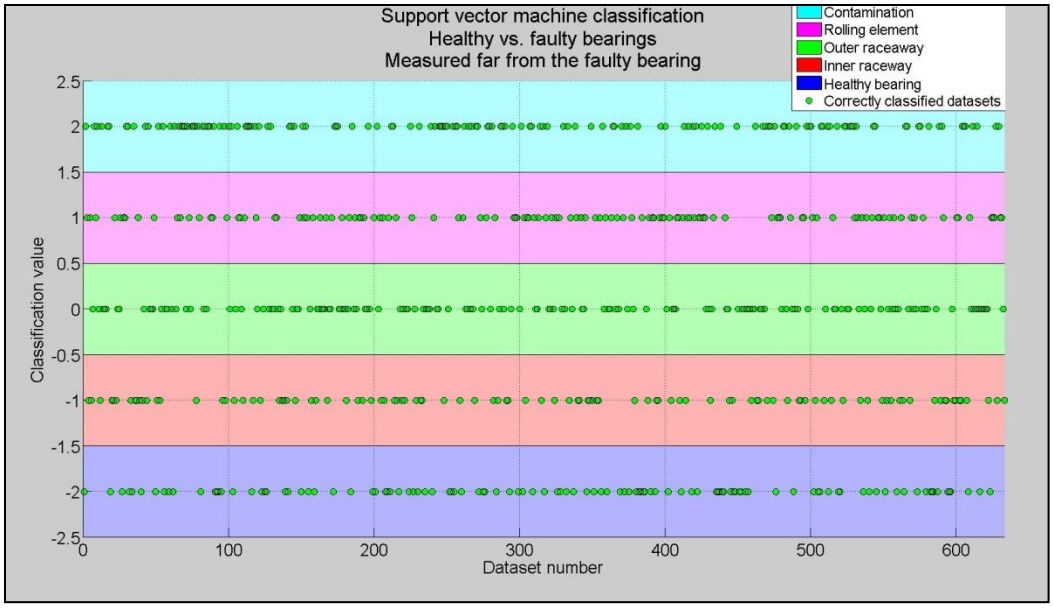

Figure 3.37: Five-class, far from the bearing, support vector machine classification

From the tests conducted on the conveyor test bench, it is clear that the condition of idler bearings can be monitored by using an accelerometer attached to the belt, regardless of sensor position. The datasets were classified with neural networks with very high accuracy. By using a support vector machine, the datasets were classified with 100% accuracy. Even the type of bearing fault was identified correctly for all the datasets. Table 3.11 shows the summary of the intelligent systems' accuracies for all three sensor positions; near and far from the faulty bearing and in the middle of the belt.

Table 3.11: Summary of Intelligent systems' accuracies

Summary of Intelligent systems' accuracies				
Sensor placement	Five-class fault classification		Two-class fault identification	
	Neural network	SVM	Neural network	SVM
Near the faulty bearing	58.90%	100%	94.41%	100%
In the middle of the belt	75.43%	100%	96.86%	100%
Far from the faulty bearing	79.30%	100%	98.74%	100%

3.2.2.4. Conclusion

Accelerometers have previously been used to monitor the health or condition of idler bearings, but these sensors were attached to the supporting structure of the idlers. These sensors only monitored a few idlers at a time and a vast number of sensors would have been needed to monitor all the idlers of a single conveyor. From these tests done in this investigation, it can be said with certainty and confidence, that an in-belt idler monitoring system has great potential of monitoring the idlers of a conveyor.

The neural network may have been very accurate, but when working with thousands of idler bearings, accuracies close to 100% are desired. The support vector machine proved to be a great classifier for the bearing conditions. Whether the sensor was placed near or far from the faulty bearing, the support vector machine classified each dataset with 100% confidence.

It was noted that the accuracies of the neural network increased as the sensor moved further away from the faulty idler. As the tests progressed, the bearing faults may have become slightly larger, making it easier to identify the fault. The bearings were all still in working condition at the end of the tests and no sign of bearing seizure was visible. The monitoring system was sensitive enough to identify a bearing in its early failing stages. It is good that the faulty bearings can be identified a while before catastrophic failure occurs, giving enough time to prepare for planned outages and before a catastrophic bearing failure causes damage.

These tests were done under fairly ideal conditions. There was no payload on the belt and the addition of a payload may create other dynamic conditions that can create noise and other frequencies in the spectrum. The effects on the accuracy of identifying and classifying a faulty bearing when a payload, although small, is added, will be investigated.

3.2.3. Measuring vibrations on the belt with the addition of payload

The investigation where the accelerometer was attached to the belt to monitor idler bearings was very successful. The tests done in that investigation were done without any payload on the belt. The presence of a payload on a conveyor belt added, to a certain degree, a dynamic aspect. The payload was expected to shift around as it travelled on the conveyor belt, adding additional noise and features to the measured signals.

To add a payload to the belt, without needing a large amount of gravel or rocks to be constantly loaded and collected, a plastic container was used and filled with rocks. Figure 3.38 shows the plastic container and some of the rocks that were added. More rocks were added and then the container was closed with its lid-locking handles. The locking mechanism of the lid allowed the same payload to be cycled with the sensor over and over again. This reduced the amount of payload that was needed to add some dynamic conditions and it was cleaner. Large rocks were chosen as they tumbled more violently than smaller rocks, creating more signal noise.

The addition of the payload was expected to add more noise to the signals. These signals were pre-processed as discussed in Chapter 2.4.2 and were used to train and test a neural network and a support vector machine to identify and classify the bearing faults. The same bearing faults were tested, but the sensor was only placed in the middle of the belt for these tests.

Figure 3.38: Payload surrounding the accelerometer

3.2.3.1. Influence of payload on the signal quality

When the conveyor was started again with the payload around the accelerometer, there was a clear, audible noise as the rocks tumbled in the container. It was however only heard as the sensor and container passed over the idler and when the container and sensor rotated around the drive and tail pulley. In the rest of the cycle there was almost no movement in the payload.

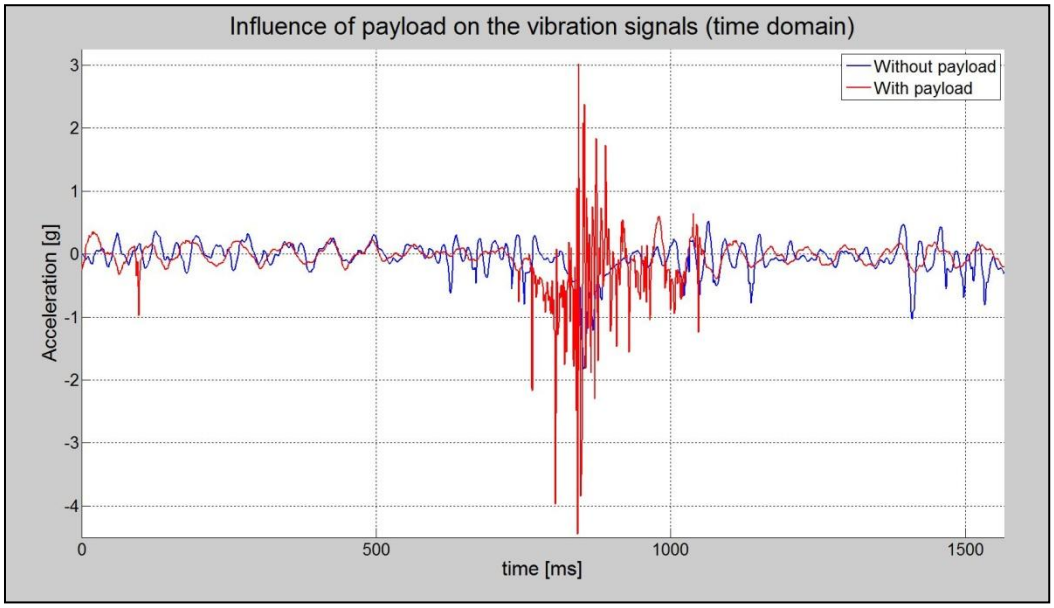

Figure 3.39: Influence of a payload in the time domain

Figure 3.39 shows a comparison between the measured vibrations, in the time domain, of a healthy bearing measured in the middle of the belt with and without the presence of a payload. The end of the steady rise in the acceleration, as seen in Figure 2.15, as the sensor rotated around the pulley from the bottom return section to the top part of the conveyor, was used as the trigger to enable the superposing of the two signals. As seen before with the case where there was no payload on the belt, there was a sharp decrease in the acceleration as the sensor passed over the idler. The sensor travelled slightly upward to the idler and downward the other side. This sudden change in the vertical direction of the sensor was what created the sharp, negative acceleration. The same sudden change in direction was what disturbed the payload in the plastic container as it travelled over the idler. The tumbling of the rocks can be seen in Figure 3.39 as the additional noise.

As the plastic container with the payload and the sensor travelled over the idler, the payload shifted around, causing some noise in the signal. This movement created a very noisy signal, but it only lasted a fraction of a second. This can be seen in Figure 3.39. After the payload settled, the signal looked like normal. An FFT was done on the two signals and is shown in Figure 3.40. The frequency spectrums for the two cases are shown up to 250 Hz. The noise continues on at the higher frequencies. The previous tests that were done without the payload were only shown to 100 Hz as there were very few peaks in the spectrum above this frequency. With a payload present, this was no longer true. There was a large amount of high-frequency noise present in the signal. The fundamental bearing frequencies were still present but the magnitudes were not as expected. The outer raceway fundamental frequency had a lower magnitude and the rolling element fundamental frequency had a higher magnitude than expected.

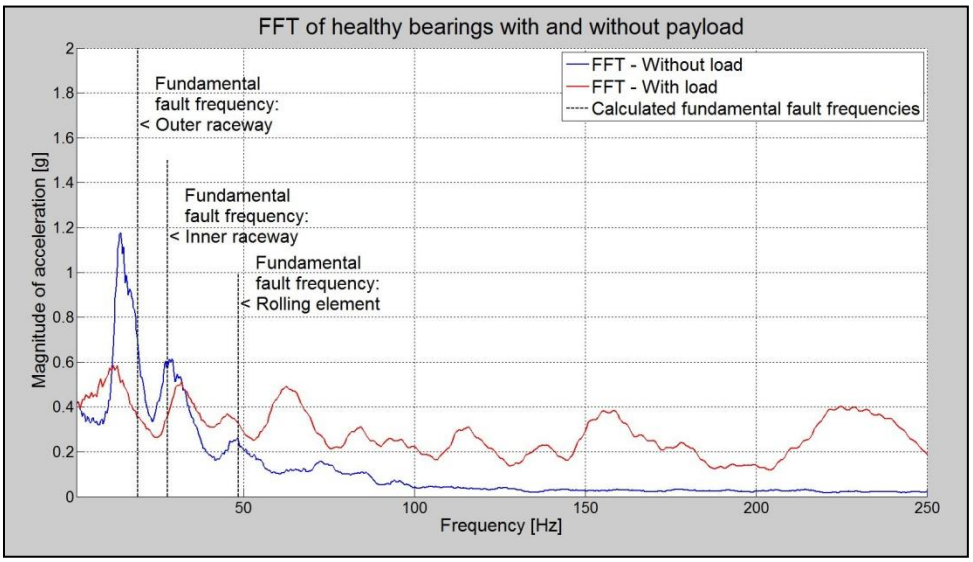

Figure 3.40: Influence of a payload on the frequency spectrum

3.2.3.2. Identification and classification of the bearing faults

Data was sampled for each of the five bearing conditions with a payload present around the sensor. A total of 1202 datasets were recorded. All these measurements were pre-processed and the energy values of each measurement calculated as discussed in Chapter 2.4.2. Each bearing condition's datasets were divided into two equal parts, one for training and the other for testing the intelligent system.

The gradient based back propagation neural network was trained and tested, as discussed in Chapter 2.5.1, with the data obtained. Firstly it was investigated to see if the neural network could distinguish a healthy bearing from a faulty bearing, regardless of the fault. It was found that the neural network had a 98.00% accuracy (589 of 601 test datasets) when distinguishing a healthy bearing from a faulty one. Table 3.12 shows the statistics for the neural network fault identification, and although the faulty bearings were all correctly classified, almost 10% of the healthy bearings were misclassified. In practice, this means that 1 out of 10 healthy idlers would be considered as faulty. This will lead to healthy idlers being replaced - unnecessary downtimes and costs will result of this. The misclassification might have been due to the neural network being over trained with the datasets of the faulty bearings, making it oversensitive to faulty bearings. Figure 3.41 shows the classifications of the healthy and faulty bearings.

Table 3.12: Neural network identification of faulty bearings with a payload

Neural network identification of faulty bearings with payload present			
Bearing condition	Number of datasets	Correctly classified	Accuracy
Healthy bearing	128	116	90.63%
Inner raceway Outer raceway Rolling element Contaminated bearing	473	473	100.00%
Total	601	589	98.00%

The neural network identified a faulty bearing with a very high accuracy. The accuracy of the neural network was tested to see how accurate it could classify the faulty bearings - not only tell if a bearing was faulty, but also classify the fault. Figure 3.42 shows the classification and Table 3.13 shows the statistics for the neural network. As expected, the overall accuracy of the neural network was lower when trying to classify the bearing faults and not only just identify them. The percentage misclassifications were still too high to be accepted but was higher than all the neural network classifications done before. The addition of the payload may have tighten the belt, helping with the transmissibility of the vibrations through the belt, or the faults in the bearings may have become a bit larger, making it easier to identify a faulty bearing.

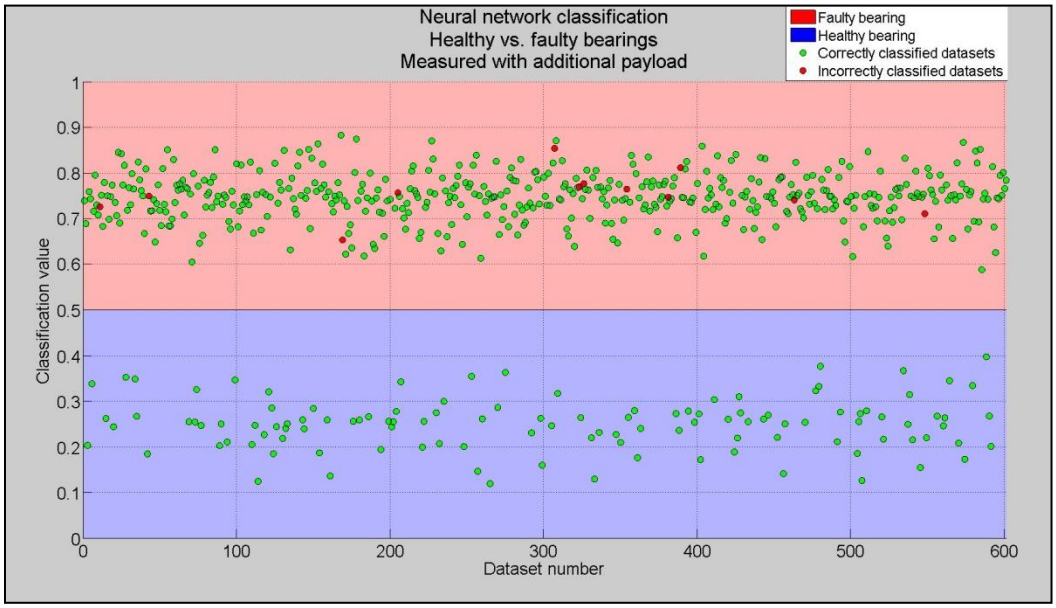

Figure 3.41: Two-class Neural network classification with additional payload

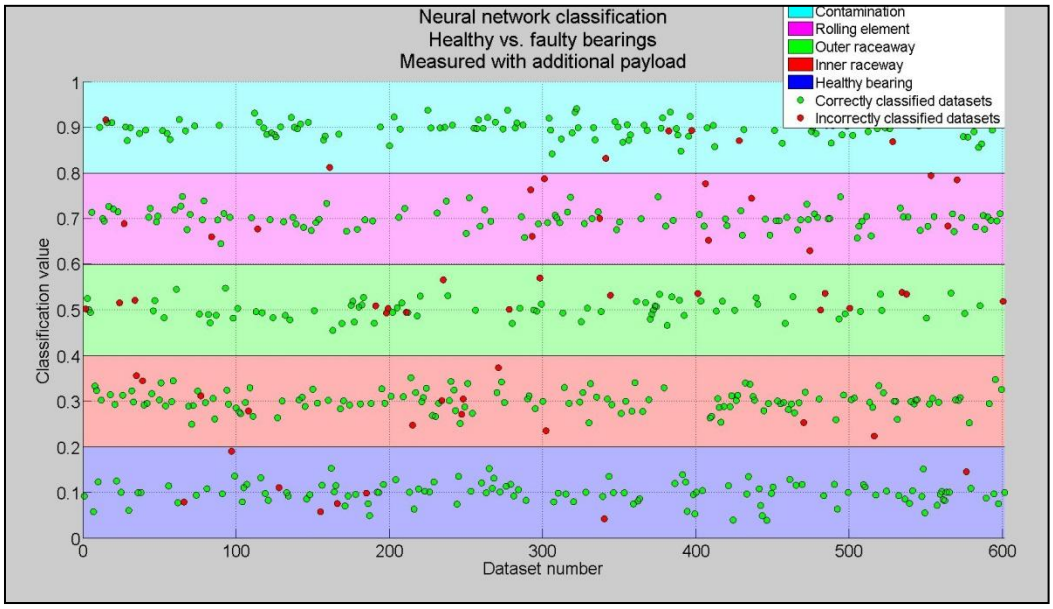

Figure 3.42: Five-class Neural network classification with additional payload

Table 3.13: Neural network classification of bearings with a payload

Neural network classification of faulty bearings with payload present			
Bearing condition	Number of datasets	Correctly classified	Accuracy
Healthy bearing	128	117	91.41%
Inner raceway	162	137	84.57%
Outer raceway	82	75	91.46%
Rolling element	111	103	92.79%
Contaminated bearing	118	110	93.22%
Total	601	542	90.18%

The support vector machine was trained and tested, as discussed in Chapter 2.5.2, with the same datasets as with the neural network. A radial base function was used and with a grid search, a cost value of 7.8365×10^5 and a gamma of 4.5672×10^{-5} was found to produce the highest accuracy. The support vector machine did not only classify the datasets into the two classes of healthy and faulty, but classified all the different faults with 100% accuracy (601 of 601 test datasets). A single support vector machine could classify a dataset into any of the five bearing conditions; healthy bearing, inner raceway defect, outer raceway defect, rolling element defect or contaminated bearing. Figure 3.43 shows the classification and Table 3.14 shows the statistics of the support vector machine.

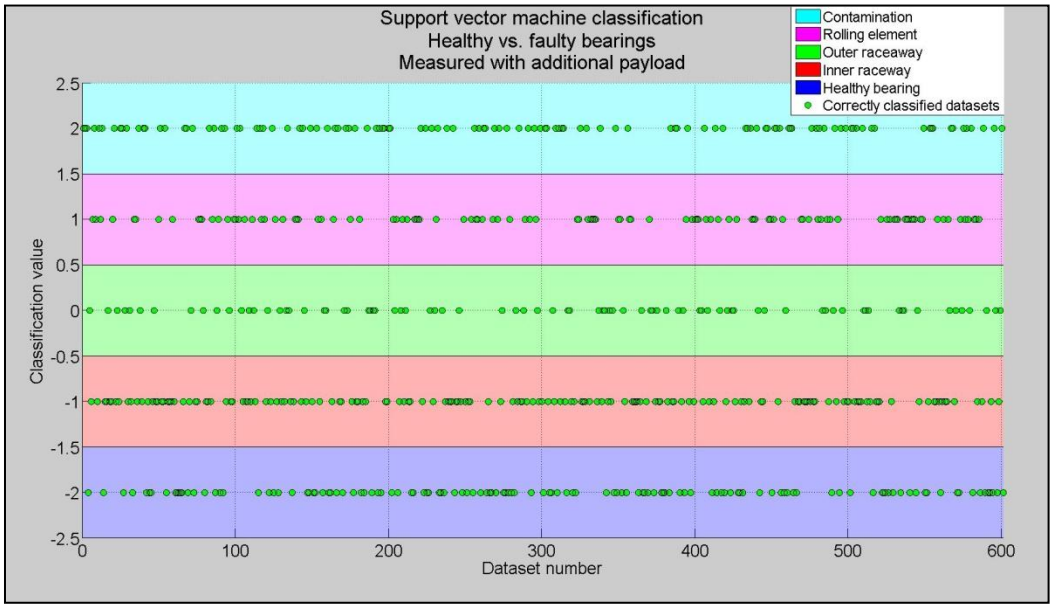

Figure 3.43: Five-class Support vector machine classification with additional payload

Table 3.14: Support vector machine classification with a payload

SVM classification of faulty bearings with payload present			
Bearing condition	Number of datasets	Correctly classified	Accuracy
Healthy bearing	128	128	100.00%
Inner raceway	162	162	100.00%
Outer raceway	82	82	100.00%
Rolling element	111	111	100.00%
Contaminated bearing	118	118	100.00%
Total	601	601	100.00%

Seeing that the support vector machine was the better classifier of the two intelligent systems and had a 100% accuracy throughout all the investigations, it was decided to combine all the data collected while the sensor was on the belt. The datasets of the near, middle and far positions were added to the datasets of the additional payload tests. This created a very large dataset of 3007 training and 3007 test signals. Each bearing fault class consisted of the data of all the tests done with the specific bearing fault. The different types of investigations of a specific bearing fault had slightly different characteristics but all belonged to the same class.

The support vector machine was trained and tested, as discussed in Chapter 2.5.2, with all the datasets collected in the different investigations. A radial base function was used and with a grid search, a cost value of 6.3719×10^{4} and a gamma of 1.2634×10^{-3} was found to produce the highest accuracy. The support vector machine classified all the different faults with 100% accuracy (3007 of 3007 test datasets). A single support vector machine could classify a dataset into any of the five bearing conditions; healthy bearing, inner raceway defect, outer raceway defect, rolling element defect or contaminated bearing. This was done regardless of the position of the sensor on the belt and if there was a payload or not. Table 3.15 shows the statistics of the support vector machine classification of all the datasets and Figure 3.44 shows the classifications.

Table 3.15: Support vector machine Classification of all the datasets

SVM classification of faulty bearings with payload present			
Bearing condition	Number of datasets	Correctly classified	Accuracy
Healthy bearing	660	660	100.00%
Inner raceway	656	656	100.00%
Outer raceway	511	511	100.00%
Rolling element	568	568	100.00%
Contaminated bearing	612	612	100.00%
Total	3007	3007	100.00%

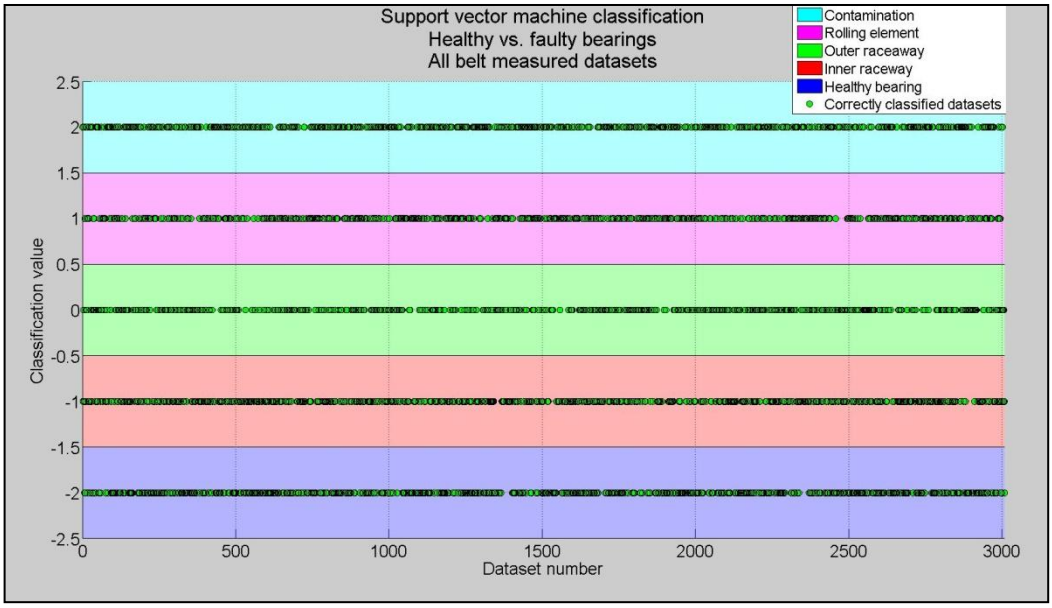

Figure 3.44: Five-class Support vector machine classification of all the on-belt measurements

3.2.3.3. Conclusion

It was seen in the tests without a payload that, when placing an accelerometer on the belt, regardless of the position, the bearing faults were be classified with 100% accuracy when a support vector machine was used. When a payload with a dynamic aspect was investigated, it was seen that the rocks tumbling around the sensor did add more noise and other energy to the signals, but the bearing faults were still classified with 100% confidence with a support vector machine. The neural network was 98.00% accurate but the 2% error was made only on healthy bearings. This 2% error in the total scheme of things translated to almost a 10% misclassification of the amount of healthy bearing datasets. In practice, this means that 1 out of 10 healthy idlers could be considered as faulty. This will lead to healthy idlers being replaced - unnecessary downtimes and costs will result of this.

The use of a support vector machine in a monitoring system is sensitive enough to identify a bearing in its early failing stages, even with the addition of a payload. It was found that the faulty bearings could be identified even before failure occurred. This can give enough time to prepare for a planned outage before a catastrophic bearing failure can cause significant damage to the belt. From the tests, it was seen that, when sufficient pre-processing was done, a support vector machine was a very powerful classifier. It is strongly advised to use a support vector machine to be used in an in-belt vibration monitoring system for conveyor idler bearings with the addition of wavelet package decomposition to pre-process the bearing signals. A substantial amount of iterative training processes went into the training of the intelligent systems, especially the support vector machines, to be able to have such high accuracies.

Chapter 4 - Conclusion

There is a need for conveyor idler monitoring, but the cost of such a system has a very large influence on the feasibility of implementation. There are several methods for monitoring or inspecting idlers but the use of vibrations enables the implementation of an on-line system. This system will reduce the labour cost of inspection and will also eliminate the possibility of human error. The use of vibrations have been found, through experiments, to be very accurate in identifying faulty idlers when the accelerometer was installed on top of the moving belt.

It was found, trough the replication of a study done on the measurements of vibrations on the supporting structure, that a faulty idler could be identified and the fault classified. Making use of wavelet package decomposition for data pre-processing and a support vector machine as a classifier, the idler bearing faults were identified and classified with 100% accuracy.

The downside of monitoring all the idlers' vibrations along the length of the conveyor, by placing the sensor against the supporting structure, is that a large number of accelerometers are needed, even if there is one accelerometer for every three or more idlers.

To reduce the number of accelerometers needed to monitor all the idler bearings, an investigation was done on the feasibility of attaching an accelerometer to the moving belt. As the accelerometer travelled along the length of the conveyor, it measured the vibrations of all the idlers it passed. From the tests done, it was found that an accelerometer could be used with great success to identify and classify idler bearing faults, regardless of the sensor position or the presence of a payload or not. The self-developed data acquisitioning system attached to the moving conveyor belt was used to identify a faulty bearing and classify the fault with a 100% success rate. Wavelet package decomposition for data pre-processing and a support vector machine was used to achieve this accuracy.

The self-developed data acquisitioning system cost a fraction of commercially available systems that complied with the size and performance needed for the data sampling. The self-developed data acquisitioning system cost less than R2000. One meter of the steel reinforced rubber belt used on the test bench, and used in the industry, costs R2500. The data acquisitioning system, as it is, needs to be improved before it can be installed in a working conveyor, but the additional costs of the improvements will still make it a financially feasible solution to a great need in the conveyor industry.

The non-linear characteristics of the on-belt system showed that the system had subharmonic and superharmonic responses to the fundamental bearing fault frequencies. Although the excitement and response frequency values did not correspond to one another, the bearing faults were still identified in the signals and the bearings were classified correctly.

By attaching the data acquisitioning equipment to the moving belt, an automatic monitoring system can be created. This reduces the need for an operator to travel the length of the conveyor with visual or acoustic monitoring equipment to identify failing or faulty idlers. The speed at which an operator has to travel along the conveyor to accurately determine if an idler is faulty, is usually walking speed, or even slower. The in-belt monitor travels at the speed of the belt and is usually much faster than an operator, and can monitor idlers in hard to reach places with ease. This means that the frequency at which all the idler bearings are monitored is much higher when an in-belt monitoring system is used, and the conditions of the bearings can be updated more regularly.

It is seen from the results that the in-belt monitor can identify a faulty bearing even before failure occurs. This allows all the faulty bearings to be identified and the needed stock can be purchased ahead of a planned outage and all the faulty bearings can be replaced. This will reduce the number of short outages that interrupts the conveyor feed and one large planned outage can be organised instead where all faulty bearings, and bearings that show signs of failing in the near future, can be replaced. The current method of monitoring cannot determine the remaining useful life of the faulty bearings. This feature will be very beneficial in the planning of an outage and should be investigated in future.

Chapter 5 - Future work and recommendations

It has been confirmed that vibrations of idler bearings can be used to identify a faulty idler and even classify the fault. There are a few improvements that need to be done on the data acquisitioning system before it can be incorporated into a fully functioning conveyor. The following improvements will have to be made and investigated:

- This system in its current state, although used with great success, is too thick to be imbedded into a belt as seen in Figure 5.1. The data acquisitioning system has to be fully imbedded into the belt and cannot protrude because it will be damaged by the idlers. The thickness reduction of the data acquisitioning system has to be addressed.

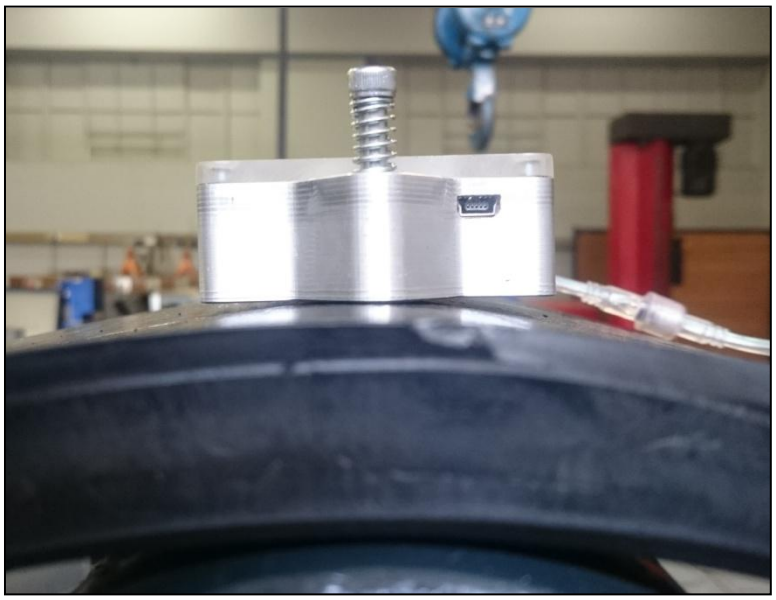

Figure 5.1: Comparison between belt and logger thickness

- The vibration data was stored on a SD card for the tests done in this investigation. The raw vibration data was transferred to a computer and the pre-processing done on the computer. Onboard pre-processing will be very beneficial to the system and a support vector machine can be loaded onto the microprocessor. Being able to pre-process the data onboard the belt and then classify it as well will reduce the need for constant communication between the monitoring system and the operator. The Teensy 3.2 has onboard fast Fourier transform and support vector machine capabilities, allowing onboard monitoring to be done. The use of multiple microcontrollers may be needed to spread the work load.
- The monitoring system is powered by a lithium-polymer battery and the battery would need to be charged regularly. The charging would ideally have to be done while the conveyor is still operational. Induction charging sections can be installed along the belt

but this can become expensive because the monitoring system will pass these sections with speed and long sections will thus be needed. Piezo-electric components can be used, with the addition of an energy harvester circuit, to charge the battery. The constant flex of the belt as it travels over and in between idlers can be a large source of piezo-electric harvested energy. The power that can be generated by solar panels is much more than piezo-electric energy and can be a constant source of power, rather than sections of induction chargers. However, the solar panels will have to be robust enough to withstand the wear and tear and be able to endure the constant flexing of the belt. The solar panels will have to be clear of any payload so that it can have direct sunlight to produce power, otherwise the efficiency of the panel will be reduced.

- Long distance transmission of large amounts of raw data is problematic. Serial communication like Bluetooth can only transmit data between 10 and 20m and is not feasible for long conveyors. Wi-Fi data transmission is faster and can be done over longer distances. Bluetooth or Wi-Fi connection spots will have to be installed along the entire length of the conveyor, making it infeasible. The other problem with Bluetooth or Wi-Fi is that between two connection points, there is usually an interruption in data transfer when a new connection is established to the next connection point. One way of eliminating the problem of transmitting large amounts of raw data is to not transmit it at all. Wavelet package decomposition and support vector machine code is available that can be added to the software of the micro-controller. This will allow for onboard pre-processing and classification to be done and the need to stream the large amounts of data no longer exists. Small GSM modules do exist that can be used to send an SMS with positioning information of the faulty bearing as soon as it is detected, or a list of faulty bearings that has been identified can be sent at predetermined periods. This requires more computational power, but newer versions of the micro-controller, the Teensy 3.6, is much more powerful and has a built-in SD card slot. The additional cost of the GSM module and the upgrade to the Teensy 3.6 should add about 10 to 15% to the cost of the data acquisitioning equipment. Short GSM towers can be erected at sites where there is no cell-phone reception. The GSM module stores the outgoing message until it has signal, so the monitoring equipment can send an update every time it is close to the operating or monitoring room if there is no signal along the conveyor.
- The current method of monitoring cannot determine the remaining useful life of the faulty bearings. This feature will be very beneficial in the planning of an outage and should be investigated in future.

After the monitoring system has been improved so that it can be fitted into a conveyor belt, real-world test will have to be done. The addition of multiple idlers and external factors will lead to additional pre-processing and support vector machine learning to be done. Tests need to be done with varying faulty idler positions, bearing faults and even different stages of bearing faults.

Further investigations need to be done on the influence that variations in the belt speed has on the measured fundamental frequencies as well as the non-linearity of the on-belt measuring system. It is clear that the system is non-linear and that this has an influence on the frequency response measured by the sensor. A better understanding of the system dynamics will enable better analysis of the measured response signals and why the excitement frequencies have a tendency to appear at subharmonic or superharmonic response frequencies when the sensor is placed on top of the belt.

Appendix A - Data acquisitioning details

A data logger was self-developed for the purpose of measuring the vibrations of conveyor idlers. A few components were combined to build a data acquisitioning system that could sample at the desired frequency and could be mobile so it could be installed on to a moving conveyor belt. The following components were used:

- Teensy 3.2 microcontroller.
- LSM6DS33 6 degrees of freedom accelerometer and gyroscope breakout board.
- SparkFun OpenLog microSD card read/writer.
- HC-05 Bluetooth transmitter/receiver.
- 2000 mAh lithium-polymer battery.
- SparkFun Lithium-polymer battery manager/charger.
- Pololu 5V step-up voltage regulator (NCP1402).

The Teensy 3.2 micro controller is the core of the data acquisitioning system and is shown in Figure A.0.1. The Teensy 3.2 has a clock speed of 96 MHz and is very fast for a microcontroller of its size. The LSM6DS33 is an accelerometer and gyroscope breakout board that has 6 degrees of freedom; 3 axis of linear acceleration and 3 axis of rotational acceleration. Figure A.0.2 shows the LSM6D33 breakout board. Only the one axis of linear acceleration is used in the application of measuring idler vibrations. The accelerometer sensor has 16 bit resolution and can measure up to a range of ±16g at a maximum frequency of 6.6 kHz. breakout board is digital and the inputs and outputs are digital values.

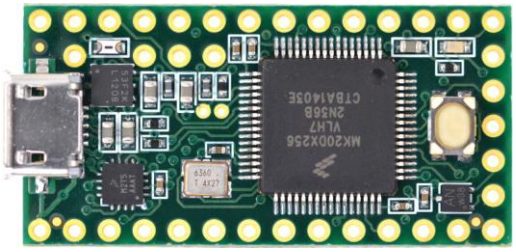

Figure A.0.1: Teensy 3.2

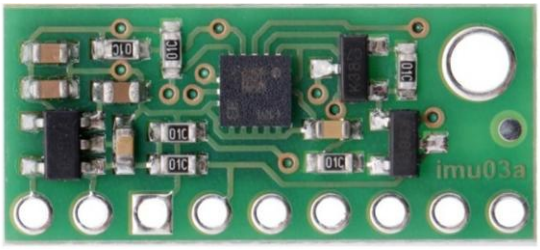

Figure A.0.2: LSM6D33 accelerometer

The microcontroller and the accelerometer breakout board communicate over an Inter-Integrated Circuit protocol (also called I^2C). This protocol allows the microcontroller to access the registers of the accelerometer sensor. The registers are where various setting values are stored and can be read or changed by the microcontroller as needed. If for instance, the

accelerometer range needs to be changed from ±16g to ±2g to better capture the small amplitude vibrations, it can be changed by altering the value of the appropriate register. It is in these registers where the acceleration values are stored each time the accelerometer samples.

Each cycle the microcontroller requests the acceleration values over the protocol and waits for a response from the accelerometer breakout board to notify it that there are acceleration values available. When the values are available they are transmitted to the microcontroller. As the acceleration values are received from the accelerometer module, they are compiled to a string and written over serial communication to the OpenLog microSD card read/writer. The OpenLog read/writer appends whatever string it receives over serial communication to the end of a text file (.txt) or a comma separated value file (.csv). This cycle is repeated, logging acceleration data, until the data acquisitioning system is turned off. Figure A.0.3 shows the OpenLog card read/writer. The microSD card slots in underneath and is not show. A microSD card of up to 64 Gb can be used with the OpenLog read/writer - more than enough storage space.

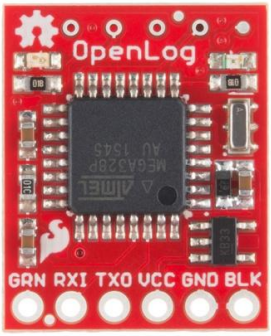

Figure A.0.3: OpenLog microSD card read/writer

The microcontroller needs a 5V source and cannot turn on at any lower voltages. A lithium-polymer battery, seen in Figure A.0.4, only supplies 3.7V. To supply the microcontroller of 5V, a step-up regulator is used. The step-up regulator, seen in Figure A.0.5, uses power electronics to enable the 3.7V source to supply higher voltages, 5V in this case. It can step-up a voltage as low as 0.5V to 5V. A battery management circuit board is used to ensure the voltage of the lithium-polymer battery does not drop below a safe voltage level. Operating the battery at low voltage can cause damage to the battery and will be disconnected automatically when its voltage becomes too low. The circuit board is also used to charge the lithium-polymer battery and can be done so with a normal micro USB charger. A 2000 mAh lithium-polymer battery is used and provides over 50 hours of logging time. The management/charging circuit board can be seen in Figure A. 0.6

Figure A.0.4: Lithium-polymer battery

Figure A.0.5: 5V step-up regulator

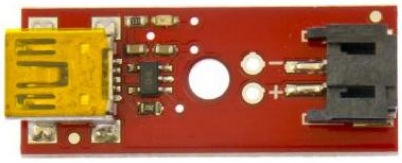

Figure A. 0.6: Battery management/charger circuit board

A Bluetooth module was also included. The Bluetooth was not used in the tests because streaming the accelerometer data over Bluetooth made the sampling frequency lower. The Bluetooth was however used to change settings of the LSM6DS33 accelerometer breakout board wirelessly when needed. This made it easier to change the settings because the data acquisitioning system could be left on the belt - was not necessary to be removed to be taken to a computer to change the settings. Any laptop, computer or cell phone that has Bluetooth can be used to change the settings if the needed software is installed and the setting commands are known.

As mentioned, the microcontroller operates at 5V. This means that the high logic level of its digital output signal is 5V (and low logic level is 0V). The LSM6DS33 accelerometer breakout board, OpenLog read/writer and the Bluetooth module operates at a 3.3V high logic level. This means that the 5V digital output signal of the microcontroller can damage the other components when it is communicating with them. A voltage divider is used between the output of the microcontroller and the input of the other components. The voltage divider is a set of two resistors that can be calculated to lower a 5V signal to 3.3V. The digital signal will not be affected in any way, except that the voltage is lower. The microcontroller can receive a 3.3V signal and recognizes it as a high logic level - no need to step-up the digital output signals from the components to the microcontroller input. Everything is grounded to a common ground.

All the components, except the LSM6DS33 accelerometer breakout board, were placed in an aluminium case that was machined by CNC. This case protects the components when tests are done against knocks and bending. Perspex covers the front so that the indication lights inside can be seen.

The case also provides strong points where the data acquisitioning system can be fixed to the moving belt. Bots were used to fix the case to the belt. Stiff springs were used between the bolt heads and the sunk holes in the case. The belt compresses when it wraps around the pulleys and idler and then the case is loose on the belt. The springs press it onto the belt so that it does

not rattle around. The battery is housed in the case underneath the circuit board to reduce the footprint. The logging section of data acquisitioning system can be seen in its aluminium case in Figure A.0.7.

The LSM6DS33 accelerometer breakout board is placed in its own, small, aluminium case. The data logging part and the accelerometer is connected with a cable that has a four-wire screw-connection so that the sensor can be moved from one position on the belt to another without needing to remove the entire data acquisitioning system. This also allows the one to be removed if needed without having to remove the other. Figure A.0.8 shows the accelerometer in its aluminium case - images not to the same scale.

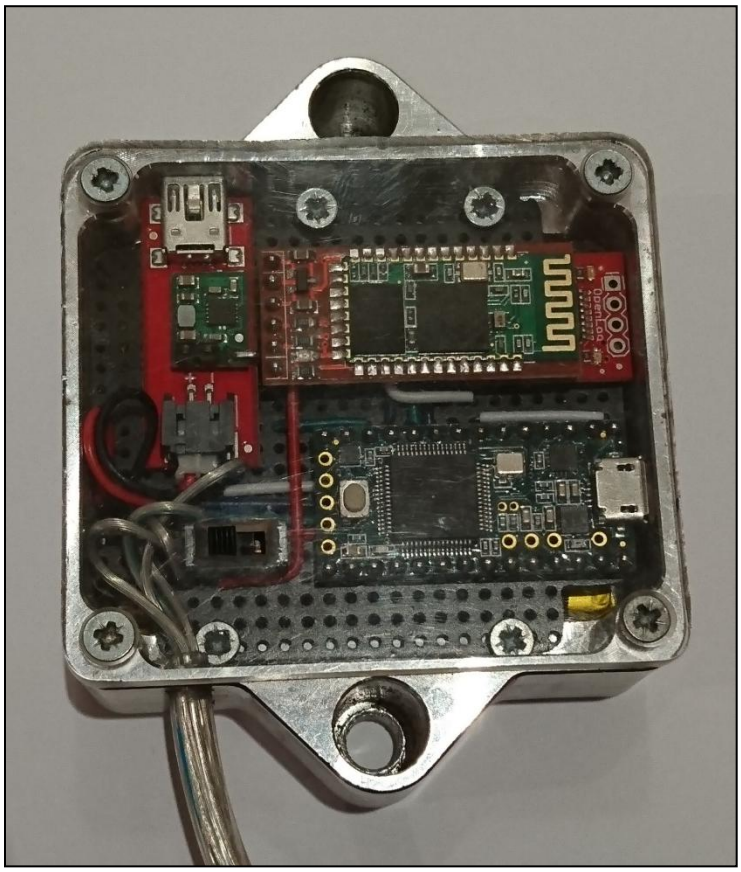

Figure A.0.7: Data acquisitioning system in its aluminium case

Figure A.0.8: Accelerometer in its aluminium case

References

Automation Supplies Ltd, n.d. *The incredible, affordable iDrive compact belt conveyor from Dorner.* [Online]
Available at: http://www.automation-supplies.com/iDrive-belt-conveyors.html
[Accessed 01 September 2015].

Bishop, C. M., 2006. *Pattern Recognition and Machine learning.* 1 ed. s.l.:Springer.

C.C.Components Pty. Ltd., n.d. *Rubber sidewall conveyor belt.* [Online]
Available at: http://www.cccomponents.com.au/products/special-purpose-belts-conveyor-components/rubber-sidewall-conveyor-belts/
[Accessed 05 September 2015].

Choi, Y. S. & Noah, S. T., 1988. Forced Periodic Vibration of Unsymmetric Piecewise-linear Systems. *Journal of Sound and Vibration,* 121(1), pp. 117-126.

CKIT, n.d. *Design guidelines and standards.* [Online]
Available at: http://www.ckit.co.za/secure/conveyor/troughed/beginners-guide/beginners_design_and_standards.htm
[Accessed 09 Septemnber 2015].

Conveyor Belt Guide, 2005. *The longest conveyor belt.* [Online]
Available at: http://www.conveyorbeltguide.com/LongestBelt.html
[Accessed 31 August 2015].

Conveytech, 2013. [Online]
Available at: http://conveytech.in/p1.html
[Accessed 05 September 2015].

Darling, D., n.d. *Encyclopedia of Science, Mobius band.* [Online]
Available at: http://www.daviddarling.info/encyclopedia/M/Mobius_band.html
[Accessed 31 August 2015].

David Brown, n.d. *Industrial conveyor systems and belt conveyor drives.* [Online]
Available at: http://www.davidbrown.com/business-units/metals-2/products/conveyor-systems-and-belt-conveyor-drives-81
[Accessed 03 September 2015].

Du Pont, 2013. *DuPont™ helps create long-term solutions for conveyor belts in the mining industry.* [Online]
Available at: http://www.dupont.ca/en/products-and-services/fabrics-fibers-

nonwovens/fibers/uses-and-applications/conveyor-belts-for-mining.html
[Accessed 17 August 2015].

Dunlop Conveyor Belting, n.d. *Steelcord belting.* [Online]
Available at: http://www.dunlopconveyorbelting.com/steelcord-belting/
[Accessed 12 September 2015].

Edilson S Ribeiro, 2012. *Idler sound monitor.* [Online]
Available at: https://www.youtube.com/watch?v=LSJcYPCpvPA
[Accessed 05 October 2015].

ESTAR, 2014. *Steel cord conveyor belts.* [Online]
Available at: http://www.estargroup-china.com/belt/product/showproduct.php?lang=en&id=18
[Accessed 03 September 2015].

FLIR, 2015. *FLIR T-Series Thermal imaging cameras.* [Online]
Available at: http://www.flir.com/instruments/display/?id=62960
[Accessed 05 October 2015].

FLUKE, 2015. *Infrared images worth thousands of dollars in saved downtime.* [Online]
Available at: http://www.fluke.com/fluke/caen/community/fluke-news-plus/articlecategories/plant-news/infrared-images-worth-thousands-of-dollars-in-saved-downtime
[Accessed 05 October 2015].

Freeman, V. N., 2010. *Apparatus and method for in-belt conveyor idler condition monitoring.* United States of America, Patent No. 7,673,739 B2.

Goodman Conveyor, n.d. *Idler selection procedure.* [Online]
Available at: http://www.beltmaintenance.com/downloads/idler_selection_procedures.pdf
[Accessed 17 November 2015].

Graney, B. P. & Starry, K., 2012. Rolling Element Bearing Analysis. *Materials Evaluation,* 70(1), pp. 78-85.

Habasit, 2011. *Introduction to light conveyor belts, history of the conveyer belt.* [Online]
Available at:
http://www.habatec.net/HNet/HabaTEC.nsf/vwWebContent/B3AFDB9C92909C37C12578BE002BB553?OpenDocument
[Accessed 31 August 2015].

Intium, 2015. *The world's first accurate and fully automated roller condition monitoring system.* [Online]
Available at: http://www.intiumsolutions.com/intium-rcm/
[Accessed 05 October 2015].

Kapp & Lehman, J., 1976. *Woven endless belt of a spliceless and Mobius strip construction.* United States of America, Patent No. 3991631.

Kim, S. K. & Lee, J. M., 1999. Analysis of the non-linear vibration characteristics of a belt-driven system. *Journal of Sound and Vibration,* 5(223), pp. 723-740.

Kinder, 2013. *Belt tracking & conveyor maintenance.* [Online]
Available at: http://www.slideshare.net/kinder13/belt-tracking-conveyor-maintenance
[Accessed 05 October 2015].

Kinder, 2015. *K-Polymer conveor rollers.* [Online]
Available at: http://www.kinder.com.au/case-study/k-polymer-conveyor-rollers/
[Accessed 05 October 2015].

Lakshmi Macfab, 2015. *Pipe conveyor.* [Online]
Available at: http://delhi.all.biz/pipe-conveyor-g72651#.VfPtSvmqrxp
[Accessed 12 September 2015].

Li, W. et al., 2013. Design of Online Monitoring and Fault Diagnosis System for Belt Conveyors Based on Wavelet Packet Decomposition and Support Vector Machine. *Advances in Mechanical Engineering,* Volume 2013, p. 10.

Maras, C., 2013. *Thermal imaging cameras a great tool for predictive maintenance inspections.* [Online]
Available at: http://www.maintworld.com/Applications/Thermal-Imaging-Cameras-a-Great-Tool-for-Predictive-Maintenance-Inspections
[Accessed 2015 October 2015].

Mjelo, N., 2013. *Inspection of Idlers (impact, carrying, return) & Idlers (carrying, trailing, return),* Camden Power Station: Eskom.

Moon, J. & Wickert, J. A., 1997. Non-linear vibration of power transmission belts. *Journal of Sound and Vibration,* 4(200), pp. 419-431.

Narayanan, S. & Jayaraman, K., 1991. Chaotic Vibration in a Non-linear Oscillator With Colomb Damping. *Journal of Sound and Vibration,* 146(1), pp. 17-31.

Norton, M. P. & Karczub, D. G., 2003. *Fundamentals of Noise and Vibration Analysis for Engineers.* 2nd ed. s.l.:Cambridge.

Nuatitech, 2015. *Better monitoring of conveyor belts using thermal cameras.* [Online]
Available at: http://nautitech.com.au/conveyor-belts/
[Accessed 05 October 2015].

Ocak, H., Loparo, K. A. & Discenzo, F. M., 2007. Online tracking of bearing wear using wavelet packet decomposition and probabilistic modeling: A method for bearing prognostics. *Journal of Sound and Vibration,* Issue 302, pp. 951-961.

Owen, P., n.d. *Condition monitoring for conveyors. A tool for increased productivity.* [Online]
Available at: http://www.saimh.co.za/beltcon/beltcon9/paper914.html
[Accessed 10 September 2015].

RAS, n.d. *ENGINEERING.* [Online]
Available at: http://www.raspulleys.com/engineering/
[Accessed 03 September 2015].

Shandong Rubber Six Xiang Te Conveyor Belt Co., Ltd., 2015. *Steel cord conveyor belt (ST630-ST5400).* [Online]
Available at: http://jiaoliu.en.made-in-china.com/product/nqjmYuDHsbRg/China-Steel-Cord-Conveyor-Belt-ST630-ST5400-.html
[Accessed 03 September 2015].

Siemens, 2013. *SIMINE Gearless Conveyor Drives.* [Online]
Available at: http://www.industry.siemens.com/verticals/global/en/mining-industry/transport/mining-conveyor-system/Documents/simine-gearless-conveyor-drives.pdf
[Accessed 17 November 2015].

SKF, n.d. *SKF idler sound monitor kit.* [Online]
Available at: http://www.skf.com/africa/en/industry-solutions/metals/Processes/upstream-steel-making/conveyors/SKF-idler-sound-monitor-kit.html
[Accessed 05 October 2015].

van Tonder, J., 2002. *Idler monitoring feasibility study 2002,* s.l.: Eskom Resources and Stratagy Research Division.

Zhang, L. & Zui, J. W., 1998. Non-linear vibration of viscoelastic moving belts, Part II: Forced vibration analysis. *Journal of Sound and Vibration,* 1(216), pp. 93-105.